Identification of Base-Isolated Structures Considering Nonlinearity and Identifiability

March 2009

Liyu Xie

Abstract

It is well documented that the rubber bearings of base-isolated structures possess strong hysteretic nonlinearity during severe earthquakes in both site and experiment observation. This thesis is devoted to discuss and present identification methods for base-isolated structures considering nonlinear behavior and identifiability in order to track and monitor the state and characteristics of the base isolation layer.

Firstly, a new method for estimating the restoring force estimation of the isolation layer in a based-isolated system is proposed. The whole base-isolated structure is separated into two substructures, the linear superstructure and the nonlinear isolation layer. The hybrid motion equation involving the modal coordinates of the superstructure and the physical coordinates of the isolation layer is derived by component mode synthesis. This significantly reduces the number of unknown parameters after the mode shape information of the superstructure is substituted and makes it possible to identify the isolation layer directly and locally. The effectiveness of this method is validated in a simulation example. It is shown that the proposed method is not sensitive to the mass distribution and the expanded mode shapes but will be scaled by the total mass.

Secondly, identifiability condition for substructural identification is investigated in the framework of closed-loop systems by spectral analysis and parametric methods. Substructures governed by linear and nonlinear feedback laws are both considered. The feedback law mechanism is shown to have greater influence on identifiability than does the model structure or the identification method.

In addition, the performance of reverse path methods applied to identify the underlying linear model of base-isolated structures is investigated. The nonlinear rubber bearings are considered as nonlinear components attached to an underlying linear model. The advantage of reverse path formulation is that it can separate the linearity and nonlinearity of the structure, extract the nonlinearity and identify the underlying linear structure. The difficulty lies in selecting the nonlinearity function of the hysteretic force due to its multi-valued property and path-dependence. In the thesis, the hysteretic force is approximated by the polynomial series of displacement and velocity. The reverse path formulation is solved by Nonlinear Identification through Feedback of Output (NIFO) methods using least-square solution. Numerical simulation is carried out to investigate the identification performance.

Finally, the proposed restoring force estimation method is applied to identify real base-isolated structures. The restoring force of the isolation layer is estimated reasonably. The difficulty lies in how to describe the state of a nonlinear device of a real structure. The amplitude-dependent equivalent stiffness and damping coefficient are adopted to describe the nonlinearity of the isolation layer. The identified results by the proposed method reconfirm the experimental observation of nonlinearity in the isolation layer made up of rubber bearings.

Acknowledgements

The first person that deserves my sincere thankfulness is my advisor Professor Akira Mita, for his encouragement and support during these years. I would like to thank him for giving me great ideas and critical advice about my research.

I would like to express my gratitude to Professor Hiromitsu Ohmori, Professor Noaki Takano and Associate Professor Masayuki Kohiyama for reviewing this thesis thoroughly and giving me valuable comments.

Special thanks to my officemates at Mita Lab for providing me with a very healthy and pleasant atmosphere to work in, for their help either in research or in life. Thanks to Takashi Kato from Hazama corporation for his valuable data about a hospital building in Kushiro city.

I have been blessed with an incredibly supportive family, whose belief in me never wavered. I acquired the insights of life and cultivated my personality from my parents. I gained the courage and hope from my family during the worst time. I am thankful to my family for their love, faith and care on me.

Contents

1 Introduction **1**

1.1 Base Isolation System 1

1.2 Hysteresis Model 3

1.3 Nonlinearity System Identification 4

1.3.1 Nonlinearity Detection 6

1.3.2 Characterization of Nonlinearity 8

1.4 Nonlinear Identification of Hysteretic Systems 9

1.4.1 Nonparametric Identification 10

1.4.2 Parametric Identification 12

1.5 Organization of the Thesis 14

2 Estimating Restoring Force by Component Synthesis Method **15**

2.1 Introduction 15

2.2 Estimating Restoring Force by Component Mode Synthesis 16

2.3 Mode Shape Expansion 23

2.4 Identification Procedure 24

2.5 Numerical Simulation 24

2.5.1 Effect of Mode Selection 35

2.5.2 Effect of Mass Estimation 35

2.6 Conclusions 37

3 Identifiability of Linear Superstructures under Feedback **38**

3.1 Introduction 38

3.2 Basic Concepts of Closed-loop Identification 40

3.2.1 System 42

3.2.2 Feedback Structure 42
3.2.3 Model 43
3.2.4 Identification Method 43
3.2.5 Experimental Conditions 44
3.2.6 Identifiability Definition 44
3.3 Identifiability Conditions for Linear Feedback Laws 44
3.3.1 Nonparametric Methods 44
3.3.2 Parametric Methods 45
3.3.3 Identifiability Conditions of Superstructures 48
3.3.3.1 Ground Excitation 48
3.3.3.2 Free Vibration 48
3.4 Numerical Simulation 49
3.5 Conclusions 53

4 Nonlinear Identification of Hysteretic Systems by Reverse Path Method 54
4.1 Introduction 54
4.2 Reverse Path 56
4.3 Nonlinear Identification through Feedback of Output Method . . . 58
4.3.1 Least Square Solution 59
4.4 Numerical Simulation 61
4.4.1 Simulation Model 61
4.4.2 Nonlinearity Function 61
4.4.3 Results by NIFO 63
4.5 Conclusions 68

5 Application to Real Buildings 69
5.1 Raiosha 69
5.1.1 Overview 69
5.1.2 Restoring Force Estimation 72
5.2 Base-Isolated Hospital Building 77
5.2.1 Overview 77
5.2.2 Restoring Force Estimation 78
5.2.2.1 Tokachi-oki Earthquake in 2003 78

5.2.2.2 Kushiro-oki Earthquake in 2004 85
5.3 Conclusions 92

6 Conclusions **93**

A Subspace Identification **95**

References **107**

List of Figures

1.1 Amplification factor 4
1.2 Nonlinear system identification process 6

2.1 Structure model 17
2.2 CMS: fixed-interface method 18
2.3 Procedure of the proposed method 25
2.4 Simulation model of 7-story base-isolated building 26
2.5 Ground acceleration observed at Hiyoshi 28
2.6 Acceleration responses of the superstructure 29
2.7 Restoring force of the isolation layer vs. displacement 29
2.8 Expanded and analytic mode shapes (1% noise) 30
2.9 Expanded and analytic mode shapes (10% noise) 30
2.10 Acceleration in the 1st modal coordinate $\ddot{\xi}_1$ (1% noise) 31
2.11 Acceleration in the 1st modal coordinate $\ddot{\xi}_1$ (10% noise) 32
2.12 Acceleration in the 2nd modal coordinate $\ddot{\xi}_2$ (1% noise) 32
2.13 Acceleration in the 2nd modal coordinate $\ddot{\xi}_2$ (10% noise) 33
2.14 Estimated restoring force of the isolation layer (1% noise) 33
2.15 Estimated restoring force of the isolation layer (10% noise) 34
2.16 Estimated restoring force vs. displacement (1% noise) 34
2.17 Estimated restoring force vs. displacement (10% noise) 35
2.18 Effect of mode selection on estimation (1% noise) 36
2.19 Effect of mass estimation (1% noise) 36
2.20 Effect of mass estimation (1% noise), (2005 2010 1541 1834 1656 2411 3790 9950 ton, from top down) 37

3.1 Structure model 39
3.2 Subsystems in a closed-loop scheme 40
3.3 A closed-loop system 41
3.4 Simulation model for a three-story building 49
3.5 Acceleration responses (initial displacement: 0.01 m on the roof, 0 elsewhere) 51
3.6 Parametric method for linear feedback case 52
3.7 Parametric method for nonlinear feedback case 52

4.1 Nonlinear model with feedback 56
4.2 Reverse path model 57
4.3 SDOF model 61
4.4 Excitation and response (standard deviation of excitation is 798.8 kN) 64
4.5 Hysteretic loop (standard deviation of excitation is 798.8 kN) . . 65
4.6 Frequency response function by NIFO using polynomial approximation of displacement and velocity 65
4.7 Frequency response function by NIFO using polynomial approximation of displacement 66
4.8 Excitation and response (standard deviation of excitation is 2403 kN) 66
4.9 Hysteretic loop (standard deviation of excitation is 2403 kN) . . . 67
4.10 Frequency response function by NIFO using polynomial approximation of displacement and velocity 67

5.1 Elevation views showing sensor allocation 70
5.2 Overview of Raiosha 70
5.3 Sensor location on the roof 71
5.4 Sensor location on the 1^{st} floor 71
5.5 Ground acceleration (in x direction) 72
5.6 Acceleration responses (#2 #4 #5 in x direction) 73
5.7 Deformation of the isolation layer (#102 in x direction) 73
5.8 Expanded mode shapes 74
5.9 Acceleration in modal coordinates 74

5.10 Restoring force of the isolation layer 75
5.11 Force-displacement plot 75
5.12 Equivalent stiffness and damping coefficient 76
5.13 Overview of a hospital building in Kushiro City 79
5.14 Acceleration response in x direction 80
5.15 Acceleration response in y direction 80
5.16 Deformation of isolation layer 81
5.17 Estimated transfer function of superstructure in x direction (input: acceleration on the 1st floor, output: acceleration on the roof) . . 82
5.18 Estimated transfer function of superstructure in y direction (input: acceleration on the 1st floor, output: acceleration on the roof) . . 82
5.19 Estimated transfer function of whole structure in x direction (input: acceleration on the ground, output: acceleration on the roof) 83
5.20 Estimated transfer function of whole structure in y direction (input: acceleration on the ground, output: acceleration on the roof) 83
5.21 Expanded 1st mode shape 84
5.22 Hysteresis loop of isolation layer in x direction 84
5.23 Hysteresis loop of isolation layer in y direction 85
5.24 Equivalent stiffness and damping coefficient in x direction (from 20 s to 180 s, 2 s per segment) 86
5.25 Equivalent stiffness and damping coefficient in y direction (from 20 s to 180 s, 2 s per segment) 86
5.26 Equivalent stiffness and damping coefficient in x direction (from 50 s to 180 s, 1 s per segment) 87
5.27 Equivalent stiffness and damping coefficient in y direction (from 50 s to 180 s, 1 s per segment) 87
5.28 Acceleration responses in x direction 88
5.29 Acceleration responses in y direction 88
5.30 Deformation of isolation layer 89
5.31 Hysteresis loop of isolation layer in x direction 90
5.32 Hysteresis loop of isolation layer in y direction 90
5.33 Equivalent stiffness and damping coefficient in x direction (from 20 s to 180 s, 2 s per segment) 91

5.34 Equivalent stiffness and damping coefficient in y direction (from 20 s to 180 s, 2 s per segment) 91

List of Tables

2.1 Modal information of superstructure 27
2.2 Parameter values 27
2.3 Identified mode shapes of superstructure 28

3.1 Modal information of the superstructure (fixed base) 50
3.2 Modal information of the overall structure 50

4.1 Parameter values 62
4.2 Simulation and NIFO parameters 63

5.1 Identified modal information of the superstructure 73

Chapter 1

Introduction

1.1 Base Isolation System

The base isolation system using laminated rubber bearings is an efficient technology for protecting structures and equipments from seismic damage. After the Northbridge (1994) and Kobe (1995) earthquakes, the importance of mitigating seismic damage is attracting more attention, which made base isolation system come into use more widely. Base isolation systems isolate the superstructure from the ground, shift its natural frequency from the destructive range of ground motion, and enable it to absorb more energy without suffering damage. They have been shown to effectively protect structures from the effects of large earthquakes, but their effectiveness is largely determined by the behavior of the isolators that assimilate a large amount of the input seismic energy and reduces interstory drifts and floor accelerations. If the isolators degrade or fail, the structure will lose its ability to resist earthquakes. Some researchers (Heaton *et al.*, 1995), have raised concerns as to the efficacy of seismic isolation during severe, impulsive earthquakes. Based on the observations from the Northbridge earthquake, base-isolated building are vulnerable to strong impulsive ground motions generated at near-source locations. Therefore, it is imperative to assess the condition of isolators for monitoring the base-isolated structures in order to protect structural or nonstructural components of superstructures.

Laminated rubber bearing has high capacity in compression and can accommodate severe shear deformation. The rubber is laminated and reinforced by steel

plates, which restrain rubber from bulging and increase the compression capacity. The damping is provided by low-damping, natural rubber bearings (NRB), which supply 2-3% of critical damping in the isolation mode. The damping of natural rubber can be improved by adding extrafine carbon blace, oils or resins, and other proprietarty fillers. High damping natural rubber (HDRB) made by this approach may provide up to 20% of the isolation mode damping. Another type is lead rubber bearing (LRB), by installing lead plugs in the laminated rubber bearings to increase energy dissipation through hysteretic damping as the lead plugs shear during large deformation motion. Both types possess high damping and have widely been used in civil and architectural structures (Naeim & Kelly, 1999; Skinner *et al.*, 1993). More information related to seismic isolation system design with rubber bearing can be found in the books written by Kelly (1997), and Naeim & Kelly (1999).

Since the performance of base-isolated systems greatly depends on the mechanical properties of rubber bearings, it is essential to understand the characteristics of bearings. Early experiments were conducted under the unidirectional large shear deformation with constant compression load (Fujita *et al.*, 1989; Mori *et al.*, 2003; Robinson, 1982). Abe *et al.* (2004) studied cyclic behaviors of laminated rubber bearings under multiaxial loading state. Hysteretic phenomenon of rubber bearing was well observed, and many models were proposed to represent the experimental results on this basis (Fujita *et al.*, 1989; Hwang *et al.*, 2002; Kikuchi & Aiken, 1997). For real structures, Tobita (1996) evaluated the dynamic properties of actual buildings by modeling the structure as a linear, time-invariant system in each time segment. The variation of the damping and frequency with the input intensity was observed, and the distinctive amplitude-dependent damping characteristics of based-isolated structures were found. Stewart *et al.* (1999) investigated the responses of four base-isolated buildings. The stiffness and damping of the seismic isolation systems evaluated, the systems were found to respond with a hysteretic action that strongly depended on the vibration amplitude. Because of hysteresis, the stiffness of the isolators decreased significantly with increasing amplitude.

1.2 Hysteresis Model

Hysteresis due to change in the material's regime results from plastic deformation of the structural materials and interface friction at the cracks in the structural elements. This is the mechanism for energy dissipation within the fabric of a structure. The energy is dissipated in materials when microscopic cracks elongate (Jeary, 1996). Although it is impractical and impossible to measure the energy dissipated by the elongation of one crack, as the aggregate effect of friction force between particles and cracks, the hysteresis is relatively straightforward to represent the energy dissipation mechanism.

One distinctive feature of hysteresis is its rate-independence, in other words, the evolution of the hysteretic loop is independent of the deformation-rate, but depends on the history path of the deformation. This phenomenon is consistent with the experimental observation that the energy loss per cycle in many materials does not depend on the deformation frequency over a wide frequency range. The high-damping rubber bearing (HDRB) possesses little rate dependency in the input range from 1 to 0.01 Hz, where the natural periods of base-isolated structures locate (Yoshida *et al.*, 2004). The rate-independent feature is also observed in the friction-type damping devices. Dynamic showed that the hysteresis loops of wire-cable isolators are almost independent of vibration frequency in the test frequency range (Demetriades *et al.*, 1993).

Hysteresis is a highly nonlinear phenomenon with path-dependent evolution. For the purpose of dynamic analysis and simulation, accurate constitutive models are required to represent the hysteretic behavior. Many hysteretic models have been developed, the Bouc-Wen model (Bouc, 1967; Wen, 1976) and Ozdemir's model (Ozdemir, 1976) are two classic examples. In engineering field, the Bouc-Wen model has been widely used to describe nonlinear hysteretic systems including hysteretic isolators. The classic Bouc-Wen, containing five unspecified parameters, can represent a wide variety of characteristics, softening or hardening, smoothly varying or bilinear hysteretic behavior. This model can also be generalized to accommodate the stiffness or strength degradation.

In order to demonstrate how the hysteresis changes the dynamic characteristics of a system, a simple case is considered here. A SDOF hysterestic structure

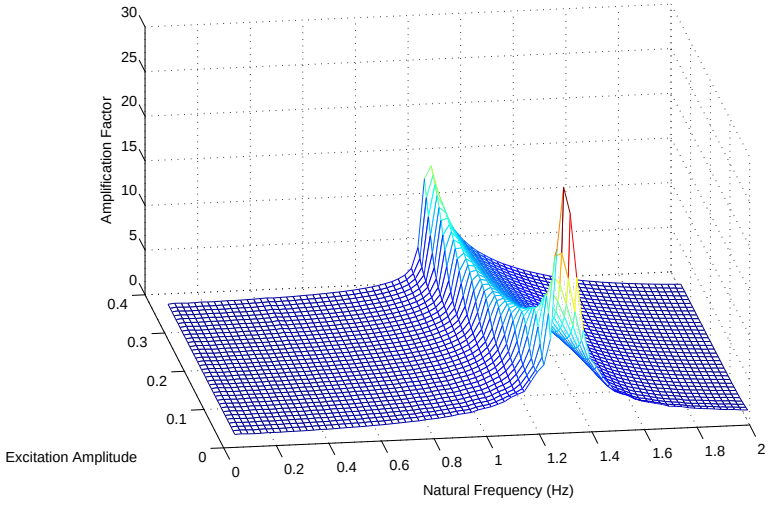

Figure 1.1: Amplification factor

modeled by Bouc-Wen model is subjected to sinusoid ground motion with various amplitudes and frequencies. The amplification factor is examined in Figure 1.1. It is clear that the dynamic response depends on the intensity of the ground motion. The natural frequency varies from 1.33 Hz when the hysteretic damper is within a small vibration range to 1 Hz when the hysteretic damper undergoes extreme plastic deformation. The amplification factor is of saddle shape, decreases dramatically with the increase of the input intensity at the beginning, after reaching its minimum begins to increase. For the case of isolation systems in which the nonlinearity is designed for the energy dissipation to mitigate the structural damage, the change of the natural frequency and the damping ratio is incapable of indicating the health condition of the system.

1.3 Nonlinearity System Identification

Mathematical models of natural and man-made systems play an essential role in today's science and technology. The applications of models range from simulation and prediction to control and diagnosis in heterogeneous fields such as all branches of engineering, economics, medicine, physiology, geophysics, and many others. System identification is the subject of building mathematical models of dynamical

systems or determining the unknown physical parameters based on observed input and output measurements of the systems.

For the purpose of dynamic analysis, most systems in nature are approximated by linear models. System identification of linear dynamic systems has been studied widely and throughly. Many approaches have been proposed to identify the mathematical models, such as, prediction error method (Ljung, 1999), subspace identification method (Van Overschee & de Moor, 1996). In the field of nondestructive evaluation and damage detection for civil structures, Doebling *et al.* (1996) made a comprehensive survey. Structural damage will result in permanent changes in structural stiffness, distribution of stiffness, and relevant material properties. These changes may be detected by monitoring dynamic behavior of the structure. Because of the direct relationship of mass, damping, and stiffness of a multi-degree-of-freedom system to the natural frequencies, mode shapes, and modal damping values, many studies have been directed at using these properties for the purpose of structural health monitoring. The damage detection is accomplished by monitoring these changes in dynamic properties. However, real structures possess nonlinear behavior more or less, due to different sources of nonlinearity. The presence of nonlinearity in a system changes its behavior, and it makes the linear model inaccurate and invalid. Therefore, these properties cannot indicate the status of a nonlinear system because in a nonlinear system they will vary with the intensity of excitation even the system is intact.

Nonlinear system identification deals with nonlinear systems to build mathematical models. Numerous methods have been proposed because of the highly individualistic nature of nonlinear systems since the 1970s. Several survey papers (Adams & Allemang, 1998; Hemez & Doebling, 2001; Kerschen *et al.*, 2006; Worden, 2000) draw a comprehensive picture about nonlinear system identification in structural dynamics. Readers can also refer to the textbooks written by Worden & Tomlinson (2001) and Nelles (2001).

Nonlinear system identification process includes three steps, namely nonlinearity detection, characterization and parameter estimation, as outlined in Figure 1.2. The first step is to detect whether a nonlinearity is present or not. Characterization step follows to determine the location, type and function form of the nonlinearity. Parameter estimation is devoted to establish a mathematic model

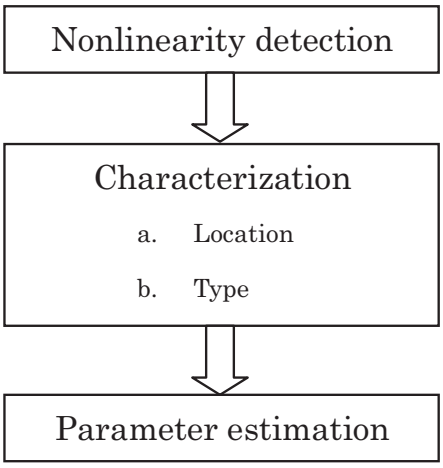

Figure 1.2: Nonlinear system identification process

with a good predictive accuracy. The dissertation focuses on mathematic models of isolation layers of base-isolated buildings, which have strong hysteresis property arose by rubber bearings. Since nonlinearity existence, location and type of isolation layers are known, the only left problem is parameter estimation. Nonlinearity detection and characterization are introduced briefly in this section, while parameter estimation process dealing with hysteretic systems will be summarized in Section 1.4. As to other types of nonlinearities, readers can refer to aforementioned survey papers.

1.3.1 Nonlinearity Detection

The detection of structural nonlinearity is the first step toward establishing a predictive model for nonlinear systems. The primary task of this step is to answer whether there exists structural nonlinearity and what's the level or extent of nonlinearity present in this system. A lot of effort has been spent in developing methods for detecting the presence of nonlinearities in a system. Some of them will be described briefly here. Details can be found in recent overviews summarized by Adams & Allemang (1998), Vanhoenacker *et al.* (2002), and Gloth & Göge (2004).

A system excited by inputs $x_1(t)$ and $x_2(t)$ generates responses $y_1(t)$ and $y_2(t)$, respectively. The principle of superposition is violated if $\alpha y_1(t) + \beta y_2(t)$ is not

the structural response to the input $\alpha x_1(t) + \beta x_2(t)$ for all constants α, β. Then, it is natural to test the superposition principle in order to detect the nonlinearity in a system. However, the time consuming aspect and the fact that no obvious identification process can be linked to this approach are the main drawbacks of this technique. As explained by Worden & Tomlinson (2001), it is of limited practical utility.

Homogeneity test, as a restricted form of the superposition principle (set $\beta = 0$), is one of the most popular detection techniques. Homogeneity is an indicator of a system, which indicates the sensitivity of a system to the magnitude of the input $x(t)$. If the frequency response function (FRF) is invariant for different magnitude levels of the input, the linearity is held. However, this test is not infallible as there are some systems that are nonlinear but nevertheless show homogeneity. The reason is that homogeneity is a weaker condition than superposition.

Nyquist plot, which combines gain and phase characteristics in a single plot, provides another way of inspecting FRFs for nonlinearity detection. If the FRF characteristics in Nyquist plots differ significantly from a circular or near-circular locus in the vicinity of the resonance frequencies, a nonlinearity should be suspected. Moreover, the isochrones, which are the lines connecting points of constant frequency for different excitation levels, should be straight lines for a linear system.

The coherence function can provide a quick visual inspection of the quality of FRFs under random excitation, which is defined as

$$\gamma^2(\omega) = \frac{|S_{yx}(\omega)|^2}{S_{xx}(\omega)S_{yy}(\omega)} = \frac{H_1(\omega)}{H_2(\omega)} \tag{1.1}$$

with

$$H_1(\omega) = \frac{S_{yx}(\omega)}{S_{xx}(\omega)}$$

$$H_2(\omega) = \frac{S_{yy}(\omega)}{S_{yx}(\omega)}$$

where $S_{xx}(\omega)$ and $S_{yy}(\omega)$ are the power spectral density (PSD) of the input and output, respectively. $S_{yx}(\omega)$ is the cross PSD between the input and output. The coherence function should be unity for all frequencies ω if and only if the system is linear. It is a rapid indicator of the presence of nonlinearity. However, the noise

can influence the calculated coherence functions seriously, which can't distinguish between nonlinearities and noise sources.

Higher-order spectra (HOS) is useful to detect the structural nonlinearity, it can also provide some qualitative information about the nonlinearity type. Bispectral analysis techniques are used by Choi *et al.* (1982) to detect nonlinearities of quadratic types. This technique is very sensitive to quadratic nonlinearities, but it is only available for random excitations and inefficient for detecting other nonlinearity types. Collis *et al.* (1998) developed techniques to detect and analyze nonlinearities based on the concepts of higher-order spectra, in particular the bispectrum and trispectrum. The bispectrum can be viewed as a decomposition of the third moment (skewness) of a signal over frequency, and it is very useful for detecting asymmetric nonlinearities. While on the contrary, the trispectrum has advantage in detecting symmetric nonlinearities, as it represents a decomposition of kurtosis over frequency. However, higher-order spectra can detect certain types of nonlinearities but not generic types.

Nichols *et al.* (2006) presented a technique for detecting the presence of nonlinearities in structures based on information-theoretic measures. The time-delayed mutual information and the time-delayed transfer-entropy provide probabilistic measures of the coupling between structural components. These measure can capture both linear and nonlinear relationships among time-series data.

Recently, many new techniques have been developed. Adams & Allemang (2001) introduced a temporal analysis approach using autocorrelation functions in discrete frequency. Autocorrelation functions of residuals from overdetermined frequency response functions are used to detect nonlinearities. Kerschen *et al.* (2003) utilized Bayesian model selection to detect nonlinearities, this technique requires a priori knowledge of an underlying model or class of models to be tested. Trendafilova *et al.* (2000) recast the nonlinearity detection into a classification problem employing a nearest neighbor approach.

1.3.2 Characterization of Nonlinearity

It is crucial to have an accurate characterization of the nonlinear behavior of the structures before parameter estimation. In characterization process, the first

step is to localize nonlinearities. By studying frequency response functions (FRF) at various excitation levels and examining the deformation shapes of the modes which are most corrupted by the nonlinear response, nonlinearities may be assumed where the relative displacements of these mode shapes are the largest. Other procedures have been proposed, for example, procedures based on the restoring force surface (RFS) method (Al-Hadid & Wright, 1989), error localization in a linear model updating framework (Fritzen *et al.*, 1998).

Nonlinearity is caused by many different mechanisms and exhibits various dynamic phenomena. It is useful to characterize the type of nonlinearity. The following questions need to be answered in this step. What causes the nonlinearity? Does it come from stiffness, damping or both? Does the stiffness have hardening or softening characteristics? Is the restoring force symmetric or asymmetric? etc.

The RFS method (Masri & Caughey, 1979) represents the restoring force as a function of the displacement and velocity, visualized the nonlinearity in a three-dimension plot. Another common way is to look at the distortion in measured FRFs of nonlinear systems by using Nyquist plots (Vakakis & Ewins, 1994), Volterra series (Chatterjee & Vyas, 2001), HOFRFs (Schoukens *et al.*, 2000), or frequency-domain ARX models (Adams, 2002).

1.4 Nonlinear Identification of Hysteretic Systems

Methods can be categorized into two classes: nonparametric and parametric identification methods. This classification is certainly not exclusive. Another common way is to categorize methods by the applied form of the signal, e.g. time-domain methods, frequency-domain methods and time-frequency analysis. Time-domain methods conduct the identification process directly based on time series of force, acceleration, etc.

1.4.1 Nonparametric Identification

Nonparametric identification does not require a prior knowledge of system structure, instead searches the best mathematic model in function space represented by a series known functions.

One fruitful nonparametric method is the restoring force surface (RFS) method, originated by Masri & Caughey (1979). RFS methods use polynomial approximation to fit the experimentally determined restoring force, which is considered as a function of displacement and velocity by an ordinary or Chebyshev polynomial series expansion. When hysteretic nonlinearity is involved, the nonlinear restoring force appears as a multivalued function of displacement and velocity due to its path-dependent nature. Therefore, the RFS method is invalid for nonlinear hysteretic systems in displacement-velocity space of force.

In order to reduce the multivaluedness of the force surface in applying the RFS method to hysteretic systems, Crawley & O'Donnell (1987) suggested that the effect of memory can be treated as an augmented state variable dependent on the state time history, and then a new higher-dimensional force state map was created in terms of the independent variables of displacement, velocity, and the augmented state. However, the augmented state could not be estimated from the measured applied force, acceleration, velocity and displacement prior to identification. Instead of using the common state space, Hammond *et al.* (1987) proposed to plot the nonlinear force surface in an appropriately selected space (subset of the state vector, SSV). They defined the restoring force derivative with respect to time as a function of velocity and restoring force. Benedettini *et al.* (1995) studied the performance of polynomial approximation of hysteretic systems in detail. It was shown that the SSV formula could fit the experimental response time histories much better than the traditional RFS formula. Ni *et al.* (1999) represented a new nonparametric identification method for nonlinear hysteretic systems. The hysteretic restoring force is mapped onto two single-valued surfaces in an appropriate subspace in terms of the state variables of displacement and restoring force by the Duhem hysteresis operator. The restoring force surfaces are almost single-valued functions of displacement and restoring force in representing most hysteretic models.

Rice & Fitzpatrick (1988), and Bendat (1990) proposed a reverse path identification method for single-input/single-output nonlinear systems. This method treats the response as the input, and the excitation force as the output. The nonlinear term is considered as a feedback term. It tracks unknown parameters in frequency domain. Rice & Fitzpatrick (1991) extended this method to identify two DOFs nonlinear systems treating each response location as a SDOF mechanical oscillator. However, this approach requires excitations to be applied at every nonlinear location.

Richards & Singh (1998) developed a conditioned reverse path method (CRP). The improved technique separates the nonlinear part of the system response from the linear part and constructs a hierarchy structure of uncorrelated response components in frequency domain. CRP removes the restriction that the excitation must be applied at the location of the nonlinearity in order to identify its unknown parameters. Adams & Allemang (2000) proposed a frequency domain method for estimating parameters of non-linear parametric models by using the spatial information and treating the nonlinear forces as internal feedback forces in the underlying linear system. This method is called Nonlinear Identification through Feedback of the Outputs (NIFO), and it requires measurements of both inputs and outputs and identifies the FRF of the underlying linear system as well as the parameters related to nonlinearities with light computational effort. Unlike CRP methods, NIFO methods estimate the linear and nonlinear coefficients in a single step.

Recently, Marchesiello & Garibaldi (2008a) developed an efficient time domain method called Nonlinear Subspace Identification (NSI) for identifying nonlinear systems by exploiting subspace identification methods. Later, Marchesiello & Garibaldi (2008b) discussed the identification problem for clearance-type nonlinearity by NSI methods. NSI is able to treat many nonlinearities at the same time, several ad hoc functions are defined and adopted in order to identify the clearance-type characteristic, showing advantages with respect to the traditional polynomial approach.

Kerschen *et al.* (2001) applied the CRP and RFS method for experimental identification of wire rope isolators, a nonlinear hysteretic system, and compared these two techniques. Both methods have specified the same functional form of

the nonlinearity. The CRP technique doesn't require numerical integration, and the mass estimation is not necessary. But, particular care is required to chose the type of nonlinearity, which must be known prior to application. A preliminary analysis based on the use of multiple and partial coherence functions between the force vector and any nonlinear vector with attempt form is used to select the approximated function form.

1.4.2 Parametric Identification

The parametric identification method assumes that the mathematical structure of nonlinear systems is known. The procedure then searches the appropriate value in parameter space by the least-squares method or optimization method. Most parametric identification methods have been implemented referring to the Bouc-Wen differential model due to its versatility.

Andronikou *et al.* (1983) first explored the identifiability of hysteretic bilinear systems. The approach was to prove that there are equivalent linear and nonlinear systems which are identifiable. And they concluded that the original hysteretic bilinear system is identifiable as long as the equivalent linear and nonlinear systems are identifiable.

Yar & Hammond (1987) used the Gauss-Newton iterative method to solve the least-squares problem for parameter identification of the Bouc-Wen model. Based on the analysis of the asymptotic properties of the estimates, they discussed the identifiability of the parameters and pointed out that the input level is important to certain parameters.

Ni *et al.* (1998) proposed a frequency domain parametric method to identify the model parameters from the experimental data of periodic vibration tests. The harmonic balance technique leads to a frequency domain least-squares problem, which is solved iteratively by the Levenberg-Marqardt (LM) algorithm. And they implemented this method to model and identify the experimental hysteresis loops of wire-cable vibration isolators.

Zhang *et al.* (2002) developed three identification algorithms, namely the Simplex, extended Kalman filter and generalized reduced gradient method, to estimate the control parameters of a generalized hysteresis model containing 13 pa-

rameters. The Simplex method is a non-gradient global search method, which is not sensitive to initial values and small measurement noise. On the contrary, the extended Kalman filter method is highly sensitive to initial values, which leads to the problem of convergence and bias. The generalized reduced gradient algorithm can easily accommodate various error functions and nonlinear constraints. However, it might yield a local minimum solution of the objective function instead of a global minimum.

Recently, the differential Evolution algorithm (Kyprianou *et al.*, 2001; Ma *et al.*, 2006), and Genetic Algorithm (GA) (Kwok *et al.*, 2007) have been used to estimate parameters of the Bouc-Wen model. Charalampakis & Koumousis (2008) presented a stochastic identification method. It is based on a hybrid evolutionary algorithm, which first locates the promising regions by a GA variant, then find the local optima by a hill-climbing technique, and finally identify the parameters constrained within feasible domain. Tang *et al.* (2006) proposed an online sequential weighted Least Squares Support Vector Machine (LS-SVM) technique to identify the structural parameters and their change due to damage.

Ma *et al.* (2004) investigated the generalized Bouc-Wen differential model and proved that the unspecified parameters of the model are functionally redundant. The parameter A is suggested to be fixed to unity. Furthermore, the parameters α and β, controlling the shape of hysteresis loops, do not have clear physical meaning and affect the entire behavior in an indirect way. A certain constraint $(\alpha + \beta)/A = 1$ is imposed to reduce the redundancy. They also studied the local and global sensitivity of parameters. The global sensitivity analysis exploited a probabilistic method, which can account for the mutual interactions of parameters. It is found that some parameter of the generalized Bouc-Wen model are rather insensitive, but none of the unspecified parameters in the classical Bouc-Wen model are insensitive. The study by Ma *et al.* (2004) provides the theoretical basis for the multi-stage estimate approach (Loh & Chung, 1993; Roberts & Sadeghi, 1990) proposed previously. One or two parameters are fixed to the assumed valued and the remaining parameters are identified (Roberts & Sadeghi, 1990). The second stage takes the final estimate of the first stage as the initial guess and identifies all the model parameters. The multi-stage scheme can improve the identification accuracy as well as convergence.

1.5 Organization of the Thesis

Chapter 1 is an introduction to the thesis. It starts with the introduction of the base isolation system, the research focus of the thesis, and stresses the hysteretic behavior of the rubber bearings, which is the primary obstacle standing in way. Then the procedure of nonlinear system identification is explained, including the nonlinearity detection, nonlinearity characterization and parameter estimation. The nonlinear identification methods for hysteretic systems are summarized in two categories, the nonparametric and parametric methods.

In Chapter 2, a new method for estimating the restoring force estimation of the isolation layer in a base-isolated system is proposed. The whole base-isolated structure is separated into two substructures, the linear superstructure and the nonlinear isolation layer. The hybrid motion equation involving the modal coordinates of the superstructure and the physical coordinates of the isolation layer is derived by component mode synthesis. The estimation procedure is elaborated by a numerical simulation.

Chapter 3 investigates the identifiability condition for substructural identification in the framework of closed-loop systems by spectral analysis and parametric methods. Substructures governed by linear and nonlinear feedback laws are both considered.

In Chapter 4, the performance of reverse path methods applied to identify the underlying linear model of base-isolated structures is investigated. The nonlinear rubber bearings are considered as nonlinear components attached to an underlying linear model. The nonlinearity function of the hysteretic force is discussed. The reverse path formulation is solved by Nonlinear Identification through Feedback of Output (NIFO) methods using least-square solution. Numerical simulation is carried out to investigate the identification performance.

In Chapter 5, the proposed restoring force estimation method is applied to identify two real base-isolated structures. The restoring force of the isolation layer is estimated reasonably. The amplitude-dependent equivalent stiffness and damping coefficient are adopted to describe the nonlinearity of the isolation layer.

Chapter 6 draws conclusions regarding to the performance of the proposed methods and the identifiability condition of substructural identification.

Chapter 2

Estimating Restoring Force by Component Synthesis Method

2.1 Introduction

A base-isolated system consists of two very different subsystems: the superstructure and the isolation layer. The isolation layer of a base-isolated structure is composed of rubber bearing isolators that typically have damping ratios up to 20%, while the superstructure is just an ordinary building with a very low damping ratio of its first mode. The conventional damage indices such as the modal frequencies and mode shapes are insensitive to local damage and thus cannot be used to quantify damage accurately. In addition, the nonlinearity of the system makes these indices invalid for damage detection. A direct and local identification method is therefore better than one using the conventional indices. This chapter presents a new algorithm for estimating the restoring force of the isolation layer by component mode synthesis. And the amplitude-dependent stiffness and damping coefficient, which are regressed from the restoring force of the isolation layer, are utilized to represent the nonlinear state of the isolation layer.

2.2 Estimating Restoring Force by Component Mode Synthesis

Component mode synthesis (CMS) is a technique used to perform the dynamic analysis of structures by means of substructuring, or decomposing the overall structure into several substructures whose boundary conditions are compatible in a specified way. This technique is quite useful for the dynamic analysis of complex structures in structural engineering, especially when the substructures have dynamic characteristics so different that the coupled structure has nonclassical vibration modes. The CMS methods presented by Hurty (1960) can be classified into four groups: fixed-interface methods, free-interface methods, hybrid-interface methods, and loaded-interface methods. These groups differ from each other mainly in the choice of the supplementary Ritz vectors, the associated generalized coordinates, and the coupling procedure. CMS methods have been reviewed by Craig (1985) and others.

Many attempts have been made to identify the element-level or substructure-level physical parameters by using CMS methods. Llorca *et al.* (1994) identified the joint stiffness parameters by using a free-interface CMS method. While, Hwang (1998) used a fixed-interface CMS method to identify the stiffness and damping coefficient parameters of connections by averaging the frequency response function in frequency domain. Yun & Bahng (2000) presented a method for estimating the element-level stiffness parameters by using a back-propagation neural network, and CMS methods are adopted for efficient generation of the patterns for training the neural network. Zhang *et al.* (2007) adopted a support vector regression method for structural identification via component mode synthesis.

In this thesis, the state of the isolation layer is our concern and the number of the accelerometers mounted is limited. A fixed-interface CMS method is used to derive the hybrid motion equation involving the modal parameters of the superstructure as well as the physical parameters of the isolation layer. This paves the way for estimating the restoring force of the isolation layer.

The base-isolated structure shown in Figure 2.1 consists of two substructures: a superstructure and a base isolation layer. The superstructure is considered

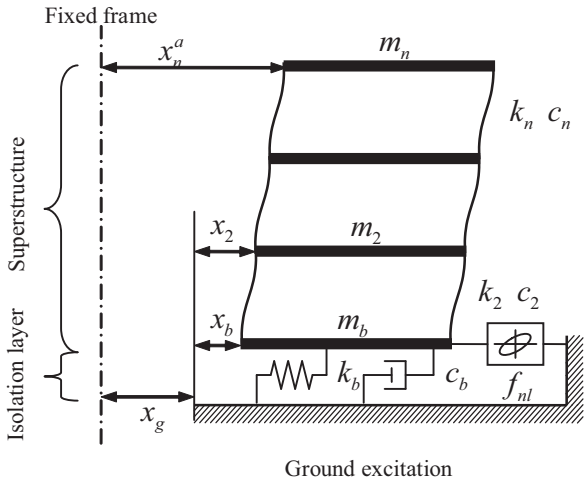

Figure 2.1: Structure model

to be a linear system, and the base isolation layer has both linear and nonlinear components. The linear one has a stiffness k_b and damping coefficient c_b, and nonlinear one has a restoring force of f_{nl}. There are many choices for the nonlinear model, but in the present case a hysteretic model is used because the rubber bearings of the isolation layer possess strong hysteresis. The model will be described in detail in numerical simulation.

The dynamic equation of the overall structure is written as

$$\mathbf{M}\ddot{\mathbf{x}} + \mathbf{C}\dot{\mathbf{x}} + \mathbf{K}\mathbf{x} + \begin{bmatrix} \mathbf{0} \\ f_{nl} \end{bmatrix} = -\mathbf{M}\mathbf{r}\ddot{x}_g \tag{2.1}$$

where $\mathbf{M}$, $\mathbf{K}$ and $\mathbf{C}$ are mass, stiffness and damping matrices, respectively. $\mathbf{r}$ is a $n \times 1$ unit vector ($\mathbf{r} = [1 \quad \dots \quad 1]^T$). $\mathbf{x}$ is the displacement relative to the ground; and $\ddot{x}_g$ is the ground acceleration.

$$\mathbf{x} = [x_n \quad x_{n-1} \quad \dots \quad x_2 \quad x_b]^T = [\mathbf{x}_s^T \quad x_b]^T$$

$$\mathbf{F}_{nl} = \begin{bmatrix} \mathbf{0} \\ f_{nl} \end{bmatrix}$$

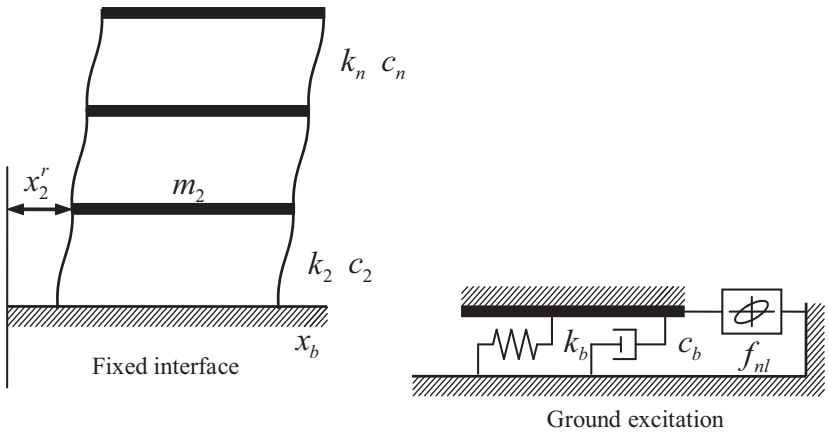

Figure 2.2: CMS: fixed-interface method

$$\mathbf{M} = \begin{bmatrix} m_n & & & 0 \\ & \ddots & & \\ & & m_2 & \\ 0 & & & m_b \end{bmatrix} = \begin{bmatrix} \mathbf{M}_s & \mathbf{0} \\ \mathbf{0} & m_b \end{bmatrix}$$

$$\mathbf{Mr} = [\, m_n \quad \cdots \quad m_2 \quad m_b \,]^T = [\, \mathbf{r}_s^T \mathbf{M}_s \quad m_b \,]^T$$

$$\mathbf{K} = \begin{bmatrix} k_n & -k_n & & & 0 \\ -k_n & k_n + k_{n+1} & -k_{n+1} & & \\ & & \vdots & & \\ & & -k_3 & k_3 + k_2 & -k_2 \\ 0 & & & -k_2 & k_2 + k_b \end{bmatrix} = \begin{bmatrix} \mathbf{K}_s & \mathbf{K}_{sb} \\ \mathbf{K}_{bs} & k_2 + k_b \end{bmatrix}$$

$$\mathbf{C} = \begin{bmatrix} c_n & -c_n & & & 0 \\ -c_n & c_n + c_{n+1} & -c_{n+1} & & \\ & & \vdots & & \\ & & -c_3 & c_3 + c_2 & -c_2 \\ 0 & & & -c_2 & c_2 + c_b \end{bmatrix} = \begin{bmatrix} \mathbf{C}_s & \mathbf{C}_{sb} \\ \mathbf{C}_{bs} & c_2 + c_b \end{bmatrix}$$

Moving the nonlinear term to the right-hand side, we obtain

$$\mathbf{M}\ddot{\mathbf{x}} + \mathbf{C}\dot{\mathbf{x}} + \mathbf{K}\mathbf{x} = -\mathbf{M}\mathbf{r}\ddot{x}_g - \mathbf{F}_{nl} \tag{2.2}$$

The whole structure is separated into two substructures that have a common interface as shown in Figure 2.2. A fixed boundary condition is imposed on this interface, making it unable to deform and move. These two substructures can therefore be treated as independent structures and can generate their own modal

information. Our focus in this thesis is not on how to retrieve the overall modal information by integrating substructures. Instead, we are trying to transform the traditional dynamic equations either in physical coordinates or modal coordinates into a hybrid form by CMS. The hybrid dynamic equations describe both the linear modal information of the superstructure and the nonlinear physical model of the isolation layer.

The equilibrium equation of the superstructure is

$$\mathbf{M}_s\ddot{\mathbf{x}}_s^r + \mathbf{C}_s\dot{\mathbf{x}}_s^r + \mathbf{K}_s\mathbf{x}_s^r = -\mathbf{M}_s\mathbf{r}_s\ddot{x}_b^a \tag{2.3}$$

where

$$x_b^a = x_g + x_b$$

and

$$\mathbf{x}_s^r = \mathbf{x}_s - x_b\mathbf{r}_s$$

with $\mathbf{r}_s$ a $(n-1)\times 1$ unit vector ($\mathbf{r}_s = [\,1 \quad \dots \quad 1\,]^T$)

The superscript r indicates coordinates relative to the fixed interface, while the superscript a indicates absolute coordinates. The subscripts s and b respectively denote the superstructure and the isolation layer. We assume the damping matrix of the superstructure is proportional to the stiffness matrix. That is, $\mathbf{C}_s = \alpha\mathbf{K}_s$. The modal damping ratios implied by the stiffness-proportional damping are proportional to the modal frequencies. Therefore, the response of higher modes will die away sooner. This is consistent with the experience that the lower modal responses are dominant in civil engineering.

Rewrite the equation of superstructure in modal coordinates, we have

$$\mathbf{\Phi}_s^T\mathbf{M}_s\mathbf{\Phi}_s\ddot{\xi}_s + \mathbf{\Phi}_s^T\mathbf{C}_s\mathbf{\Phi}_s\dot{\xi}_s + \mathbf{\Phi}_s^T\mathbf{K}_s\mathbf{\Phi}_s\xi_s = -\mathbf{\Phi}_s^T\mathbf{M}_s\mathbf{r}_s\ddot{x}_b^a \tag{2.4}$$

where $\mathbf{\Phi}_s$ is the fixed-interface mode shape matrix of the superstructure and ξ_s is the modal coordinates. $\mathbf{x}_s^r$ is related to the modal coordinates as follows: $\mathbf{x}_s^r = \mathbf{\Phi}_s\xi_s$.

If $\mathbf{\Phi}_s$ is normalized in such a way that

$$\mathbf{M}_s^* = \mathbf{\Phi}_s^T\mathbf{M}_s\mathbf{\Phi}_s = \mathbf{I}$$

We have the relations

$$\mathbf{K}_s^* = \mathbf{\Phi}_s^T \mathbf{K}_s \mathbf{\Phi}_s = \mathbf{\Omega}^2$$

and

$$\mathbf{C}_s^* = \mathbf{\Phi}_s^T \mathbf{C}_s \mathbf{\Phi}_s = \alpha \mathbf{\Omega}^2$$

where $\mathbf{\Omega}$ is the undamped frequency matrix of the superstructure, ω_i is the i^{th} undamped frequency.

$$\mathbf{\Omega} = \begin{bmatrix} \omega_1 & & & \mathbf{0} \\ & \ddots & & \\ & & \omega_{n-2} & \\ \mathbf{0} & & & \omega_{n-1} \end{bmatrix}$$

Therefore, Eq. (2.4) can be expressed by

$$\mathbf{M}_s^* \ddot{\xi}_s + \mathbf{C}_s^* \dot{\xi}_s + \mathbf{K}_s^* \xi_s = -\mathbf{\Phi}_s^T \mathbf{M}_s \mathbf{r}_s \ddot{x}_b^a \tag{2.5}$$

The physical displacements of the superstructure in local coordinates are expressed as a linear combination of its substructure modes. After some algebraic transformations, the displacements of superstructure in general coordinates can be represented by a set of Ritz vectors:

$$\mathbf{x}_s = \mathbf{Q} \begin{bmatrix} \xi_s \\ x_b \end{bmatrix} \tag{2.6}$$

where x_b is the displacement of the isolation layer representing the interface displacement. The boundary condition of its fixed interface determines the Ritz vectors (Craig & Bampton, 1968) as

$$\mathbf{Q} = [\, \mathbf{\Phi}_s \quad \mathbf{\Psi}_s \,] \tag{2.7}$$

where $\mathbf{\Psi}_s$ is the constraint mode associated with the fixed interface. It is the superstructure deformation obtained by imposing one unit displacement on the fixed interface. In this case the superstructure is constrained only by the base layer. So $\mathbf{\Psi}_s = [\, 1 \quad \dots \quad 1 \,]^T$.

The overall physical coordinates can be transformed to the hybrid coordinate which contains the modal coordinates of the superstructure ξ_s and the physical coordinate of the base isolator $\ddot{x}_b$.

$$\mathbf{x}_s = \mathbf{\Phi}_s \xi_s + \mathbf{\Psi}_s x_b \tag{2.8}$$

$$\mathbf{x} = \begin{bmatrix} \mathbf{x}_s \\ x_b \end{bmatrix} = \begin{bmatrix} \mathbf{\Phi}_s & \mathbf{\Psi}_s \\ \mathbf{0} & 1 \end{bmatrix} \begin{bmatrix} \xi_s \\ x_b \end{bmatrix} = \mathbf{\Phi}\xi \tag{2.9}$$

Substituting this into the motion equation of the overall structure and multiplying both sides by $\mathbf{\Phi}^T$, we get from Eq. (2.2)

$$\mathbf{\Phi}^T\mathbf{M}\mathbf{\Phi}\ddot{\xi} + \mathbf{\Phi}^T\mathbf{C}\mathbf{\Phi}\dot{\xi} + \mathbf{\Phi}^T\mathbf{K}\mathbf{\Phi}\xi = -\mathbf{\Phi}^T\mathbf{M}\mathbf{r}\ddot{x}_g - \mathbf{\Phi}^T\mathbf{F}_{nl} \tag{2.10}$$

which we can simplify as follows

$$\mathbf{M}^*\ddot{\xi} + \mathbf{C}^*\dot{\xi} + \mathbf{K}^*\xi = -\mathbf{\Phi}^T\mathbf{M}\mathbf{r}\ddot{x}_g - \mathbf{\Phi}^T\mathbf{F}_{nl} \tag{2.11}$$

where

$$\mathbf{\Phi}^T\mathbf{F}_{nl} = \begin{bmatrix} \mathbf{\Phi}_s^T & \mathbf{0} \\ \mathbf{\Psi}_s^T & 1 \end{bmatrix} \begin{bmatrix} \mathbf{0} \\ f_{nl} \end{bmatrix} = \begin{bmatrix} \mathbf{0} \\ f_{nl} \end{bmatrix} = \mathbf{F}_{nl}$$

$$\mathbf{M}^* = \mathbf{\Phi}^T\mathbf{M}\mathbf{\Phi} = \begin{bmatrix} \mathbf{\Phi}_s^T & \mathbf{0} \\ \mathbf{\Psi}_s^T & 1 \end{bmatrix} \begin{bmatrix} \mathbf{M}_s & \mathbf{0} \\ \mathbf{0} & m_b \end{bmatrix} \begin{bmatrix} \mathbf{\Phi}_s & \mathbf{\Psi}_s \\ \mathbf{0} & 1 \end{bmatrix}$$
$$= \begin{bmatrix} \mathbf{I} & \mathbf{\Phi}_s^T\mathbf{M}_s\mathbf{r}_s \\ \mathbf{r}_s^T\mathbf{M}_s\mathbf{\Phi}_s & tr(\mathbf{M}) \end{bmatrix}$$

$$\mathbf{K}^* = \mathbf{\Phi}^T\mathbf{K}\mathbf{\Phi} = \begin{bmatrix} \mathbf{\Phi}_s^T & \mathbf{0} \\ \mathbf{\Psi}_s^T & 1 \end{bmatrix} \begin{bmatrix} \mathbf{K}_s & \mathbf{K}_{sb} \\ \mathbf{K}_{bs} & k_2 + k_b \end{bmatrix} \begin{bmatrix} \mathbf{\Phi}_s & \mathbf{\Psi}_s \\ \mathbf{0} & 1 \end{bmatrix}$$
$$= \begin{bmatrix} \mathbf{\Phi}_s^T\mathbf{K}_s\mathbf{\Phi}_s & \mathbf{0} \\ \mathbf{0} & k_b \end{bmatrix} = \begin{bmatrix} \mathbf{\Omega}^2 & \mathbf{0} \\ \mathbf{0} & k_b \end{bmatrix}$$

$$\mathbf{C}^* = \mathbf{\Phi}^T\mathbf{C}\mathbf{\Phi} = \begin{bmatrix} \mathbf{\Phi}_s^T & \mathbf{0} \\ \mathbf{\Psi}_s^T & 1 \end{bmatrix} \begin{bmatrix} \mathbf{C}_s & \mathbf{C}_{sb} \\ \mathbf{C}_{bs} & c_2 + c_b \end{bmatrix} \begin{bmatrix} \mathbf{\Phi}_s & \mathbf{\Psi}_s \\ \mathbf{0} & 1 \end{bmatrix}$$
$$= \begin{bmatrix} \mathbf{\Phi}_s^T\mathbf{C}_s\mathbf{\Phi}_s & \mathbf{0} \\ \mathbf{0} & c_b \end{bmatrix} = \begin{bmatrix} \alpha\mathbf{\Omega}^2 & \mathbf{0} \\ \mathbf{0} & c_b \end{bmatrix}$$

$$\mathbf{K}_{bs} = \begin{bmatrix} 0 & \cdots & 0 & -k_2 \end{bmatrix} = \mathbf{K}_{sb}^T$$

$$\mathbf{C}_{bs} = \begin{bmatrix} 0 & \cdots & 0 & -c_2 \end{bmatrix} = \mathbf{C}_{sb}^T$$

and

$$\mathbf{\Psi}_s^T\mathbf{K}_s + \mathbf{K}_{bs} = 0$$

The final form of the motion equation in the hybrid coordinates is

$$\begin{bmatrix} \mathbf{I} & \boldsymbol{\Phi}_s^T \mathbf{M}_s \mathbf{r}_s \\ \mathbf{r}_s^T \mathbf{M}_s \boldsymbol{\Phi}_s & tr(\mathbf{M}) \end{bmatrix} \ddot{\xi} + \begin{bmatrix} \alpha \boldsymbol{\Omega}^2 & \mathbf{0} \\ \mathbf{0} & c_b \end{bmatrix} \dot{\xi} + \begin{bmatrix} \boldsymbol{\Omega}^2 & \mathbf{0} \\ \mathbf{0} & k_b \end{bmatrix} \xi = -\boldsymbol{\Phi}^T \mathbf{M} \mathbf{r} \ddot{x}_g - \mathbf{F}_{nl} \tag{2.12}$$

The new coordinate system could reduce the number of physical parameters significantly. Another advantage of this form is that the complete modal information of the superstructure is not required. The participation factors of higher modes are relatively low for base-isolated buildings. We assume here that only the first l orders of the superstructure mode shapes are known.

When we consider only first l modes as expressed in the form

$$\mathbf{x}_s = \bar{\boldsymbol{\Phi}}_s \bar{\xi}_s + \boldsymbol{\Psi}_s x_b$$

$$\mathbf{x} = \begin{bmatrix} \mathbf{x}_s \\ x_b \end{bmatrix} = \begin{bmatrix} \bar{\boldsymbol{\Phi}}_s & \boldsymbol{\Psi}_s \\ \mathbf{0} & \mathbf{I} \end{bmatrix} \begin{bmatrix} \bar{\xi}_s \\ x_b \end{bmatrix} = \bar{\boldsymbol{\Phi}} \bar{\xi}$$

where $\bar{\xi}_s$ is the first l modal coordinates, and $\bar{\xi}_s$ is the first l columns of $\boldsymbol{\Phi}_s$, in other words, the first l orders of mode shapes.

Following the same procedure, we obtain

$$\begin{bmatrix} \mathbf{I} & \bar{\boldsymbol{\Phi}}_s^T \mathbf{M}_s \mathbf{r}_s \\ \mathbf{r}_s^T \mathbf{M}_s \bar{\boldsymbol{\Phi}}_s & tr(\mathbf{M}) \end{bmatrix} \ddot{\bar{\xi}} + \begin{bmatrix} \alpha \bar{\boldsymbol{\Omega}}^2 & \mathbf{0} \\ \mathbf{0} & c_b \end{bmatrix} \dot{\bar{\xi}} + \begin{bmatrix} \bar{\boldsymbol{\Omega}}^2 & \mathbf{0} \\ \mathbf{0} & k_b \end{bmatrix} \bar{\xi} = -\bar{\boldsymbol{\Phi}}^T \mathbf{M} \mathbf{r} \ddot{x}_g - \bar{\boldsymbol{\Phi}}^T \mathbf{F}_{nl} \tag{2.13}$$

Substitute ξ, $\boldsymbol{\Phi}_s$, $\mathbf{Mr}$ and $\mathbf{F}_{nl}$ by matrix forms in Eq. (2.12)

$$\begin{bmatrix} \mathbf{I} & \boldsymbol{\Phi}_s^T \mathbf{M}_s \mathbf{r}_s \\ \mathbf{r}_s^T \mathbf{M}_s \boldsymbol{\Phi}_s & tr(\mathbf{M}) \end{bmatrix} \begin{bmatrix} \ddot{\xi}_s \\ \ddot{x}_b \end{bmatrix} + \begin{bmatrix} \alpha \boldsymbol{\Omega}^2 & \mathbf{0} \\ \mathbf{0} & c_b \end{bmatrix} \begin{bmatrix} \dot{\xi}_s \\ \dot{x}_b \end{bmatrix} + \begin{bmatrix} \boldsymbol{\Omega}^2 & \mathbf{0} \\ \mathbf{0} & k_b \end{bmatrix} \begin{bmatrix} \xi_s \\ x_b \end{bmatrix}$$
$$= -\begin{bmatrix} \boldsymbol{\Phi}_s^T & \mathbf{0} \\ \boldsymbol{\Psi}_s^T & 1 \end{bmatrix} \begin{bmatrix} \mathbf{M}_s \mathbf{r}_s \\ m_b \end{bmatrix} \ddot{x}_g - \begin{bmatrix} \mathbf{0} \\ f_{nl} \end{bmatrix} \tag{2.14}$$

Extract the second row related to the base isolation, we can obtain the following SDOF equation of motion for the isolation layer.

$$m_b \ddot{x}_b + c_b \dot{x}_b + k_b x_b = -tr(\mathbf{M}_s)(\ddot{x}_b + \ddot{x}_g) - m_b \ddot{x}_g - \mathbf{r}_s^T \mathbf{M}_s \boldsymbol{\Phi}_s \ddot{\xi}_s - f_{nl} \tag{2.15}$$

Therefore, the identification of the isolation layer has become as simple as possible. The restoring force of isolation layer can be expressed as follows

$$F = c_b \dot{x}_b + k_b x_b + f_{nl} = -tr(\mathbf{M})(\ddot{x}_b + \ddot{x}_g) - \mathbf{r}_s^T \mathbf{M}_s \boldsymbol{\Phi}_s \ddot{\xi}_s \tag{2.16}$$

The restoring force consists of two parts. The first term represents the rigid inertial force of the superstructure, and the second term is the inertial force in modal coordinates.

2.3 Mode Shape Expansion

For economy, accelerometers are usually not installed on every floor. Therefore the measured mode shapes consist of a limited number of degrees of freedom (DOF), typically smaller than the number of DOF in the analytic model. The full length vector of mode shapes is, however, indispensable in the calculation of the equivalent external force acting on the isolation layer. It is necessary to expand the measured mode shapes for matching the other unmeasured DOFs. Guyan static expansion proposed by Guyan (1965) is suggested in this thesis because of its simplicity.

The Guyan static expansion method is based on the assumption that inertial forces acting on the unmeasured DOFs are negligible with respect to the elastic forces. This assumption is implemented by setting $\mathbf{M} = \mathbf{0}$ in the following modal force equilibrium equation

$$\left(\begin{bmatrix} \mathbf{K}_{aa} & \mathbf{K}_{ao} \\ \mathbf{K}_{oa} & \mathbf{K}_{oo} \end{bmatrix} - \omega_i^2 \begin{bmatrix} \mathbf{M}_{aa} & \mathbf{M}_{ao} \\ \mathbf{M}_{oa} & \mathbf{M}_{oo} \end{bmatrix} \right) \begin{bmatrix} \varphi_{ai} \\ \varphi_{ao} \end{bmatrix} = \mathbf{0} \tag{2.17}$$

The subscripts a and o respectively represent the locations of the measured and unmeasured DOFs. This equation leads to an exact analytical relationship between the mode shapes at the measured and unmeasured DOFs

$$\varphi_{ao} = -\mathbf{K}_{oo}^{-1}\mathbf{K}_{oa}\varphi_{ai} \tag{2.18}$$

Usually there is no preknowledge about the stiffness distribution of the superstructure, so we have to use an alternative way to describe it. We assume that the stiffness distribution of a building is proportional to its mass distribution. This assumption is roughly reasonable for buildings with conventional shapes.

2.4 Identification Procedure

The procedure of the proposed method is illustrated in Figure 2.3. After the identification process for the superstructure, the number of the unknown parameters to be identified could be reduced greatly as shown in Eq. (2.15). Only partial modal information is required for the estimation of the restoring force, which makes this method workable when the number of sensors is limited. It is easy to incorporate the nonlinearity in the isolation layer by selecting nonlinear models for the restoring force.

$$F = c_b\dot{x}_b + k_b x_b + f_{nl} = -tr(\mathbf{M})(\ddot{x}_b + \ddot{x}_g) - \mathbf{r}_s^T\mathbf{M}_s\mathbf{\Phi}_s\ddot{\xi}_s$$

What we want to identify is the total restoring force on the left-hand side of this equation. To do this we first need to specify the mass distribution $\mathbf{M}_s\mathbf{r}_s$, the mode shape matrix $\mathbf{\Phi}_s$, and the acceleration in modal coordinates $\ddot{\xi}_s$ on the right-hand side. Given that the acceleration response on floors is observable, the ground excitation and the acceleration response in the isolation layer and on several other floors are known. It is not difficult to retrieve the mode shape information by using subspace identification methods. Only partial modal information is required for the estimation of the restoring force, but the mode shapes need to be expanded at unmeasured DOFs. Then the acceleration in modal coordinates $\ddot{\xi}_s$ can be obtained by the transformation from the physical coordinates. The mass distribution $\mathbf{M}_s\mathbf{r}_s$ is treated by taking the design value of real buildings, since the mass of buildings hardly changes unless significant rebuilding or retrofitting takes place.

2.5 Numerical Simulation

A multistory structure supported by a base isolation layer is considered here. We refer to the part of the structure above the base as the superstructure, and we make the following assumptions:

1. The superstructure is of the shear type, its stiffness and mass may vary from floor to floor, it remains within elastic range even during an earthquake, and its only nonlinearity is associated with the base isolation system.

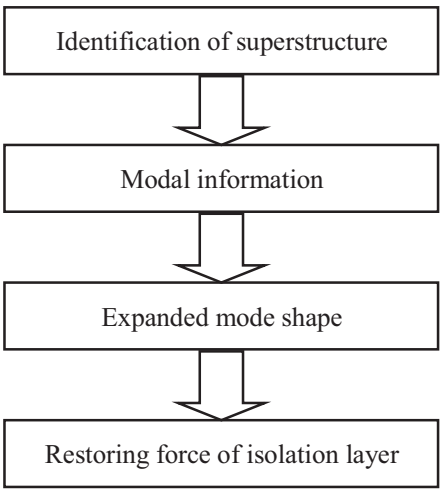

Figure 2.3: Procedure of the proposed method

2. The base isolation layer consists of an elastic spring, a hysteretic damper, and a viscous damper.

According to the experimental observation, Yoshida *et al.* (2004) concluded that the elastomeric bearings and friction-type isolators exhibit little rate dependence and quite stable hysteresis loops, a smooth and differential hysteresis model is adopted for the hysteretic dampers in the dynamic simulation. A widely accepted one is the Bouc-Wen hysteresis model proposed by Bouc (1967) and generalized by Wen (1976). Baber & Noori (1986) and other researchers incorporate the deterioration of hysteretic characteristics. Although it is not in total accordance with the plasticity theory and sometimes it predicts negative dissipated energy, as pointed out by Carli (1999), it has been widely used in seismic engineering.

The differential equation of the Bouc-Wen model is

$$D_y \dot{z} = A\dot{u} - (\gamma \mathrm{sgn}(z\dot{u}) + \beta) \left|z\right|^p \dot{u} \tag{2.19}$$

and the hysteretic force of the isolation layer is given by

$$f_{nl} = F_y z$$

The terms D_y and F_y are respectively the yield displacement and force of the hysteretic damper; z is a dimensionless parameter; A, β and γ are parameters

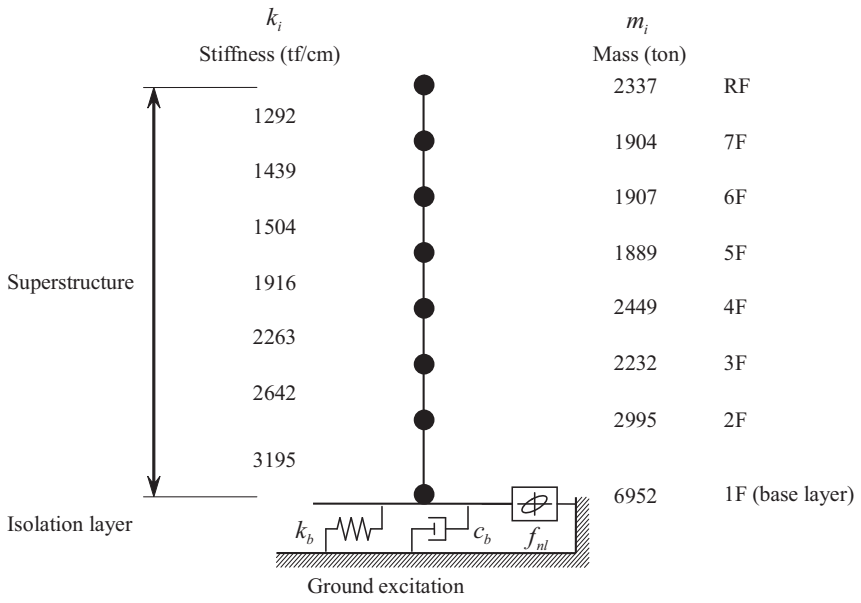

Figure 2.4: Simulation model of 7-story base-isolated building

that describe the shape of the hysteresis loop; and u and $\dot{u}$ are respectively the displacement and velocity of the isolation layer. The smoothness of transition from elasticity to plasticity is determined by p, and when $p \to \infty$ the hysteresis model is reduced to a bilinear case.

A 7-story base-isolated building is considered and the mass and stiffness matrices of the superstructure are defined in Figure 2.4. The damping matrix is assumed to be proportional to the stiffness matrix and the first order of the damping ratio is 1%. The modal information of the superstructure is listed in Table 2.1. The accelerometers are installed in the basement, on the 1^{st} floor, on the 4^{th} floor, and on the roof. The parameters related to the isolation layer are listed in Table 2.2. The restoring force of the isolation layer is given by

$$F = k_b x_b + c_b \dot{x}_b + f_{nl} \tag{2.20}$$

The earthquake that happened 23^{rd} July 2005 in Chiba Prefecture, Japan, is selected as the ground input. The ground acceleration was observed at Hiyoshi Campus of Keio University and recorded by the Raiosha monitoring system (Yoshimoto *et al.*, 2003). The maximum acceleration in this record is 70.13 cm/s^2 and the sampling rate is 100 Hz (Figure 5.5).

Table 2.1: Modal information of superstructure

	Frequency (Hz)	Damping ratio (%)
1^{st}	1.09	1.00
2^{nd}	2.82	2.59
3^{rd}	4.61	4.22
4^{th}	6.06	5.55
5^{th}	7.36	6.74

Table 2.2: Parameter values

Argument	Value
k_b	475000 kN/m
c_b	6000 kN·s/m
A	1
β	0.6
γ	0.4
p	1
D_y	1.5 mm
F_y	655.4 kN

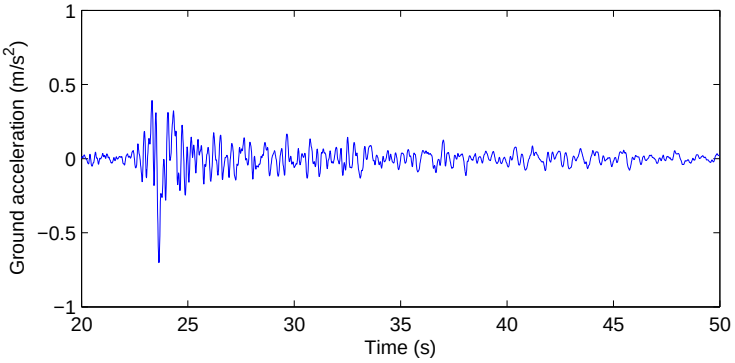

Figure 2.5: Ground acceleration observed at Hiyoshi

Table 2.3: Identified mode shapes of superstructure

	1% noise		10% noise	
	Roof	4$^{\text{th}}$ floor	Roof	4$^{\text{th}}$ floor
1$^{\text{st}}$	1	0.4419	1	0.4385
2$^{\text{nd}}$	1	-1.0053	1	-1.0281

The simulation was conducted using Simulink MATLAB®. The acceleration response of the superstructure is illustrated in Figure 2.6 and the restoring force is plotted against displacement in Figure 2.7.

Two cases are under consideration: one with the acceleration response contaminated by 1% white noise and the other with the acceleration response contaminated by 10% white noise. Taking the acceleration on the 1$^{\text{st}}$ floor as the ground input to the superstructure and the accelerations on the 4$^{\text{th}}$ floor and the roof as the responses, the mode shapes of the superstructure were identified by the subspace identification method (N4SID: refer to Appendix A) using the toolbox in Matlab. After the first two mode shapes at measured DOFs were extracted (Table 2.3), they were expanded to the unmeasured DOFs by using Eq. (2.18) as shown in Figure 2.8 and 2.9. In this calculation, the stiffness distribution was assumed to be proportional to the mass distribution.

The acceleration in modal coordinates $\ddot{\xi}_s$ is corresponding to the physical acceleration obtained by coordinate transformation

$$\ddot{\xi}_s = \mathbf{\Phi}_s^{\dagger} \ddot{\mathbf{x}}_s^r \tag{2.21}$$

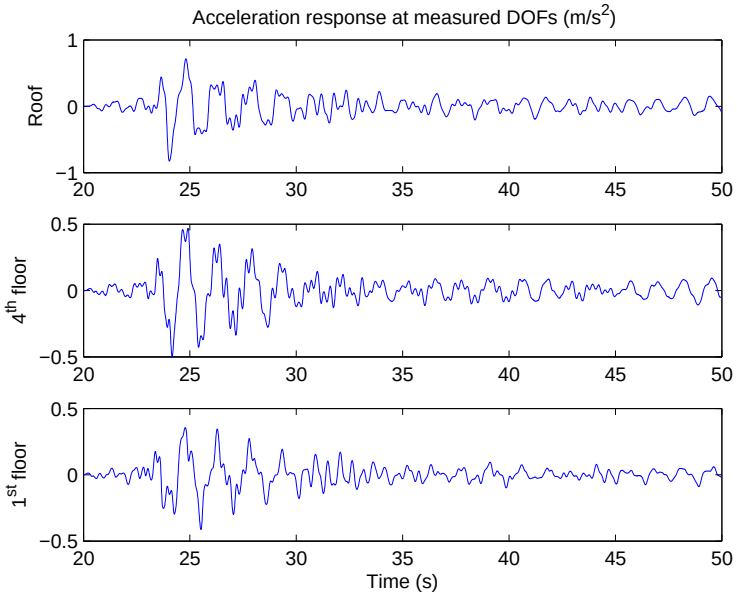

Figure 2.6: Acceleration responses of the superstructure

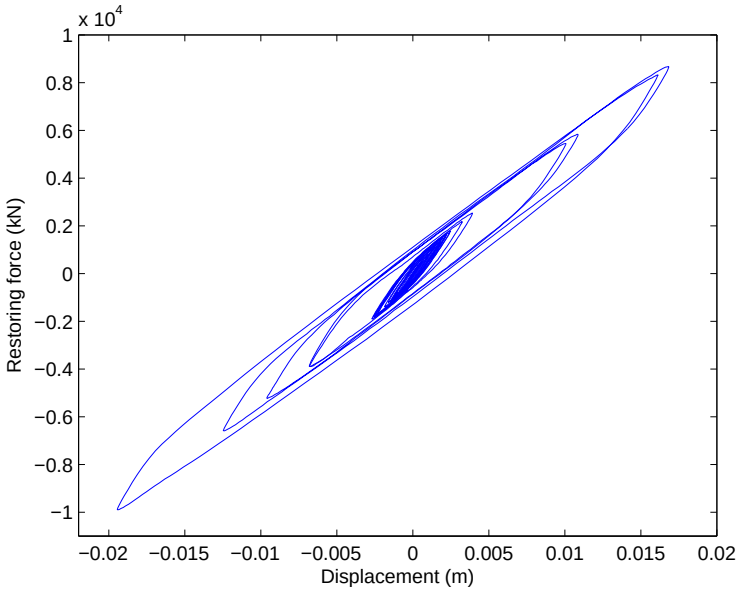

Figure 2.7: Restoring force of the isolation layer vs. displacement

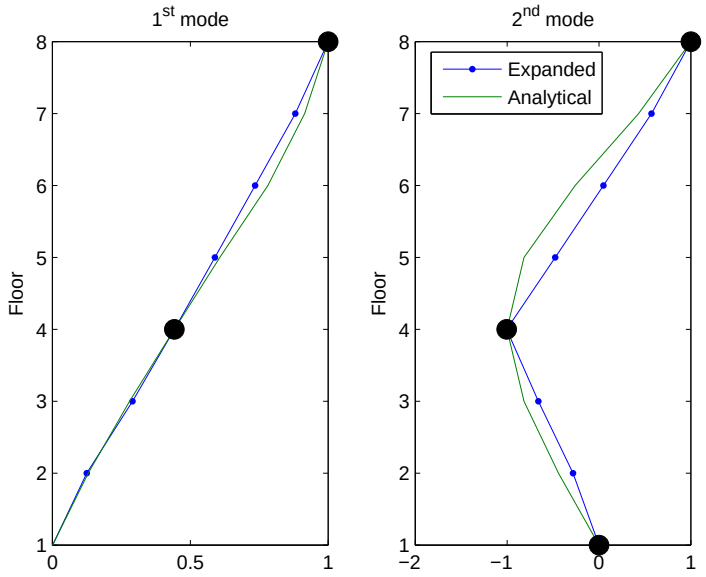

Figure 2.8: Expanded and analytic mode shapes (1% noise)

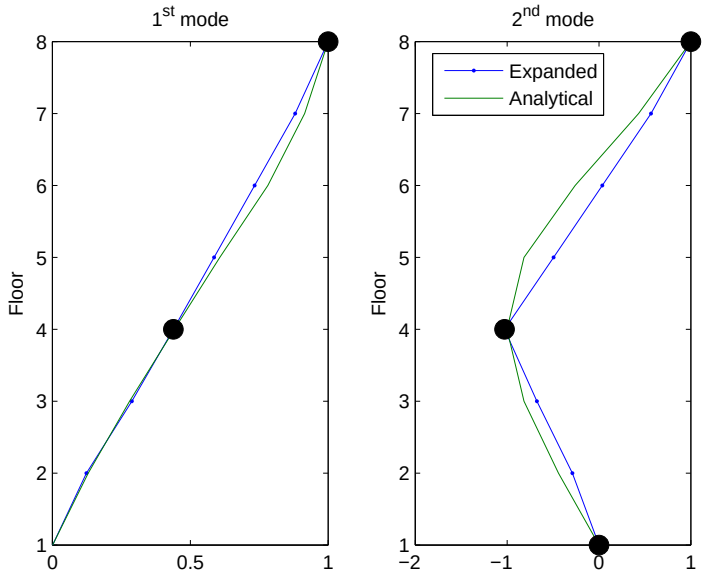

Figure 2.9: Expanded and analytic mode shapes (10% noise)

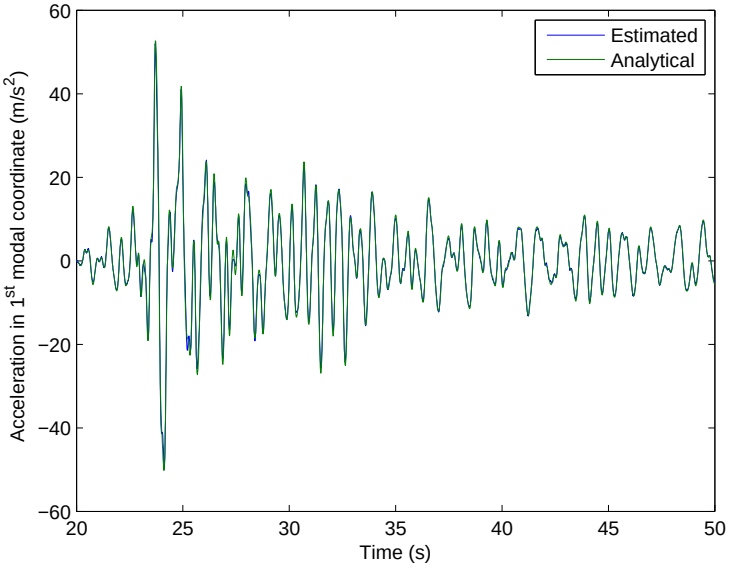

Figure 2.10: Acceleration in the 1st modal coordinate $\ddot{\xi}_1$ (1% noise)

$\mathbf{\Phi}_s^{\dagger}$ is the pseudo-inverse matrix of the expanded mode shape matrix of $\mathbf{\Phi}_s$. The evaluated results and analytical values are plotted in Figures 2.10, 2.11, 2.12 and 2.13.

All the unknown parameters in Eq. (2.16) needed for estimating the restoring force of the isolation layer were determined assuming the mass to be the same as that in the simulation model. Figures 2.14 and 2.15 illustrates the difference between the estimated restoring force and the analytical one. Although they are consistent at a rather high level, the estimated force-displacement is distorted a lot (Figures 2.16 and 2.17). These cases with different noise levels show that noise degrades the identification results, the modal information, and the modal acceleration has little effect on the estimated restoring force. The reason is that the dominant part of the restoring force comes from the inertia force of the superstructure, and the part coming from modal inertia forces doesn't count as much.

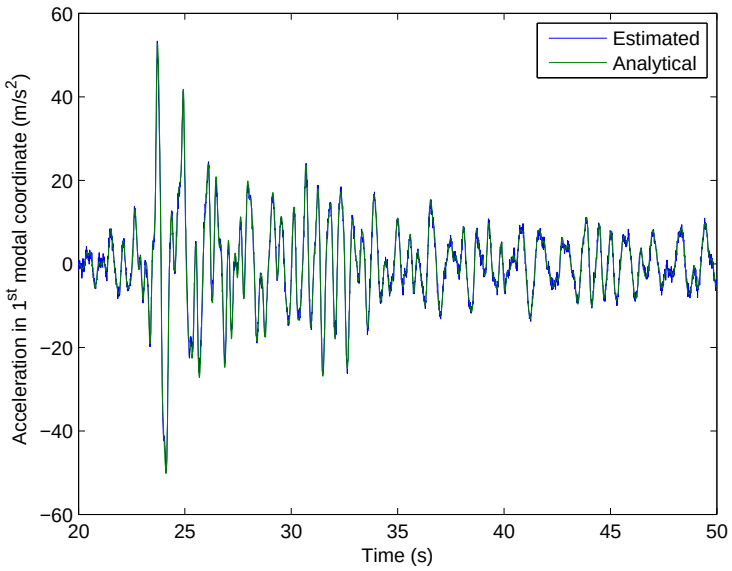

Figure 2.11: Acceleration in the 1$^{\text{st}}$ modal coordinate $\ddot{\xi}_1$ (10% noise)

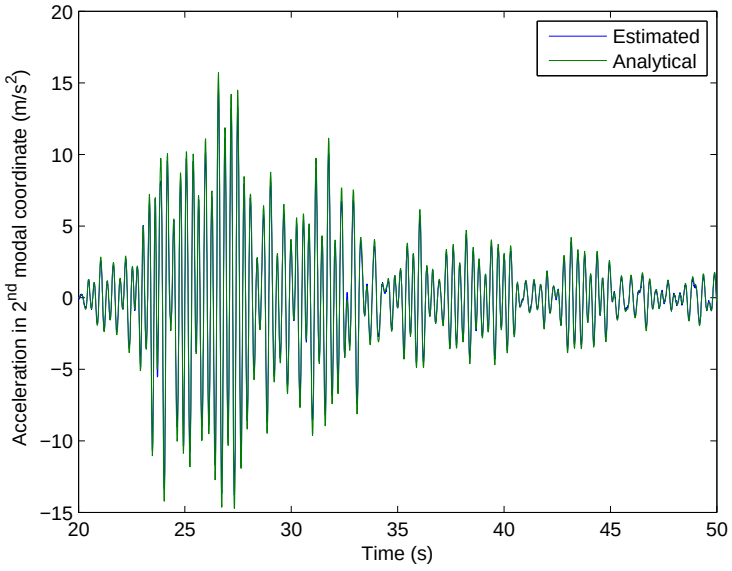

Figure 2.12: Acceleration in the 2$^{\text{nd}}$ modal coordinate $\ddot{\xi}_2$ (1% noise)

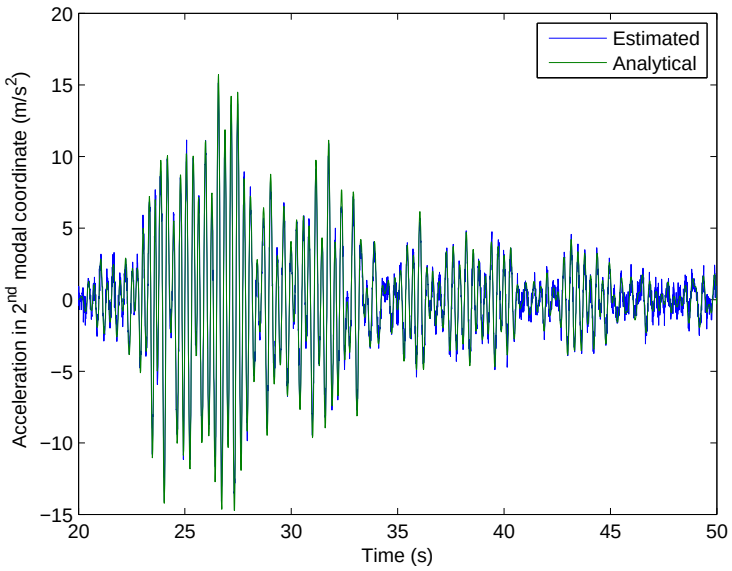

Figure 2.13: Acceleration in the 2$^{\text{nd}}$ modal coordinate $\ddot{\xi}_2$ (10% noise)

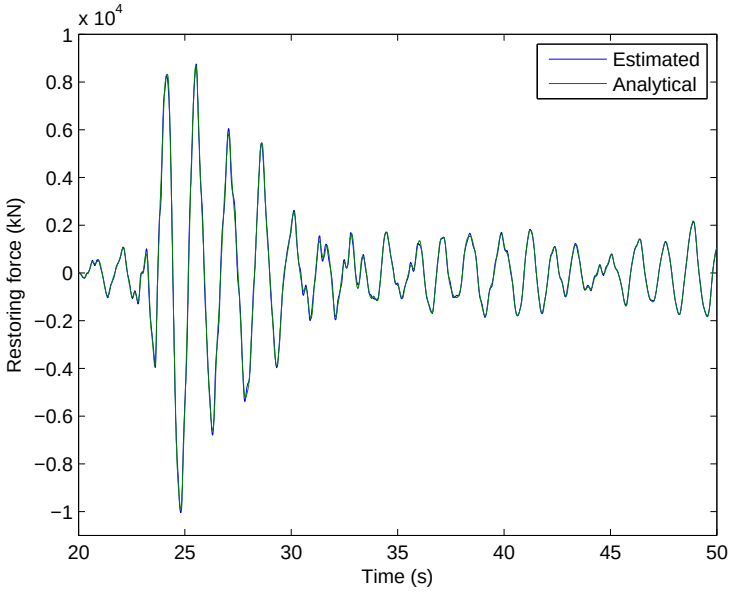

Figure 2.14: Estimated restoring force of the isolation layer (1% noise)

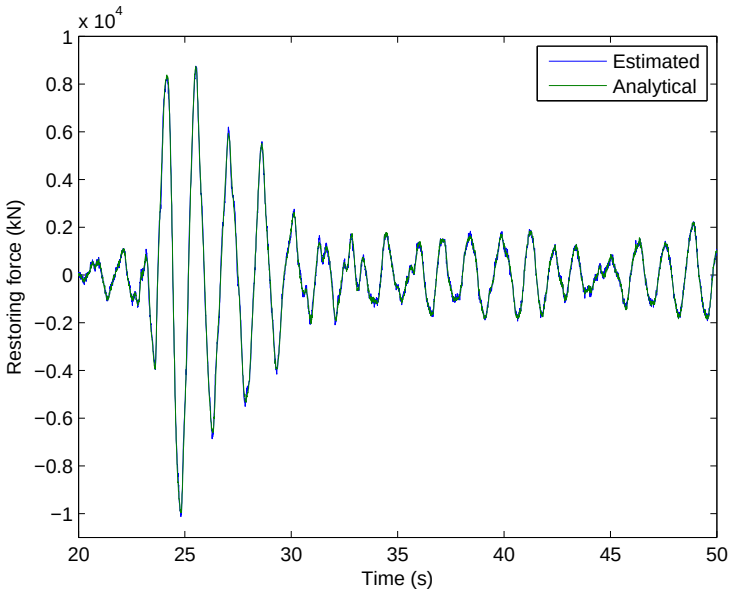

Figure 2.15: Estimated restoring force of the isolation layer (10% noise)

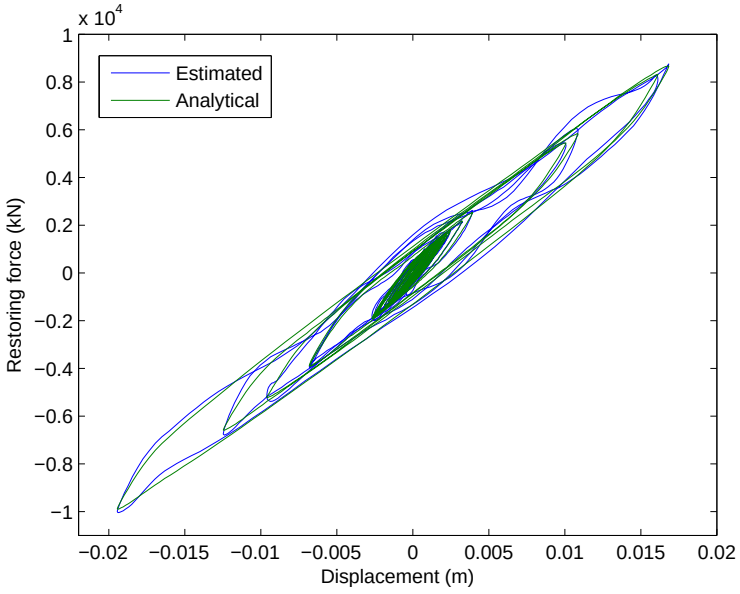

Figure 2.16: Estimated restoring force vs. displacement (1% noise)

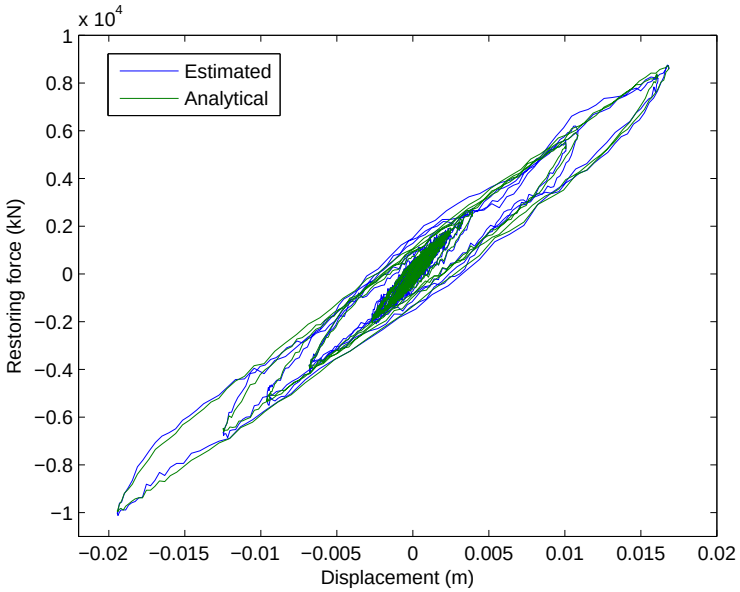

Figure 2.17: Estimated restoring force vs. displacement (10% noise)

2.5.1 Effect of Mode Selection

The effect of mode selection was examined for three different choices: the first mode, the first two modes, and the first three modes. As illustrated in Figure 2.18, the first two modes can generate acceptable results. In most cases, the response of the structure is dominated by the low-order vibration modes with high participation factors.

2.5.2 Effect of Mass Estimation

The effect of the mass estimation was evaluated by investigating two kinds of mass variation. First, the mass estimation was scaled to its simulation value, in this case, by 90%, and the first two modes were selected for the restoring force estimation. As illustrated in Figure 2.19, the estimated value retains the shape but is scaled by the same degree. This is due to the reason that the rigid inertial force, which dominates the restoring force, is proportional to the total.

The second kind of mass variation was that the mass is normally distributed around the simulation value with a certain standard deviation (in this case, 20

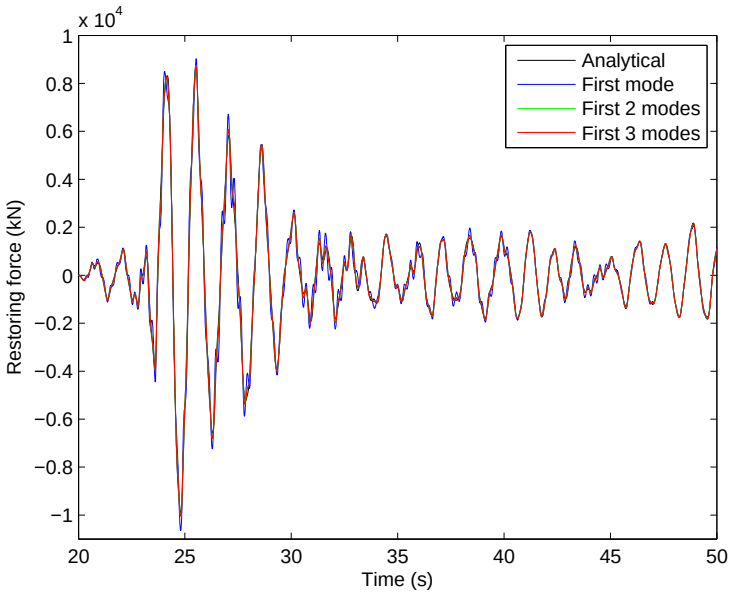

Figure 2.18: Effect of mode selection on estimation (1% noise)

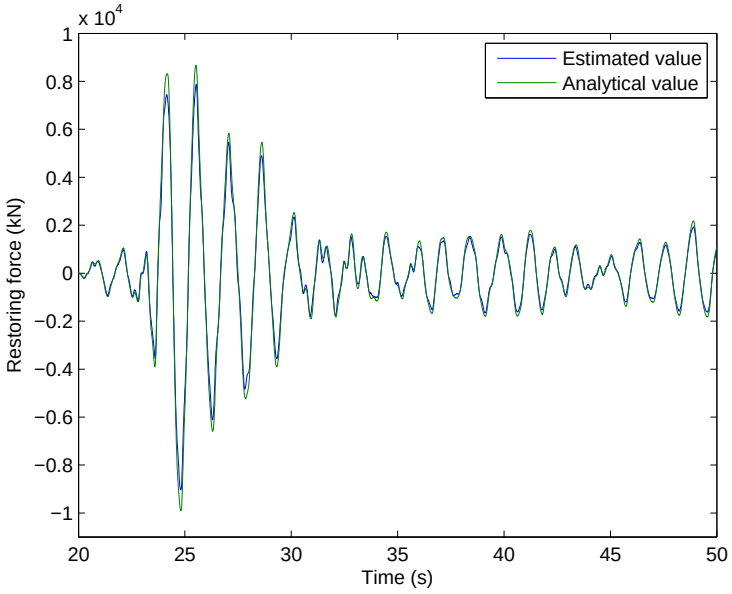

Figure 2.19: Effect of mass estimation (1% noise)

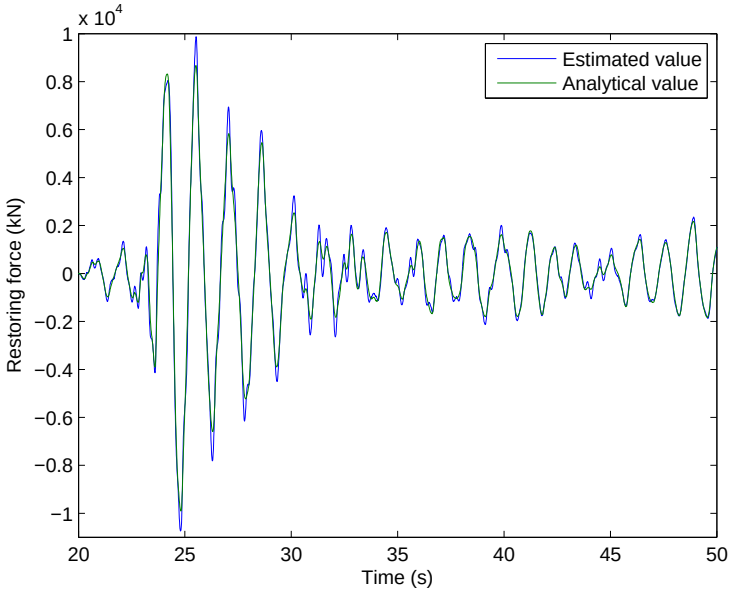

Figure 2.20: Effect of mass estimation (1% noise), (2005 2010 1541 1834 1656 2411 3790 9950 ton, from top down)

of the simulation value). As shown in Figure 2.20, in this case also the estimated value fit the analytical value very well. From these two examples, it is concluded that the estimation of the restoring force is insensitive to the mass distribution but will be scaled by the estimated total mass.

2.6 Conclusions

This chapter represented a new method, based on component mode synthesis, for estimating the restoring force of an isolation layer. The hybrid motion equation involving the modal coordinates and the physical coordinates is derived by using a substructuring technique. This method is applicable even when the number of sensors is limited because only the mode shape information of the superstructure and the estimated mass estimation are needed for estimating the restoring force. It was shown that the proposed method is not sensitive to the mass distribution and the expanded mode shapes but will be scaled by the total mass. The effectiveness of this method was validated in simulations.

Chapter 3

Identifiability of Linear Superstructures under Feedback

3.1 Introduction

The structural engineering community takes for granted that substructural identification of a superstructure is equivalent to the case in which a structure is subject to ground motion, if the base story of the superstructure is considered as the ground. Structural engineers assume that identification will never fail if the input and output signals are known. Substructural identification of the superstructure sometimes fails, however, in the case of free vibration. This can't be explained by the theory of open-loop identification, even though the input and output signals of the substructure are both known. Therefore, investigating the identifiability condition requires new insight, with substructural identification moved into the framework of closed-loop systems.

In this chapter, we take the example of a base-isolated structure decomposed into two substructures: a superstructure, and a base isolation layer. The superstructure is considered a linear system. The base isolation layer can be either linear or nonlinear. We first investigate the linear case, in which the isolation layer is represented by a linear model with stiffness k_b and damping coefficient c_b, as illustrated in Figure 3.1. Here, x is the displacement relative to the ground, $\ddot{x}_g$ is the ground acceleration, and the superscript a refers to the absolute coordinates.

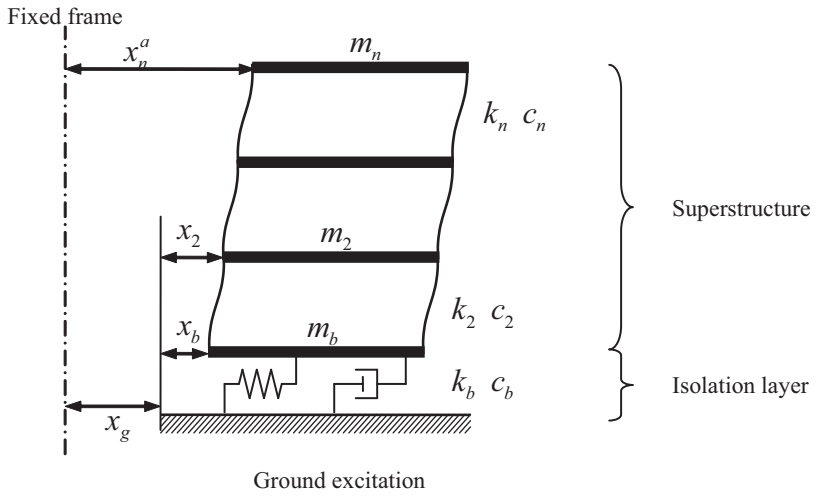

Figure 3.1: Structure model

The motion equation of the overall structure is written as

$$\mathbf{M}\ddot{\mathbf{x}} + \mathbf{C}\dot{\mathbf{x}} + \mathbf{K}\mathbf{x} = -\mathbf{M}\mathbf{r}\ddot{x}_g \tag{3.1}$$

where $\mathbf{K}$, $\mathbf{C}$, and $\mathbf{M}$ are the stiffness, damping, and mass matrices, respectively; and $\mathbf{Mr}$ is the diagonal vector of $\mathbf{M}$.

After decomposing the structure into the superstructure and the isolation layer, these two subsystems compose a complete closed-loop system, as shown in Figure 3.2. The superstructure is taken as the plant, while the isolation layer is the regulator. The subscripts s and b denote the superstructure and the isolation layer, respectively. The ground acceleration functions as the reference signal, a persistent excitation of any order, and is the input to the overall system. The output of the plant is contaminated by unmeasured noise sources. We assume that there are no process disturbances between the plant and the controller, and that the unmeasured noise doesn't affect the controller, meaning that there is no correlation between the noise and the input. The noise sources are modeled within output signals; therefore, they are located outside the feedback loop. The isolation layer generates the feedback, which is the relative acceleration of this layer with respect to the ground. The feedback added via the reference signal is equal to the absolute acceleration of the layer exciting the plant.

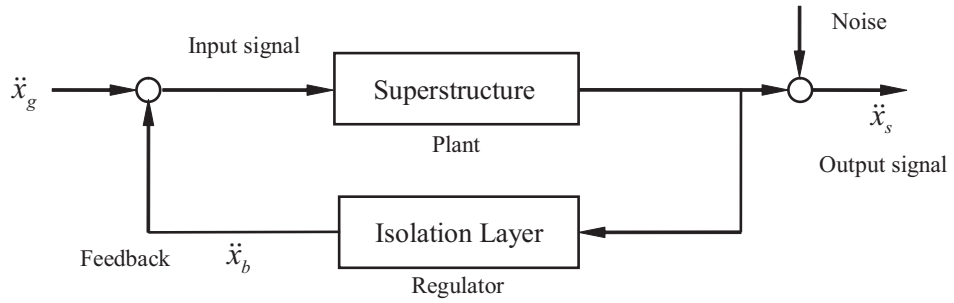

Figure 3.2: Subsystems in a closed-loop scheme

This chapter is organized as follows. Section 3.2 addresses the basic concepts of closed-loop identification. Section 3.3 investigates the identifiability problem for linear systems under linear feedback laws, by examining spectral analysis and parametric methods. We also derive the identifiability condition for parametric methods. Section 3.4 briefly explains the identifiability of linear systems under nonlinear feedback laws. Then, in Section 3.5, we apply the identifiability condition to study the identification of a superstructure by numerical simulation. Finally, the last section summarizes our main results.

3.2 Basic Concepts of Closed-loop Identification

The essential concept in closed-loop identification is identifiability, which means that there exists an identified model $M(\theta)$ that can describe the true system S when the number of measurements tends to infinity. In the case of a closed-loop system, as shown in Figure 3.3, the input and the unmeasurable noise, which is inside the feedback loop, are correlated whenever the feedback controller exists. This is why several methods that can be applied in open loops fail when applied to closed-loop data.

The identifiability problem of linear systems under linear feedback was first investigated by Akaike (1967) by using spectral analysis, showing that under pure feedback conditions, spectral analysis fails to yield informative results for

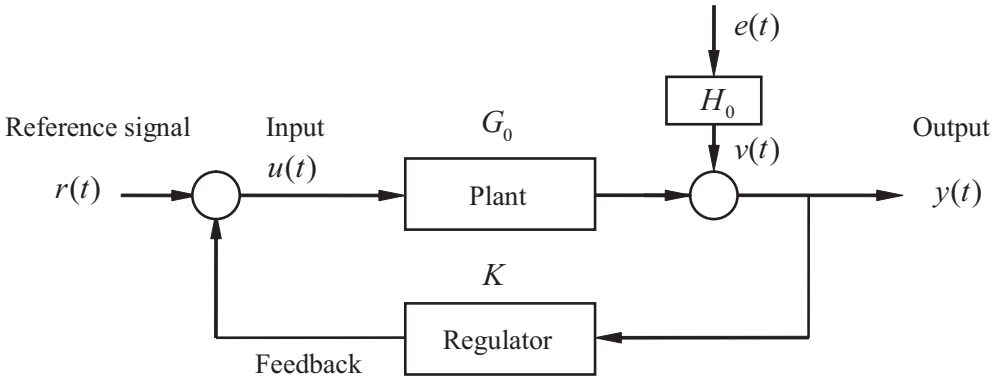

Figure 3.3: A closed-loop system

the plant. Box & MacGregor (1974) concluded an identical result by using correlation methods, which are not applicable to the causality of true systems. Ljung *et al.* (1974) explored the same problem by direct, parametric approaches and proved that by shifting between different linear regulators, it is always possible to achieve identifiability for pure feedback systems. The required number of regulators depends only on the numbers of inputs and outputs. Söderström *et al.* (1975) then included noise sources in the regulator and external input signals for a general configuration. Ng *et al.* (1977) derived the identifiability conditions for joint input-output approaches, which require that there be no correlation between the noise in the forward and reverse paths. The presence of delays in either the plant or the regulator is necessary to avoid an algebraic loop, as Ljung *et al.* (1974) and Söderström *et al.* (1976) pointed out. This can be relaxed to a condition relating to the absence of algebraic loops in closed-loop systems (Sohn, 2003). Wang *et al.* (2004) used a fast-sampling direct approach to lift these restrictive identifiability conditions for a closed-loop system without external signals. Finally, Forssell & Ljung (1999) and Gustavsson *et al.* (1977) provided comprehensive surveys of closed-loop identifiability.

In the structural engineering community, the identifiability of substructural identification has seldom been considered. It is vitally important to determine under what conditions it is possible to obtain reliable, identified results for closed-loop systems. Generally speaking, the result of identification depends on the

following items, as classified by Gustavsson *et al.* (1977):

1. System
2. Feedback structure
3. Model structure
4. Identification method
5. Experimental conditions

3.2.1 System

Consider a linear time-invariant dynamical system in a discrete-time representation

$$S : y(t) = G_0(q)u(t) + v(t), \qquad v(t) = H_0(q)e(t) \tag{3.2}$$

where $y(t) \in R^p$ is a p-dimensional output signal; $u(t) \in R^m$ is an m-dimensional input signal; $e(t) \in R^p$ is a sequence of independent random variables with zero mean and covariance matrix $E[e(t)e^T(t)] = \Lambda > 0$; and $G_0(q)$ and $H_0(q)$ are rational transfer function matrices, with $H_0(q)$ being an inversely stable, monic filter. q denotes the forward shift operator, e.g. $q^{-1}u(t) = u(t - \Delta t)$.

3.2.2 Feedback Structure

Assume that this system is operated under a linear feedback law

$$u(t) = r(t) + K(q)y(t) \tag{3.3}$$

where $r(t)$ is a m-dimensional reference signal assumed to be independent of the noise v, which is either an additional measurable signal or a noise disturbance in the regulator output; and $K(q)$ is a linear, time-invariant regulator of appropriate dimensions. The feedback structure plays a vital role in the identifiability conditions of a closed-loop system. The number of regulators or the complexity of the regulator can influence the identifiability of a closed-loop system.

3.2.3 Model

To determine a model of the system S, we consider a model set

$$M : y(t) = G_\theta(q)u(t) + H_\theta(q)\varepsilon(t), \qquad \theta \in \Theta \subset R^d \tag{3.4}$$

where $\varepsilon(t)$ is a sequence of independent, random vectors with zero mean values and covariances $\tilde{\Lambda}$; $G_\theta(q)$ and $H_\theta(q)$ are the dynamics model and the noise model respectively, and both are appropriate rational transfer function matrices depending on a real-valued parameter vector θ. When θ varies within a feasible region, Eq. (3.4) represents a family of models, sometimes called a model structure. We assume that G is causal and H is both monic and causal.

3.2.4 Identification Method

The procedure to determine the parameter vector is called the identification method. For a closed-loop system, identification methods can be classified into three main groups:

1. The direct approach: Ignore the feedback and identify the system directly by measuring the input and output, exactly as if it was an open-loop system.

2. The indirect approach: If the regulator is known, then the closed-loop system as a whole can be identified. The corresponding open-loop system is determined through knowledge of the regulator.

3. The joint input-output approach: Jointly consider both the input and the output as the output from a system driven by some extra input or noise. The corresponding open-loop system is identified by estimating the characteristics of this augmented system.

Each group includes several different methods, such as correlation and spectral analysis, the parametric identification method (Ljung, 1999), and the subspace identification method (Van Overschee & de Moor, 1996). If there is a time delay in either the system or the regulator, and if the regulator noise is independent of the system noise, then the direct and joint input-output approaches are equivalent for determining identifiability. Furthermore, the indirect approach has no advantage

over direct identification in terms of either identifiability or accuracy. Therefore, we adopt the direct identification approach in this part.

3.2.5 Experimental Conditions

Basically, the experimental conditions consist of the sampling rate and the length of the experiment, which describe how the input is determined. An experimental system can be operated in an open loop, or the experimental conditions can be determined by the feedback of a given regulator. Traditionally, the conditions include the regulator characteristics. In this chapter, however, we exclude these characteristics from the experimental conditions and instead regard the regulator characteristics as a dependent item, called the feedback structure.

3.2.6 Identifiability Definition

The property of identifiability is related to the consistency of parameter estimation. There are several definitions on different levels, as defined by Ljung *et al.* (1974). For a certain model structure, experimental conditions, and identification method, a system is said to be system identifiable (SI) if an identified model $M(\theta)$ converges to the true system S when the number of measurements tends to infinity. If a system is SI for all possible model structures, then it is said to be strongly system identifiable (SSI).

3.3 Identifiability Conditions for Linear Feedback Laws

3.3.1 Nonparametric Methods

As a classical, well-established method, spectral analysis was first used by Akaike (1967) to study the identifiability problem with nonparametric identification methods on closed-loop data. The frequency response function can be obtained from the spectrum analysis

$$G(\omega) = \frac{\Phi_{uy}(\omega)}{\Phi_u(\omega)} \tag{3.5}$$

where $\Phi_u(\omega)$ and $\Phi_{uy}(\omega)$ are the power spectrum of input u and the cross-spectrum between input u and output y, respectively. Another formulation of $G(\omega)$ is the following

$$G(\omega) = \frac{G_0(e^{i\omega})\Phi_r(\omega) + K(e^{i\omega})|H_0(e^{i\omega})|^2\sigma_e^2}{\Phi_r(\omega) + |K(e^{i\omega})|^2|H_0(e^{i\omega})|^2\sigma_e^2} \tag{3.6}$$

where $\Phi_r(\omega)$ is the power spectrum of the reference signal r. When the reference signal exists, the frequency response gives a weighted average of the true process frequency response and the frequency response of the controller's inverse. If there is no persistent excitation signal, meaning that $\Phi_r(\omega) = 0$, then nonparametric methods identify only the inverse of the feedback controller

$$G(\omega) = \frac{1}{K(e^{i\omega})} \tag{3.7}$$

This shows that spectral analysis will not yield information about the plant if applied to a pure feedback operation. Box & MacGregor (1974) concluded an identical result by using correlation methods. Nonparametric methods fail to yield informative results because the causality of true systems is not able to be implied by these methods. Instead, these methods only identify the best correlation relationship between the input and output, which is represented by the feedback law.

3.3.2 Parametric Methods

Söderström *et al.* (1976) generalized the identifiability conditions for a system by including the noise sources in the regulator and the external input signals. The regulator is assumed to shift among r different feedback laws

$$u(t) = r(t) + K_i(q)y(t) \qquad 1 \leq i \leq r \tag{3.8}$$

Each case applies during a nontrivial period of the total time of an experiment. Here, we introduce some abbreviations to facilitate concise description. We denote $G = G_0(q)$, $\hat{G} = G_\theta(q)$, $H = H_0(q)$, $\hat{H} = H_\theta(q)$ and $K_i = K_i(q)$. Eq. (3.2) and Eq. (3.8) give

$$y(t) = GK_iy(t) + Gr(t) + He(t) \tag{3.9}$$

Simplify it, $y(t)$ is expressed by

$$y(t) = (I - GK_i)^{-1}Gr(t) + (I - GK_i)^{-1}He(t) \tag{3.10}$$

Then, the input can be written as

$$u(t) = [K_i(I - GK_i)^{-1}G + I]r(t) + K_i(I - GK_i)^{-1}He(t) \tag{3.11}$$

We also introduce the following notation for the feedback law K_i

$$P_i = (I - GK_i)^{-1}G \tag{3.12}$$

Now, we consider direct identification. The residual $\varepsilon(t)$ is given as

$$\begin{aligned} \varepsilon(t) &= \hat{H}^{-1}[y(t) - \hat{G}u(t)] \\ &= \hat{H}^{-1}[P_i - \hat{G}(K_iP_i + I)]r(t) + \hat{H}^{-1}(I - \hat{G}K_i)(I - GK_i)^{-1}He(t) \end{aligned} \tag{3.13}$$

Since K_i is causal and the input $u(t)$ is independent of $e(t)$, the minimum variance prediction error $\varepsilon(t)$ is asymptotically given as

$$\varepsilon(t) \equiv e(t)$$

Therefore, Eq. (3.13) implies the following

$$\begin{cases} \hat{H}^{-1}[P_i - \hat{G}(K_iP_i + I)] = 0 \\ \hat{H}^{-1}(I - \hat{G}K_i)(I - GK_i)^{-1}H = I \end{cases} \qquad 1 \le i \le r \tag{3.14}$$

Both sides of the first equation are added with a term $H^{-1}[(GK_i - I)P_i + G]$, which is equal to zero according to Eq. (3.12). Thus it can be rewritten in this form

$$\begin{aligned} &(\hat{H}^{-1}\hat{G} - H^{-1}G)(-K_iP_i - I) + (\hat{H}^{-1} - H^{-1})P_i \\ &= H^{-1}[(GK_i - I)P_i + G] = 0 \end{aligned} \tag{3.15}$$

The second equation is simplified as

$$-(\hat{H}^{-1}\hat{G} - H^{-1}G)K_i + (\hat{H}^{-1} - H^{-1}) = 0 \tag{3.16}$$

Thus, we rewrite Eq. (3.14) in matrix form

$$\begin{aligned} &\begin{bmatrix} \hat{H}^{-1} - H^{-1} & H^{-1}G - \hat{H}^{-1}\hat{G} \end{bmatrix} \begin{bmatrix} P_i & I \\ K_iP_i + I & K_i \end{bmatrix} \\ &= \begin{bmatrix} \hat{H}^{-1} - H^{-1} & H^{-1}G - \hat{H}^{-1}\hat{G} \end{bmatrix} \begin{bmatrix} I & 0 \\ K_i & I \end{bmatrix} \begin{bmatrix} P_i & I \\ I & 0 \end{bmatrix} = \begin{bmatrix} 0 & 0 \end{bmatrix} \end{aligned} \tag{3.17}$$

Because the matrix $\begin{bmatrix} P_i & I \\ I & 0 \end{bmatrix}$ is nonsingular, we finally have

$$\begin{bmatrix} \hat{H}^{-1} - H^{-1} & H^{-1}G - \hat{H}^{-1}\hat{G} \end{bmatrix} R_r = \begin{bmatrix} 0 & 0 \end{bmatrix} \tag{3.18}$$

$$R_r = \begin{bmatrix} I_1 & \cdots & I_1 & 0 & \cdots & 0 \\ K_1 & \cdots & K_r & I_2 & \cdots & I_2 \end{bmatrix}$$

where I_1 has order $n_y|n_y$, 0 has order $n_y|n_r$, K_i has order $n_u|n_y$, and I_2 has order $n_u|n_r$. Thus, R_r is a matrix of order $n_y + n_u|r(n_y + n_r)$. Here, r is the number of regulators, and n_y, n_u and n_r are the numbers of plant outputs, plant inputs, and reference signals, respectively. If the identification result converges to the true model, then we have

$$\hat{H} = H, \hat{G} = G$$

This implies that

$$\begin{aligned} \hat{H}^{-1} - H^{-1} &= 0 \\ H^{-1}G - \hat{H}^{-1}\hat{G} &= 0 \end{aligned} \tag{3.19}$$

This requires that R_r should be nonsingular.

In conclusion, the identifiability condition for a linear system under linear feedback can be summarized as follows: For a linear multivariate system, if there is a reference signal, it must be a persistent excitation of any finite order. Assume that there is a time delay in either the system or the regulator, such that $G(0)K_i(0) = 0$. Then, the system is SSI if and only if

$$\text{rank}(R_r) = n_y + n_u \tag{3.20}$$

A necessary condition for Eq. (3.20) to hold is that

$$r \geq (n_y + n_u)/(n_y + n_r) \tag{3.21}$$

The presence of a delay in either the plant or the regulator, given by $G(0)K_i(0) = 0$, avoids algebraic relations between the input and output and necessary to guarantee identifiability. Here, this is represented strictly, but Sohn (2003) relaxed this classic delay-structure condition for the identifiability of closed-loop systems.

3.3.3 Identifiability Conditions of Superstructures

We can now apply the derived identifiability condition to the case of superstructures, for two situations: ground excitation, and free vibration.

3.3.3.1 Ground Excitation

In the case of ground excitation, the reference signal is of the same dimension as the input signal, i.e., $n_u = n_r$; and the regulator is not replaceable, i.e., $r = 1$. Then, the identifiability condition becomes

$$\operatorname{rank} \begin{bmatrix} I_1 & 0 \\ K_1 & I_2 \end{bmatrix} = n_y + n_u \tag{3.22}$$

Therefore, no matter what the feedback might be, the necessary condition from Eq. (3.21) always holds if there is ground motion. In other words, if the input and output of the plant are given, the superstructure in the case of an earthquake is SSI.

3.3.3.2 Free Vibration

The case of free vibration means a situation with pure linear feedback laws, so $n_r = 0$. Then, the identifiability condition becomes

$$\operatorname{rank} \begin{bmatrix} I_1 & \cdots & I_1 \\ K_1 & \cdots & K_r \end{bmatrix} = n_y + n_u \tag{3.23}$$

Therefore, the necessary condition from Eq. (3.21) for the free-vibration case is given as

$$r \geq 1 + n_u/n_y \tag{3.24}$$

This means even if no reference signal exists, the presence of at least two linear feedback laws guarantees the system identifiability of the superstructure.

If the identifiability condition is not satisfied, the system is not SSI. It can, however, be SI for certain model structures. Söderström *et al.* (1975) investigated the identifiability of a pure feedback system without external inputs for certain model structures and derived the necessary and sufficient condition for identifiability. This condition requires that the order of the regulator be higher than that of the plant for identifiability to hold.

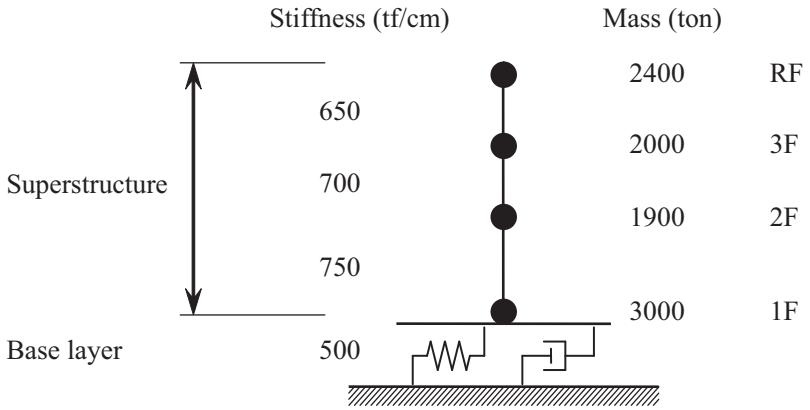

Figure 3.4: Simulation model for a three-story building

When the regulator is operated by a nonlinear feedback law, Eq. (3.6) can not clarify the identifiability of the plant, because the description of the regulator in the frequency domain is invalid. In parametric approaches, if the feedback law is nonlinear, it can be viewed as a different linear regulator during every short time segment. Therefore, the complexity of the nonlinear regulator guarantees the identifiability of the plant in the case of pure feedback, and in the case with external signals, as well.

3.4 Numerical Simulation

In this simulation, we considered a three-story structure. The part of the structure above the base layer was defined as the superstructure. The superstructure was of the shear type and assumed to remain within its elastic range. The stiffness and mass could vary from floor to floor, as illustrated in Figure 3.4. The damping coefficient matrix was proportional to the stiffness matrix as $\mathbf{C} = \alpha\mathbf{K}$, with $\alpha = 0.001$. Tables 3.1 and 3.2 list the modal information for the superstructure and the overall structure, respectively. The time step for the simulation was $\Delta t = 0.01$ second. The structure was placed in a state of free vibration by setting its initial displacement. The acceleration response was contaminated by 1% white noise (i.e., the standard deviation of the noise was 1% of the standard deviation of the response).

Table 3.1: Modal information of the superstructure (fixed base)

	Frequency (Hz)	Damping ratio (%)
1st	1.2762	0.0040
2nd	3.6125	0.0113
3rd	5.3489	0.0168

Table 3.2: Modal information of the overall structure

	Frequency (Hz)	Damping ratio (%)
1st	0.9113	0.0029
2nd	2.4803	0.0078
3rd	4.0756	0.0128
4th	5.5001	0.0173

Autoregressive moving average models with exogenous inputs (ARMAX models) includes disturbance dynamics, can flexibly describe a disturbance as a moving average of white noise. The model is given as following

$$\begin{aligned} y(t) + a_1 y(t-1) + \cdots + a_{n_a} y(t-n_a) = b_1 u(t-1) + \cdots + b_{n_b} u(t-n_b) \\ + e(t) + c_1 e(t-1) + \cdots + c_{n_c} e(t-n_c) \end{aligned} \tag{3.25}$$

where a_i, b_i and c_i are the coefficients of the AR, X and MA part, respectively. n_a, n_b and n_c are model orders of each part. This model can also be rewritten

$$A(q)y(t) = B(q)u(t) + C(q)e(t) \tag{3.26}$$

where

$$A(q) = 1 + a_1 q^{-1} + \cdots + a_{n_a} q^{-n_a}$$

$$B(q) = b_1 q^{-1} + \cdots + b_{n_b} q^{-n_b}$$

$$C(q) = 1 + c_1 q^{-1} + \cdots + c_{n_c} q^{-n_c}$$

$A(q)y(t)$ is the auto-regression part of the output, $B(q)u(t)$ describes a process of exogenous inputs, and $C(q)e(t)$ represents the disturbance dynamics, is the moving average of a stationary white noise $e(t)$. And this corresponds to Eq. (3.2) with

$$G(q,\theta) = \frac{B(q)}{A(q)}, \qquad H(q,\theta) = \frac{C(q)}{A(q)} \tag{3.27}$$

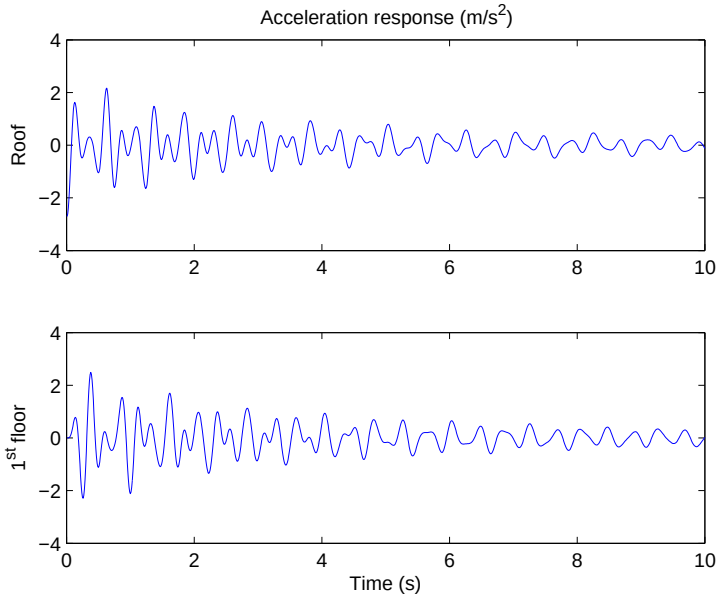

Figure 3.5: Acceleration responses (initial displacement: 0.01 m on the roof, 0 elsewhere)

For further information about the model estimation, readers can refer to the book written by Ljung (1999).

Thus, an ARMAX model is used for identification, using the acceleration on the first floor for the input signals and the acceleration on the roof for the outputs signals, as shown in Figure 3.5. When the regulator (i.e., the base story) was governed by a linear feedback law, the parametric method obviously failed to identify the superstructure, as illustrated in Figure 3.6.

To ensure the nonlinearity of the regulator, a cubic hardening stiffness was added to the base layer: $F_n = \beta k_b x_b^3$ ($\beta = 10000$), where x_b was the displacement relative to the ground. As shown in Figure 3.7, the result identified by the ARMAX model is consistent with that of the analytical model.

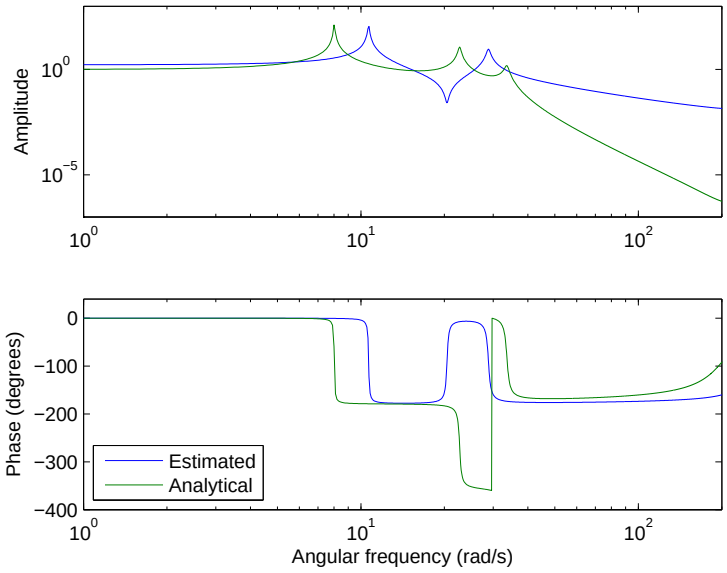

Figure 3.6: Parametric method for linear feedback case

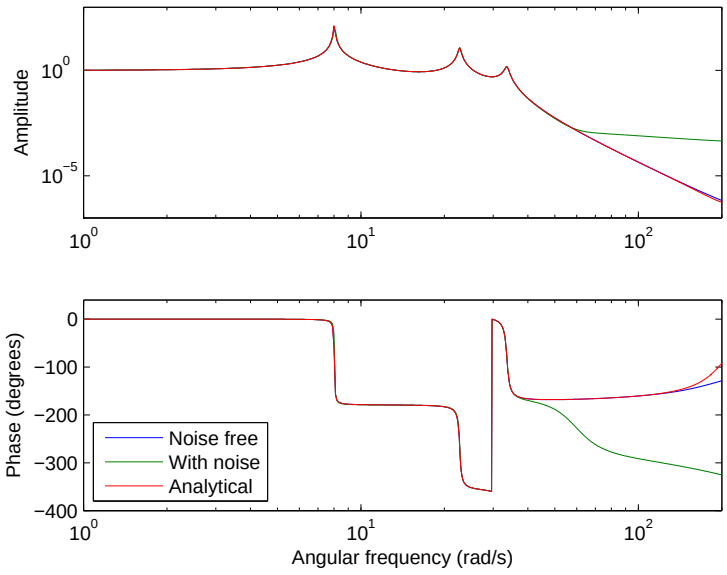

Figure 3.7: Parametric method for nonlinear feedback case

3.5 Conclusions

We have explored the identifiability condition for substructural identification in cases of free vibration. As explained by Akaike (1967), spectral analysis in the frequency domain cannot obtain the identifiability of a superstructure. If the base layer is governed by a linear feedback law, the identifiability of the superstructure is lost unless there are at least two regulators. By making the regulators nonlinear, identifiability can be regained with parametric methods. In a free-vibration field test, the identification of a linear substructure under linear feedback laws can be guaranteed if a nonlinear device is attached to the rest of the structure. The feedback, determined by the characteristics of the regulator, has a greater influence on the identifiability than does the model structure or the identification method.

Chapter 4

Nonlinear Identification of Hysteretic Systems by Reverse Path Method

4.1 Introduction

For the purpose of system identification, most structures are approximated by a linear model. And the modal parameters (frequency, modal shape, etc.) or physical parameters (stiffness and damping coefficient) describe the status of linear structures, the variance of these parameters indicates the damage to the structure. However, nonlinearity exists inevitably in a real world, and sometimes it behaves so strongly that the methods for linear structures fail to identify the system and detect the damage by linear approximation. For example, it is well observed that base-isolated buildings exhibit nonlinear and hysteretic properties under experiment situation. The dynamic parameters will vary with the intensity of excitation even if the system is intact, consequently the change of these parameters can not indicate the status of nonlinear systems.

In recent years, system identification of nonlinear dynamic structures has made significant progress. Kerschen *et al.* (2006) investigated the past and recent developments in nonlinear system identification methods. Although the number of methods is large, there are no method to identify any type of nonlinearity.

Rice & Fitzpatrick (1988), and Bendat (1990) proposed a reverse path identification method for single-input/single-output nonlinear systems. This method treats the response as the input, and the excitation force as the output. The nonlinear term is considered as a feedback term. It tracks unknown parameters in frequency domain. Rice & Fitzpatrick (1991) extended this method to identify two DOFs nonlinear systems treating each response location as a SDOF mechanical oscillator. However, this approach requires excitations to be applied at every nonlinear location.

Richards & Singh (1998) developed a conditioned reverse path method (CRP). The improved technique separates the nonlinear part of the system response from the linear part and constructs a hierarchy structure of uncorrelated response components in frequency domain. CRP removes the restriction that the excitation must be applied at the location of the nonlinearity in order to identify its unknown parameters. Adams & Allemang (2000) proposed a frequency domain method for estimating parameters of nonlinear parametric models by using the spatial information and treating the nonlinear forces as internal feedback forces in the underlying linear system. This method is called Nonlinear Identification through Feedback of the Outputs (NIFO), and it requires measurements of both inputs and outputs and identifies the Frequency Response Function (FRF) of the underlying linear system as well as the parameters related to nonlinearities with light computational effort. Unlike CRP methods, NIFO methods estimate the linear and nonlinear coefficients in a single step.

Recently, Marchesiello & Garibaldi (2008a) developed an efficient time domain method called Nonlinear Subspace Identification (NSI) for identifying nonlinear systems by exploiting subspace identification methods. Later, Marchesiello & Garibaldi (2008b) discussed the identification problem for clearance-type nonlinearity by NSI methods. NSI is able to treat many nonlinearities at the same time, several ad hoc functions are defined and adopted in order to identify the clearance-type characteristic, showing advantages with respect to the traditional polynomial approach.

The advantage of reverse path formulation is that it can separate the linearity and nonlinearity of the structure, extract the nonlinearity and identify the un-

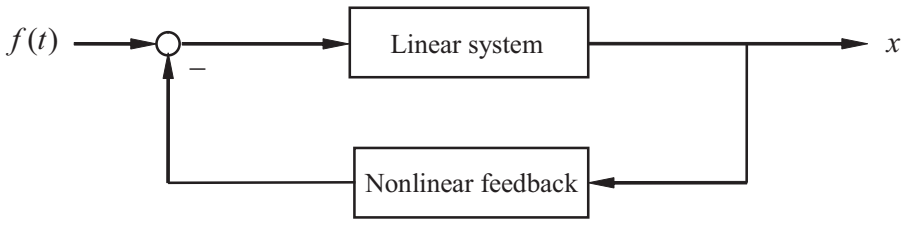

Figure 4.1: Nonlinear model with feedback

derlying linear structure. Therefore, the modal and physical parameters of the underlying linear structure become meaningful again.

Here, we use NIFO methods to identify the underlying linear model of hysteretic systems subjected to external force. The hysteretic restoring force is modeled by polynomial approximation of displacement and velocity. Numerical simulation is carried out to investigate the identification performance.

4.2 Reverse Path

The reverse path method exploits traditional spectral analysis techniques to identify nonlinear systems, treating the input-output relationship of excitation and response in a reversal way. The advantage of this method is that it can utilize the well-established linear analysis techniques for nonlinear systems. This idea is illustrated via a simple example. Let's consider the symmetric Duffing equation

$$m\ddot{x} + c\dot{x} + kx + k_3x^3 = f(t) \tag{4.1}$$

where m, c and k are the mass, damping coefficient and stiffness of the underlying linear system, respectively. k_3 is the coefficient of the cubic nonlinear term. $f(t)$ is the external excitation.

Generally, a nonlinear system can be described by Figure 4.1, as a linear system with nonlinear feedback. The underlying linear system is defined by the linear frequency response function

$$H(\omega) = \frac{1}{-\omega^2 m + i\omega c + k} \tag{4.2}$$

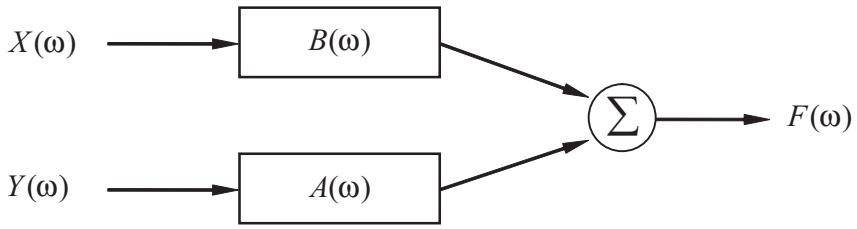

Figure 4.2: Reverse path model

where $i = \sqrt{-1}$. This transfer function relates an "effective" excitation $f_e(t)$ with displacement response x, where the effective excitation force is defined as

$$f_e(t) = f(t) - k_3 x^3 \tag{4.3}$$

with $k_3 x^3$ as nonlinear feedback.

Now, we consider the above nonlinear system in an alternative viewpoint. Taking the Fourier transform $\mathcal{F}[\bullet]$ of Eq. (4.1) gives

$$B(\omega)X(\omega) + A(\omega)Y(\omega) = F(\omega) \tag{4.4}$$

where $B(\omega) = 1/H(\omega)$, $X(\omega) = \mathcal{F}[x(t)]$ and $F(\omega) = \mathcal{F}[f(t)]$. For the nonlinear term, $A(\omega) = k_3$ and $Y(\omega) = \mathcal{F}[x^3(t)]$.

By exchanging the roles of the input and output, the displacement response x is considered as the input and the excitation force $f(t)$ as the output. Thus, the SDOF nonlinear system is viewed as a two-input/single-output system as illustrated in Figure 4.2.

Multiplying Eq. (4.4) by $X(\omega)$ and taking the expectation, we obtain

$$B(\omega)S_{xx}(\omega) + A(\omega)S_{xy}(\omega) = S_{xf}(\omega) \tag{4.5}$$

Similarly, Multiplying Eq. (4.4) by $Y(\omega)$ gives

$$B(\omega)S_{yx}(\omega) + A(\omega)S_{yy}(\omega) = S_{yf}(\omega) \tag{4.6}$$

These two equations form a set of simultaneous equations. By solving them, we can obtain unknown $B(\omega)$ and $A(\omega)$ at every frequency.

$$\begin{bmatrix} S_{xx}(\omega) & S_{xy}(\omega) \\ S_{yx}(\omega) & S_{yy}(\omega) \end{bmatrix} \begin{pmatrix} B(\omega) \\ A(\omega) \end{pmatrix} = \begin{pmatrix} S_{xf}(\omega) \\ S_{yf}(\omega) \end{pmatrix} \tag{4.7}$$

It is worth noting that the coefficient $A(\omega)$ is estimated as a complex function with respect to frequency. The real part of the result represents the coefficient k_3, and the imaginary part is meaningless with magnitude much smaller than the real part. The limitation of this method for MDOF systems is that the excitation must be applied at the location of nonlinearities.

4.3 Nonlinear Identification through Feedback of Output Method

The NIFO method is a spectral approach for identifying MDOF nonlinear systems, developed by Adams & Allemang (2000). It interprets the nonlinearities as the unmeasured internal feedback forces, and exploits the spatial information of type of nonlinearities.

Let's consider the Duffing equation again. We can rewrite Eq. (4.4) in the frequency domain as

$$B(\omega)X(\omega) = F(\omega) - A(\omega)Y(\omega) \tag{4.8}$$

The nonlinear forces, viewed as internal feedback forces, are the functions of the measured output (cubic function of the displacement x^3). Eq. (4.8) shows that the underlying linear system is excited by two forces: one is the external force $F(\omega)$, the other is the internal nonlinear feedback due to the nonlinearity $Y(\omega)$. Premultiplying Eq. (4.8) by the transfer function of the underlying linear system $H(\omega)$ gives

$$X(\omega) = H(\omega)F(\omega) - H(\omega)A(\omega)Y(\omega) \tag{4.9}$$

in matrix form, we have

$$X(\omega) = \begin{bmatrix} H(\omega) & H(\omega)A(\omega) \end{bmatrix} \begin{pmatrix} F(\omega) \\ -Y(\omega) \end{pmatrix} \tag{4.10}$$

where $Y(\omega) = \mathcal{F}[x^3(t)]$ is a known nonlinear function. This suggests that the type of nonlinearities should be known as a function of measured outputs before we identify nonlinear systems. The configuration of nonlinearity types is the spatial

information of nonlinear systems. Solving Eq. (4.10) gives the estimates of the FRFs of the underlying linear system $H(\omega)$ and the coefficient $A(\omega)$ of nonlinearities in a single step. A stable least-square solution with spectral averaging is suggested to identify the parameters related to structural nonlinearities.

If the NIFO method is applied to MDOF nonlinear systems, Eq. (4.10) can be given in matrix form

$$\mathbf{X}(\omega) = \left[\begin{array}{cccc} \mathbf{H}(\omega) & \mathbf{H}(\omega)\mathbf{A}_1(\omega) & \cdots & \mathbf{H}(\omega)\mathbf{A}_n(\omega) \end{array} \right] \left(\begin{array}{c} \mathbf{F}(\omega) \\ -Y_1(\omega) \\ \vdots \\ -Y_n(\omega) \end{array} \right) \tag{4.11}$$

where $\mathbf{X}(\omega)$ is a p-dimensional output vector, and $\mathbf{F}(\omega)$ is a q-dimensional input vector. $Y_n(\omega)$ represents different types of nonlinearities. $\mathbf{H}(\omega)$ is the frequency response function of the underlying linear structure, a $p \times q$-dimensional matrix. $\mathbf{A}_n(\omega)$ indicates the location of nonlinear types, a $q \times 1$-dimensional matrix.

Rewrite Eq.(4.11) in a compact form

$$\mathbf{X}(\omega) = \mathbf{H}_o(\omega)\mathbf{F}_o(\omega) \tag{4.12}$$

where $\mathbf{H_o}(\omega)$ is a $p\times(q+n)$-dimensional matrix, and $\mathbf{F_o}(\omega)$ is a $(q+n)$-dimensional vector.

4.3.1 Least Square Solution

Assuming that data length of measurements is N, we divide it in n_s segments possible overlapped. Then, an overdetermined set of linear equations is obtained.

$$\{\mathbf{Z}(\omega)\}_{n_s\times p} = \{\mathbf{P}(\omega)\}_{n_s\times(q+n)}\{\mathbf{H}_o(\omega)^T\}_{(q+n)\times p} \tag{4.13}$$

and

$$\{\mathbf{Z}(\omega)\}_{n_s\times p} = \left[\begin{array}{cccc} \mathbf{X}(\omega)_1 & \mathbf{X}(\omega)_2 & \cdots & \mathbf{X}(\omega)_{n_s} \end{array} \right]^T \tag{4.14}$$

$$\{\mathbf{P}(\omega)\}_{n_s\times(q+n)} = \left[\begin{array}{cccc} \mathbf{F}_o(\omega)_1 & \mathbf{F}_o(\omega)_2 & \cdots & \mathbf{F}_o(\omega)_{n_s} \end{array} \right]^T \tag{4.15}$$

where the superscript T means transpose of a matrix.

Eq. (4.13) is the well-known least-square problem with the solution at fixed frequency

$$\mathbf{P}(\omega)^T\mathbf{P}(\omega)\mathbf{H}_o(\omega)^T = \mathbf{P}(\omega)^T\mathbf{Z}(\omega) \tag{4.16}$$

where $\mathbf{P}(\omega)^T\mathbf{P}(\omega)$ is called the information matrix. In order to avoid possible ill-conditioning from the formation of $\mathbf{P}(\omega)^T\mathbf{P}(\omega)$, the orthogonal decomposition is suggested via Gram-Schmidt orthogonalization.

For convenience, ω is omitted in matrix representation. For example, $\mathbf{P}(\omega)$ is abbreviated as $\mathbf{P}$. The classical Gram-Schmidt orthogonalization factorizes $\mathbf{P}$ by Cholesky decomposition as

$$\mathbf{P} = \mathbf{WS} \tag{4.17}$$

where

$$\mathbf{S} = \begin{bmatrix} 1 & s_{12} & s_{13} & \cdots & s_{1(q+n)} \\ & 1 & s_{23} & \cdots & s_{1(q+n)} \\ & & \ddots & \ddots & \vdots \\ & & & 1 & s_{(q+n-1)(q+n)} \\ & & & & 1 \end{bmatrix} \tag{4.18}$$

is a $(q+n)\times(q+n)$ unit upper triangular matrix, and

$$\mathbf{W} = \begin{bmatrix} \mathbf{w}_1 & \cdots & \mathbf{w}_{q+n} \end{bmatrix} \tag{4.19}$$

is a $n_s \times (q+n)$ matrix with orthogonal columns that satisfy

$$\mathbf{W}^T\mathbf{W} = \mathbf{D} \tag{4.20}$$

and $\mathbf{D}$ is a positive diagonal matrix.

The Gram-Schmidt procedure calculates $\mathbf{S}$ one column at one time and orthogonalizes $\mathbf{P}$ as follows.

$$\left.\begin{array}{l} \mathbf{w}_1 = \mathbf{p}_1 \\ s_{ik} = \frac{<\mathbf{w}_i, \mathbf{p}_k>}{<\mathbf{w}_i, \mathbf{w}_i>}, 1 \le i < k \\ \mathbf{w}_k = \mathbf{p}_k - \sum_{i=1}^{k-1} s_{ik}\mathbf{w}_i \end{array}\right\} k = 2, \cdots, q+n \tag{4.21}$$

where $<,>$ denotes the inner product.

Define

$$\mathbf{g} = \mathbf{D}^{-1}\mathbf{W}^T\mathbf{Z} \tag{4.22}$$

then the unknown matrix $\mathbf{H}_o$ can be obtained using backward substitution.

$$\mathbf{S}{\mathbf{H}_o}^T = \mathbf{g} \tag{4.23}$$

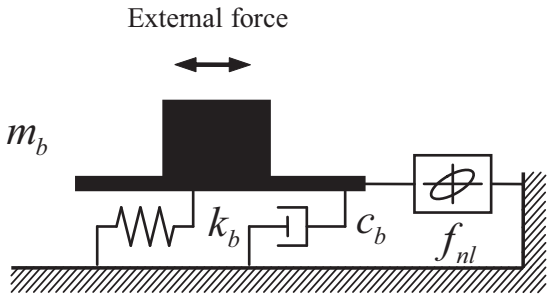

Figure 4.3: SDOF model

4.4 Numerical Simulation

4.4.1 Simulation Model

The Bouc-Wen hysteresis model is adopted for the hysteretic dampers in the dynamic simulation. The differential equation of the Bouc-Wen model is described by Eq. (2.19). A simplest case is considered to study the performance of proposed methods. A single DOF base-isolated system, as shown in Figure 4.3, is subjected to the external force. The equation of motion of this system is

$$m_b\ddot{x} + c_b\dot{x} + k_b x + f_{nl} = F \tag{4.24}$$

where m_b, c_b and k_b are the mass, damping coefficient and stiffness of the SDOF system, respectively. The parameters of the system are defined as in Table 4.1. This system is excited by Gaussian noise with various variance. Obviously, the response depends on the intensity of excitation.

4.4.2 Nonlinearity Function

The nonlinearity function is required to be known before application. This problem can be overcome by assuming a function space as a search space, when the nonlinearity type is not clear. Masri & Caughey (1979) and Masri *et al.* (1982) proposed a nonparametric method named restoring force surface (RFS) methods by using polynomial approximation to fit the experimentally determined restoring force. The nonlinear restoring force is considered as a function of displacement and velocity by an ordinary or Chebyshev polynomial series expansion.

Table 4.1: Parameter values

Argument	Value
m_b	8000 ton
k_b	475000 kN/m
c_b	6000 kN·s/m
β	0.6
γ	0.4
p	1
D_y	1.5 mm
F_y	655.4 kN

When hysteretic nonlinearity is involved, the nonlinear restoring force appears as a multivalued function of displacement and velocity due to its path-dependent nature. The choice of nonlinearity type poses a cumbersome matter. The polynomial approximation of displacement to fit the nonlinear restoring force will result in a memoryless nonlinear stiffness model, losing hysteretic characteristics. The polynomial approximation of displacement and velocity representing the hysteretic force could relax the memoryless property in a certain level, but could not eliminate its multivalued-function property. Hammond *et al.* (1987) proposed to plot the surface of nonlinear force in a selected space (subset of the state vector, SSV). They defined the restoring force derivative with respect to time as a function of velocity and restoring force. Benedettini *et al.* (1995) studied the performance of polynomial approximation of hysteretic systems in detail. It was shown that the SSV formula could fit the experimental response time histories much better than the traditional formula. However, a recursive procedure is required to solve the problem that the hysteretic force is a evaluated through the integration of its derivative. Here, the traditional formula are used to describe the nonlinear force, further investigation will explore the way of integrating SSV models with NIFO methods.

The hysteretic force is approximated by the following series

$$F_h = \sum a_{ij} x^i v^j \tag{4.25}$$

where v is velocity and a_{ij} are coefficients of polynomial terms. The linear terms of

Table 4.2: Simulation and NIFO parameters

Argument	Value
$\Delta t(s)$	0.005
Time span (s)	500
Block size	10000
Overlap (%)	90
Averages n_s	89

displacement and velocity are excluded because they are remained to be identified as a part of the underlying linear system. Each polynomial term could be viewed as a nonlinearity type.

4.4.3 Results by NIFO

The SDOF system is excited by a zero-mean Gaussian random input, whose standard deviation is 798.8 kN so that the maximum displacement response is comparable with the yield displacement of the hysteretic damper, as shown in Figures 4.4 and 4.5. Numerical integration is conducted by using Simulink MATLAB® , and a total number of 10^5 samples has been generated for the NIFO application (Table 4.2).

Polynomial approximation of hysteretic force is up to third order.

$$F_h = a_{20}x^2 + a_{11}xv + a_{02}v^2 + a_{30}x^3 + a_{21}x^2v + a_{12}xv^2 + a_{03}v^3 \tag{4.26}$$

As shown in Figure 4.6, the NIFO and linear estimates are compared with the underlying linear frequency response function. Although the NIFO estimate achieved better performance than the linear estimate, it still can not retrieve the accurate information of the underlying linear system. The reason is that the multivalued-property remains so that the polynomial approximation can not represent the hysteretic force accurately. Figure 4.7 shows the NIFO estimate by using polynomial approximation of displacement only. The memoryless property of the nonlinear approximation function makes the performance worse near the vicinity of resonant frequency.

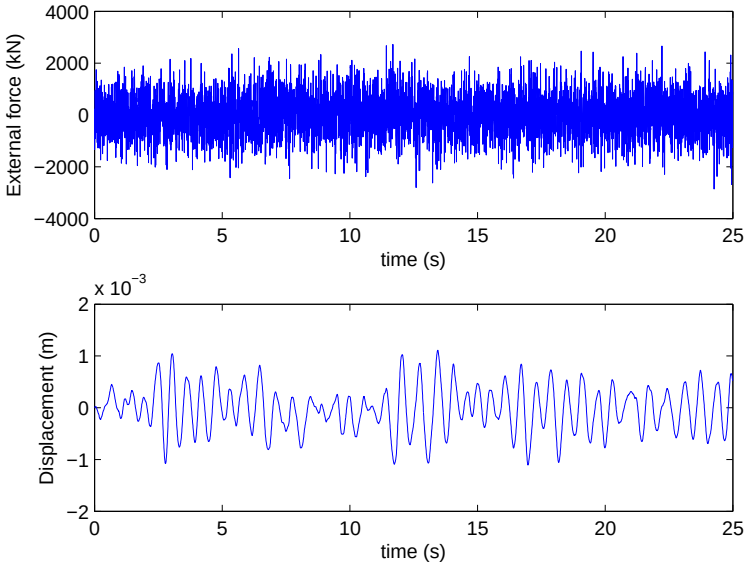

Figure 4.4: Excitation and response (standard deviation of excitation is 798.8 kN)

The system is subject to a more intensive Gaussian random input, whose standard deviation is 2403 kN. The maximum displacement is more than two times of the yield displacement, as shown in Figures 4.8 and 4.9. The NIFO estimate in Figure 4.10 deviates further away from the linear value, when the nonlinearity gets stronger.

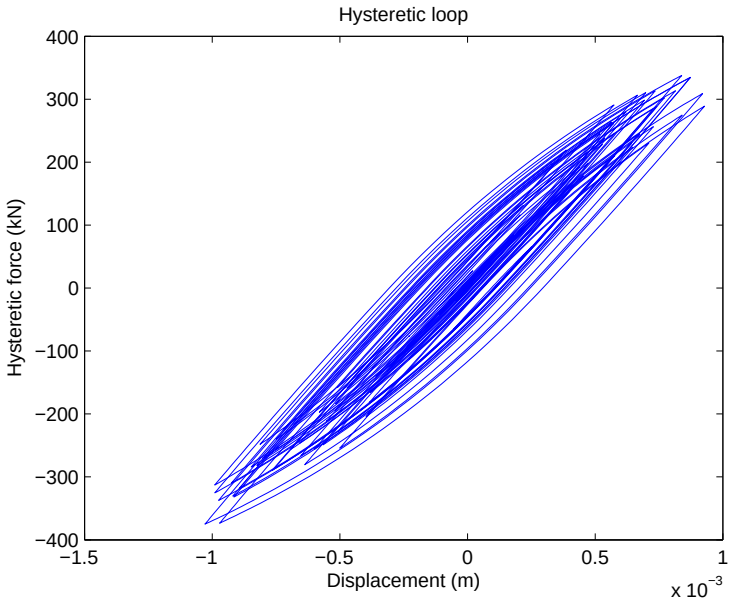

Figure 4.5: Hysteretic loop (standard deviation of excitation is 798.8 kN)

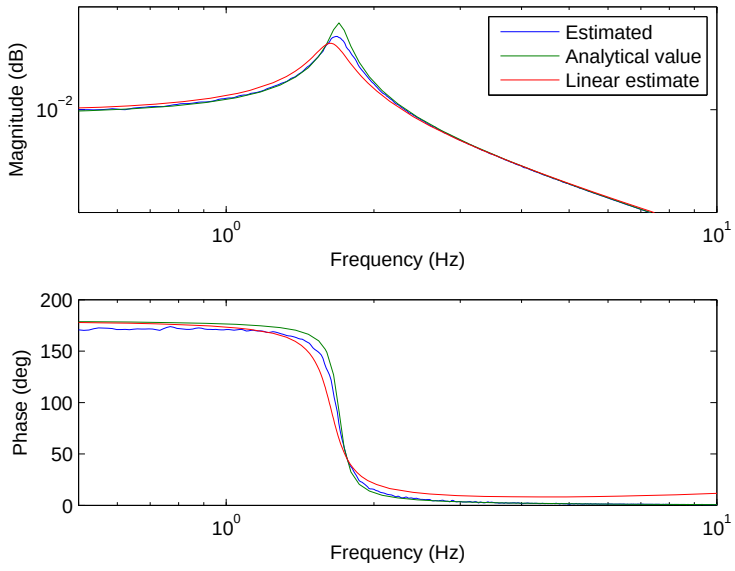

Figure 4.6: Frequency response function by NIFO using polynomial approximation of displacement and velocity

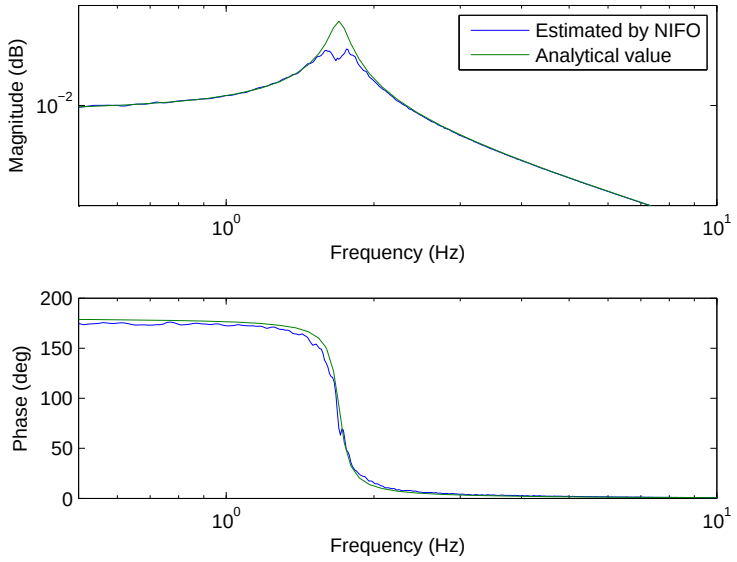

Figure 4.7: Frequency response function by NIFO using polynomial approximation of displacement

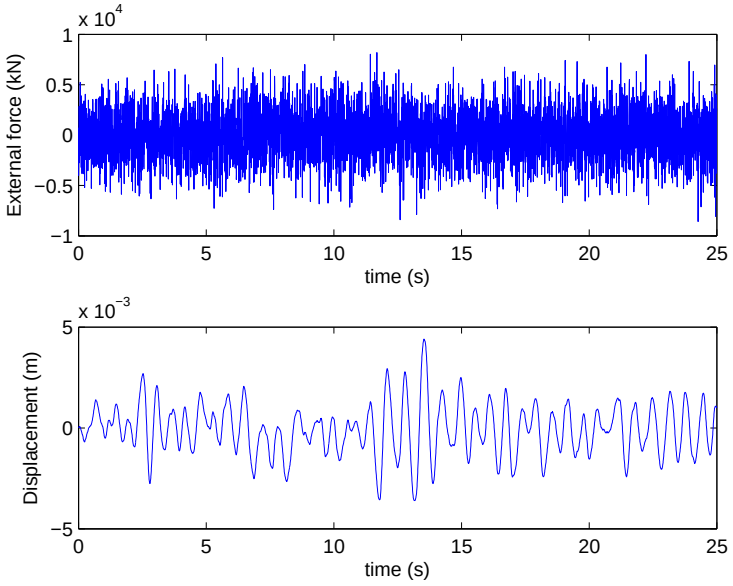

Figure 4.8: Excitation and response (standard deviation of excitation is 2403 kN)

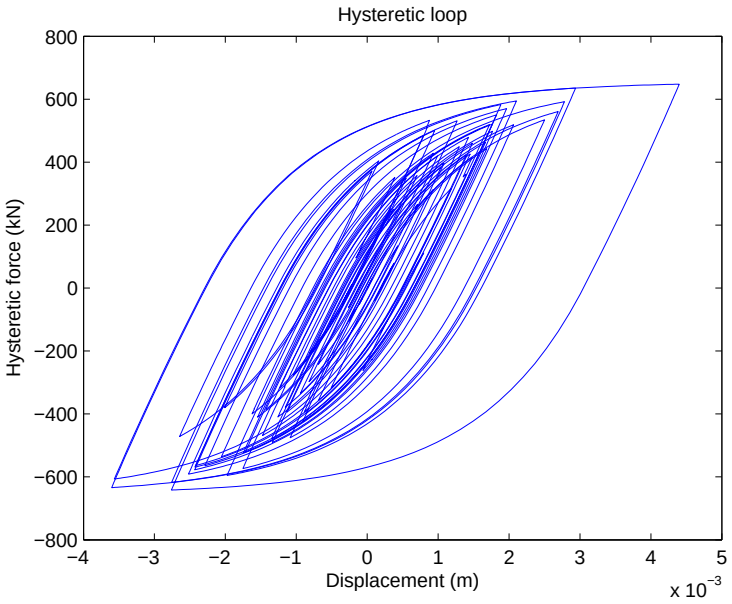

Figure 4.9: Hysteretic loop (standard deviation of excitation is 2403 kN)

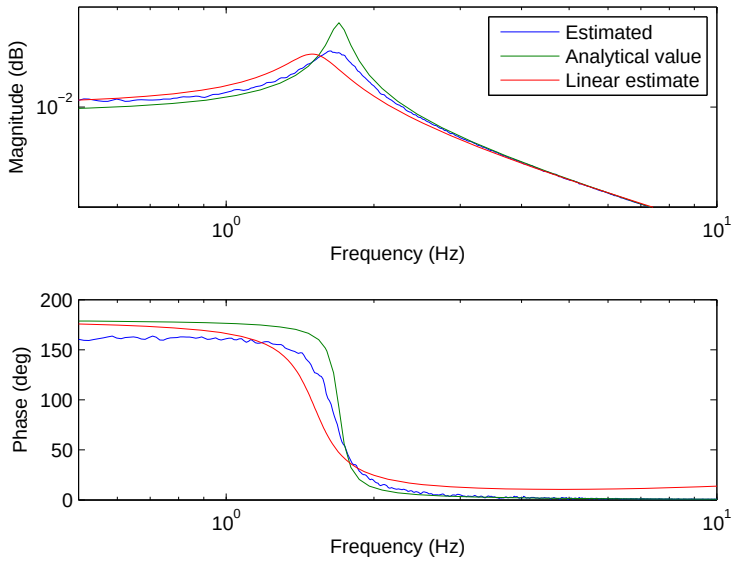

Figure 4.10: Frequency response function by NIFO using polynomial approximation of displacement and velocity

4.5 Conclusions

A nonlinear identification technique named NIFO has been presented to identify hysteretic systems. The hysteretic restoring force is modeled by polynomial approximation of displacement and velocity. The idea of reverse path is attractive for its simplicity. It is able to extract the underlying linear model out of nonlinear systems, and it makes the traditional dynamic characteristics (modal frequencies, mode shapes, etc.) meaningful for indicating the state of nonlinear systems. However, polynomial approximation can not yield the exact hysteretic force due to the inherent multivalued-property of hysteretic systems, so that NIFO can not identify the exact underlying linear model. To overcome the difficulties, SSV model is suggested to model the nonlinear hysteretic force. Further study should be made to explore possible algorithms of nonlinear identification methods.

Chapter 5

Application to Real Buildings

5.1 Raiosha

5.1.1 Overview

The proposed method is applied to a building named Raiosha at Keio University in Yokohama City, Japan. It is a 7-story based-isolated building, 30.95 meters high. The structure of the superstructure is steel frame and the supporting columns are concrete-filled tubes. The base isolation layer is equipped with three kinds of devices: 55 high-damping rubber bearings of 750-900mm in diameter, 6 oil dampers in each direction, and 9 elastic sliding bearings. As illustrated in Figure 5.1, the monitoring system installed in this building has 16 accelerometers at 7 locations and 3 displacement sensors at 2 locations. The sampling frequency of these sensors is 100 Hz. The measurements are stored in a monitoring server and, can be accessed and downloaded via the web.

The earthquake that happened 23 July 2005 in Chiba Prefecture, Japan, was used for analysis. The movement in the x plane was considered for the analysis. The ground motion is plotted in Figure 5.5, the acceleration collected by #1, #2, #4 and #5 (shown in Figure 5.1) in the x direction and the deformation of the isolation layer collected by #102 in the x direction are shown in Figures 5.6 and 5.7.

Yoshimoto *et al.* (2005) developed an algorithm based on the subspace identification to identify the stiffness of the isolation layer and applied it to Raiosha. In

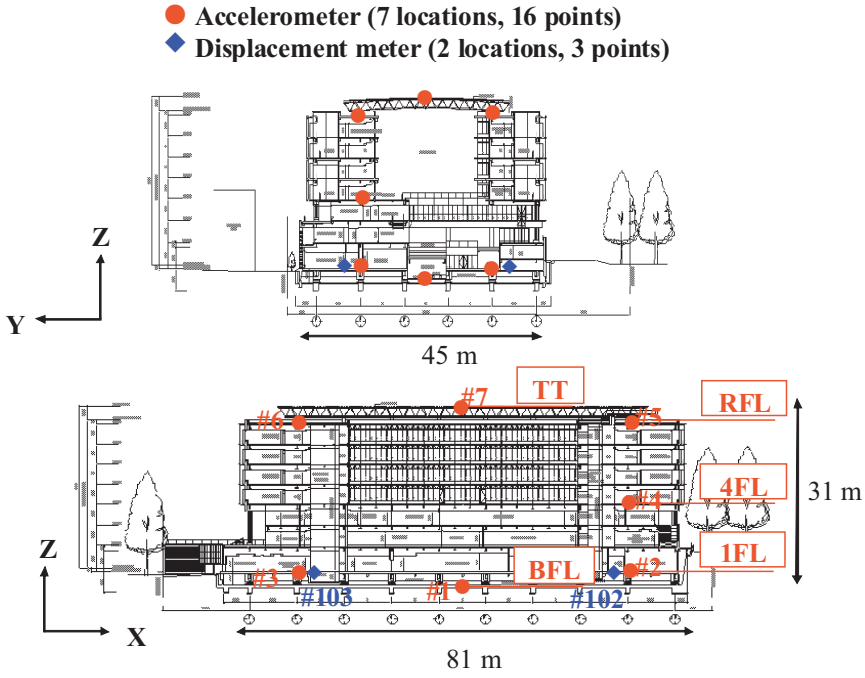

Figure 5.1: Elevation views showing sensor allocation

Figure 5.2: Overview of Raiosha

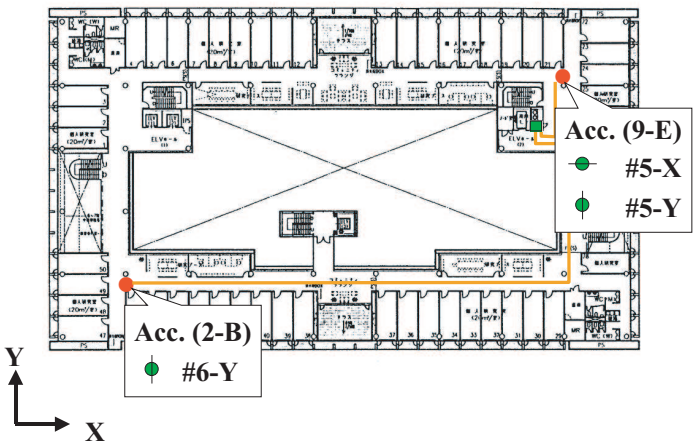

Figure 5.3: Sensor location on the roof

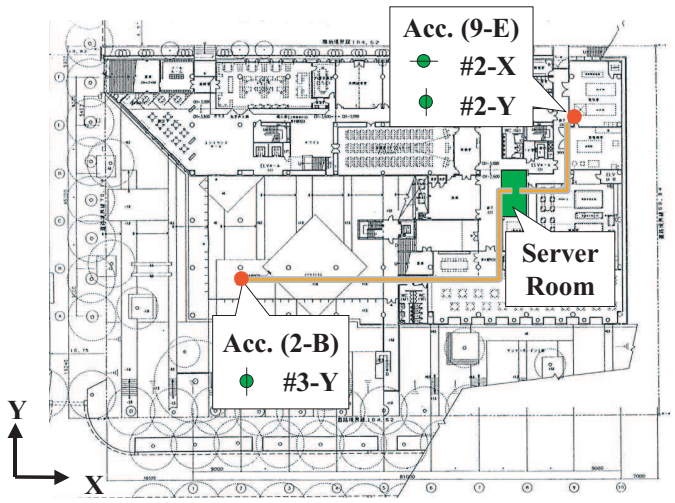

Figure 5.4: Sensor location on the 1st floor

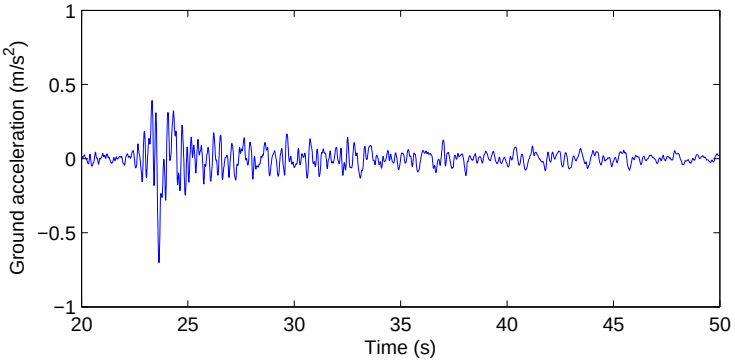

Figure 5.5: Ground acceleration (in x direction)

the paper, when the deformation of the layer is small (with the maximum value 0.76 mm in y direction), the identification succeeded in applying to the simulation case and the existing building under earthquakes. The method is based on linear models, however, and thus nonlinear behaviors are not explicitly considered. The nonlinearity in the isolations is the crucial feature accounting for the behavior of the base-isolated system. This nonlinearity will be illustrated by the force-displacement plot showing the hysteresis, and the amplitude-dependent stiffness and damping coefficient are adopted to relate the nonlinearity with the deformation.

5.1.2 Restoring Force Estimation

The identification of the superstructure is performed under the assumption that it is a linear lightly damped structure. The mode shapes of the superstructure that are identified by the subspace identification method (N4SID) when the acceleration on the 1^{st} floor is taken as the excitation and the accelerations on the 4^{th} floor and the roof are taken as the responses listed in Table 5.1 along with other modal information. We then expand the first two modes (Figure 5.8) and use the expanded mode shapes to estimate the restoring force. The accelerations in modal coordinates are calculated by coordinate transformation (Figure 5.9).

Assuming the estimated mass to be the simulation value, we were able to estimate the restoring force expressed in Eq. (2.16). Figure 5.10 shows the estimated result, and Figure 5.11 shows the force-displacement plot.

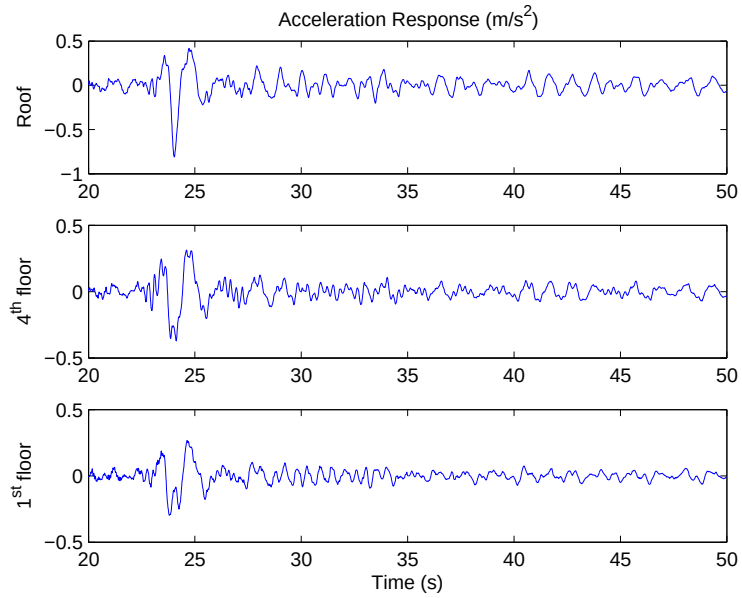

Figure 5.6: Acceleration responses (#2 #4 #5 in x direction)

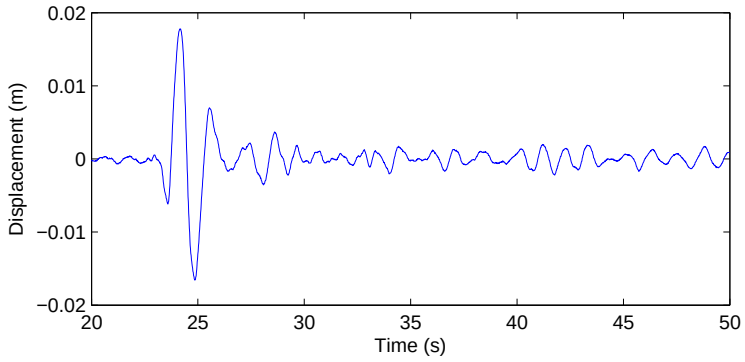

Figure 5.7: Deformation of the isolation layer (#102 in x direction)

Table 5.1: Identified modal information of the superstructure

			Mode shape	
	Frequency (Hz)	Damping ratio (%)	Roof	4$^{\text{th}}$ floor
1$^{\text{st}}$	1.0819	0.0347	1	0.3680
2$^{\text{nd}}$	3.4720	0.0445	1	-1.4671

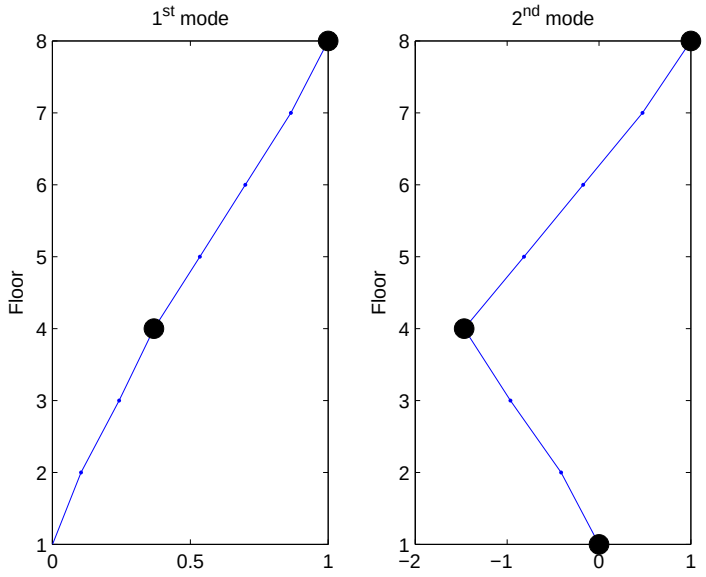

Figure 5.8: Expanded mode shapes

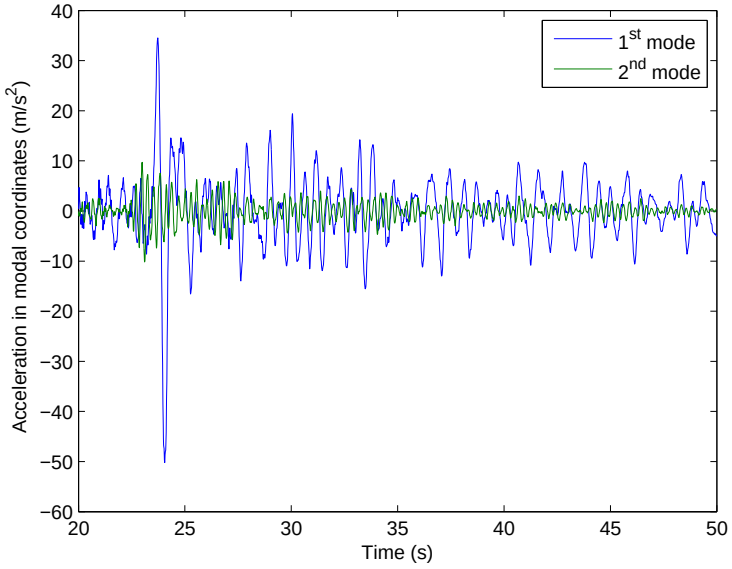

Figure 5.9: Acceleration in modal coordinates

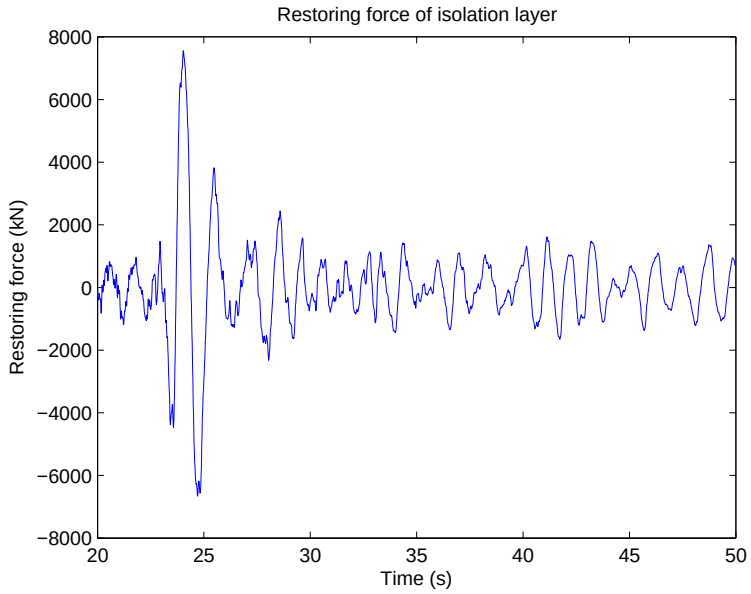

Figure 5.10: Restoring force of the isolation layer

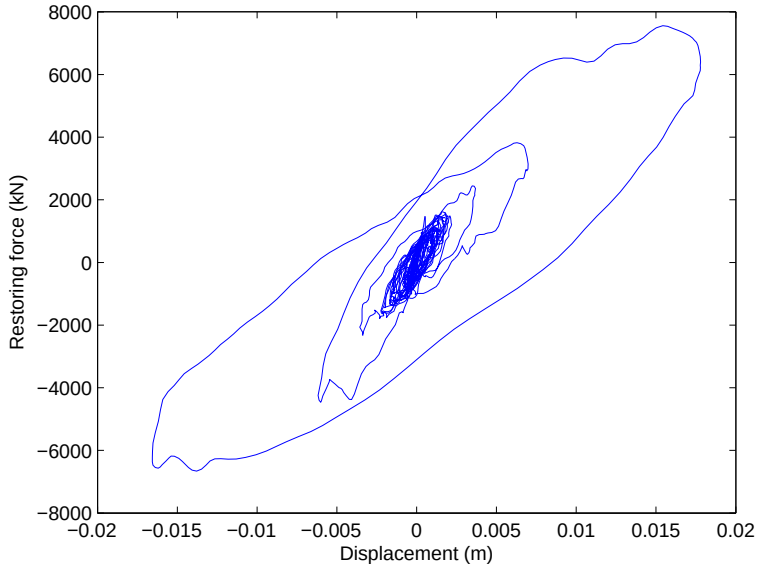

Figure 5.11: Force-displacement plot

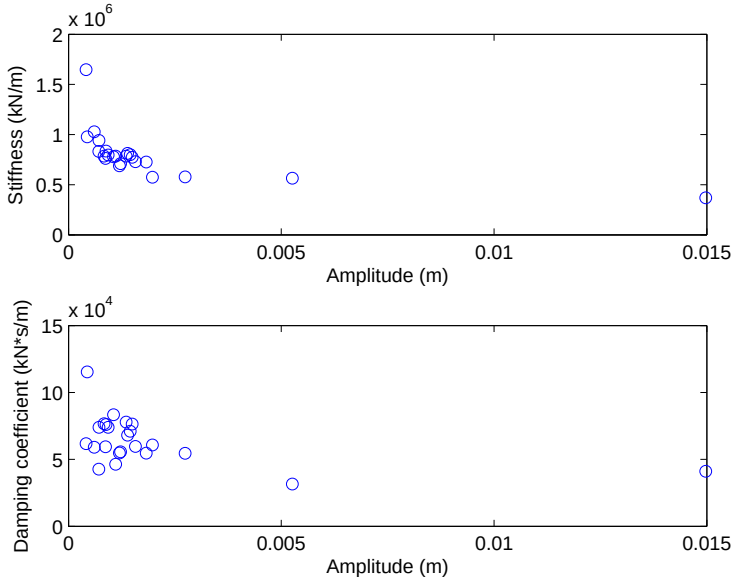

Figure 5.12: Equivalent stiffness and damping coefficient

Figure 5.11 indicates that the isolation layer has strong hysteresis due to its large deformation. However, it is difficult to extract intrinsic state information of the isolation layer from the force-displacement plot. As stated by Stewart *et al.* (1999) and Tobita (1996), the performance of the base-isolated system depends on the vibration intensity. Therefore, it is feasible to represent the state condition of the isolation layer by the equivalent stiffness and damping coefficient, which are evaluated with respect to the deformation of the isolation layer.

If we assume the restoring force consists of the equivalent elastic force and the equivalent viscous force, we can write

$$f(\dot{x}_b, x_b) = k_{eq} x_b + c_{eq} \dot{x}_b \tag{5.1}$$

Restoring force at time t can be estimated by substituting the recorded displacement and velocity into this equation

$$f(t) = \begin{bmatrix} x_b(t) & \dot{x}_b(t) \end{bmatrix} \begin{bmatrix} k_{eq} \\ c_{eq} \end{bmatrix} = \mathbf{H}_t \mathbf{P} \tag{5.2}$$

The minimum least-squares approximation of the coefficient is given by

$$\mathbf{P} = (\mathbf{H}^T \mathbf{H})^{-1} \mathbf{H}^T \mathbf{f} \tag{5.3}$$

where

$$\mathbf{H} = \begin{bmatrix} H_{\Delta t} \\ H_{2\Delta t} \\ \vdots \\ H_t \end{bmatrix} = \begin{bmatrix} x_b(\Delta t) & \dot{x}_b(\Delta t) \\ x_b(2\Delta t) & \dot{x}_b(2\Delta t) \\ \vdots & \vdots \\ x_b(t) & \dot{x}_b(t) \end{bmatrix}$$

and

$$\mathbf{f} = \begin{bmatrix} f(\Delta t) \\ f(2\Delta t) \\ \vdots \\ f(t) \end{bmatrix}$$

The recorded data is sliced into segments, and the equivalent coefficients are estimated within each segment. The average amplitude of the displacement is evaluated by using the following equation

$$A_{eq} = \sqrt{2}\mathrm{RMS}(x_b) \tag{5.4}$$

where RMS means root mean square function.

The estimated stiffness and damping coefficient in the x plane are plotted against the displacement amplitude in Figure 5.12. Both of them decrease with increasing amplitude, as usual, the estimation of the equivalent stiffness is more stable than that of the damping coefficient. The stiffness is very sensitive in the small amplitude range and might drop 50% at a shear strain of 2.5% (the 100% shear strain is at 0.2-m displacement in the design book for Raiosha). Compared to the small amplitude experiment performed by Abe *et al.* (2004), the same decreasing pattern is confirmed.

5.2 Base-Isolated Hospital Building

5.2.1 Overview

The second real application is a hospital building located in Kushiro City, Japan. Base isolation system has been adopted to protect the medical devices and sustain the functionality of this hospital when earthquakes happen. It is a 3-story reinforced-concrete building, 45 meters long in x direction and 40 meters wide in y direction, as illustrated in Figure 5.13. The reinforced-concrete superstructure

is supported by 50 high-damping rubber bearings of 600-750 mm in diameter. The height of rubber bearing is 16.2 cm.

Accelerometers have been installed at three locations in order to monitor the building during earthquakes. The acceleration responses on the ground and the 1^{st} floor are measured in both horizontal (x and y direction) and vertical directions, while the acceleration responses on the roof are measured only in horizontal direction. A thermometer located at the isolation layer is set considering the temperature effect to rubber bearings. Because the air conditioning system in the hospital is in operation 24 hours a day and the isolation layer is sealed for heat preservation, the temperature effect to rubber bearings is not considered in this application. The analysis is conducted in x and y direction, respectively, without considering the coupling effect between these two directions.

5.2.2 Restoring Force Estimation

5.2.2.1 Tokachi-oki Earthquake in 2003

The acceleration record was obtained during Tokachi-oki earthquake on September 26^{th}, 2003, as in Figures 5.14 and 5.15. The deformation of the isolation layer is calculated by Fourier transformation from acceleration difference between the ground and the 1^{st} floor. The acceleration difference is first filtered by a band-pass filter to remove the slow drift and high frequency noise. Then, the Fourier transformation of deformation is derived from that of the filtered signal due to their mathematical connection in frequency domain. The deformation in time domain is computed by inverse Fourier transformation. The deformation of the isolation layer is plotted in plan view in Figure 5.16. The maximum deformation is 13.4 cm in x direction, the rubber bearing experienced extremely large deformation with over 80% shear strain (maximum deformation/height of rubber bearing).

Before the restoring force estimation, nonparametric methods are utilized to get some prior information about the building. The transfer function of the superstructure is shown in Figures 5.17 and 5.18, taking the acceleration on the 1^{st} floor as inputs and the acceleration on the roof as outputs. The first resonant

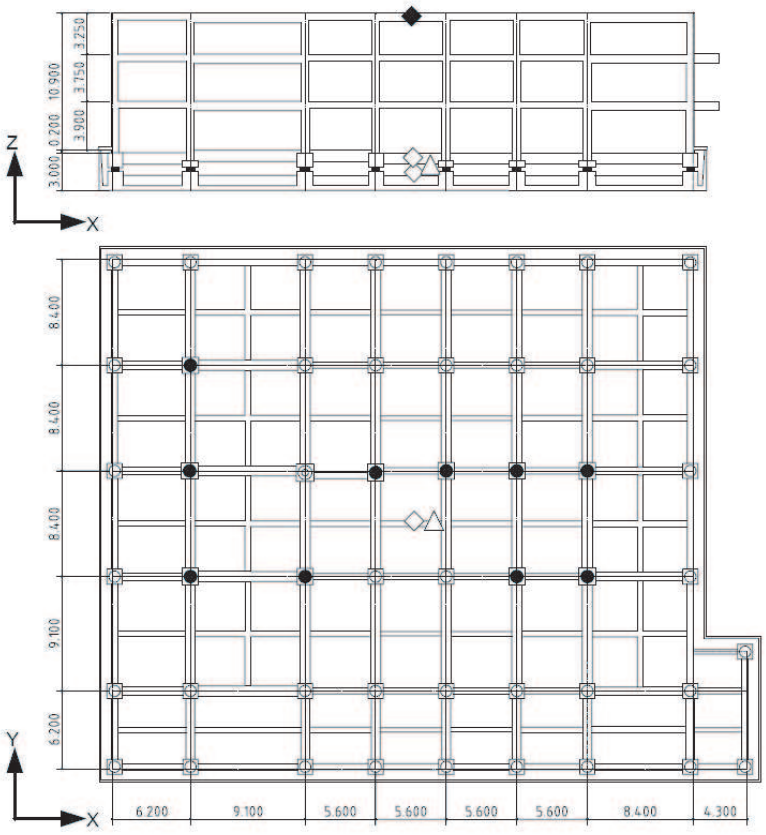

Figure 5.13: Overview of a hospital building in Kushiro City

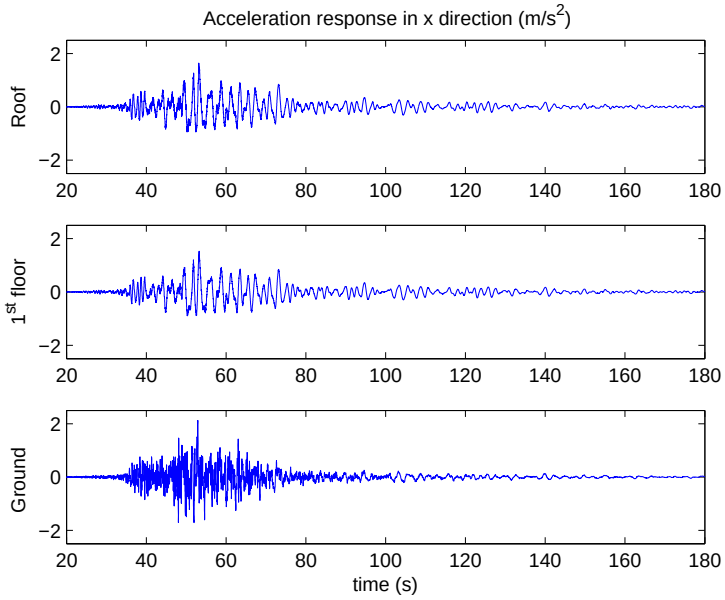

Figure 5.14: Acceleration response in x direction

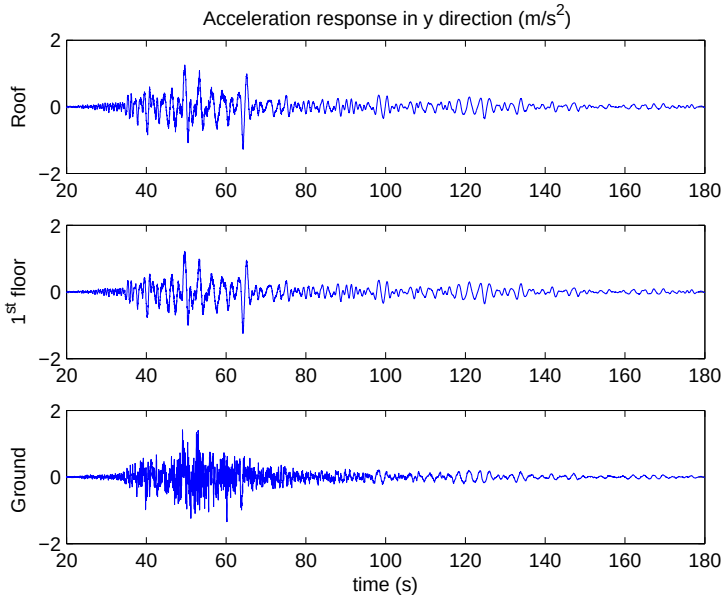

Figure 5.15: Acceleration response in y direction

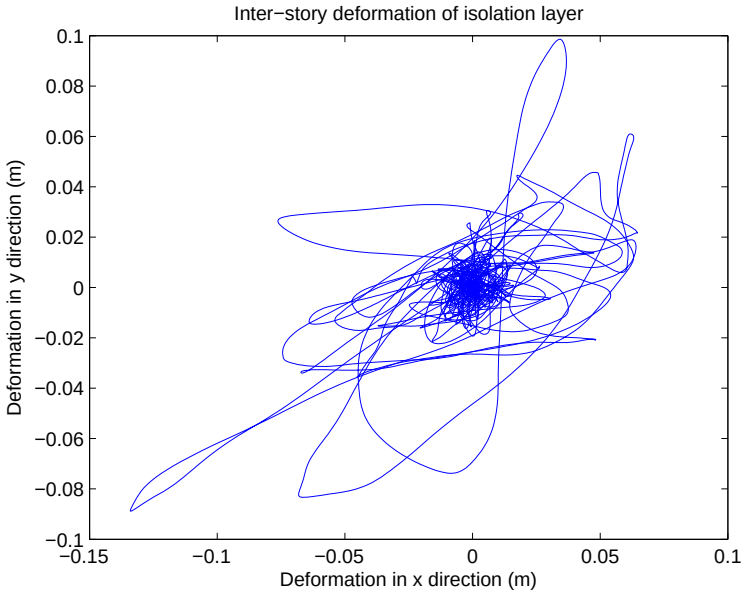

Figure 5.16: Deformation of isolation layer

frequencies in both directions are around 4.5 Hz. It tells that the reinforced-concrete superstructure is quite stiff in both directions. The transfer function of the whole structure is shown in Figures 5.19 and 5.20, taking the acceleration on the ground as inputs and the acceleration on the roof as outputs. The first resonant frequencies in both directions are around 0.5 Hz, far smaller than that of the superstructure. The rubber bearings effectively isolate the superstructure from the ground and elongate the period.

The mode shapes of the superstructure are identified by the subspace identification method (N4SID) from the data set between 20 s to 180 s. Because the superstructure is rather rigid, only the first mode shape (Figure 5.21) is selected to estimate the restoring force. The hysteresis loops are illustrated in Figures 5.22 and 5.23.

By the same procedure applied to Raiosha, the equivalent stiffness and damping coefficient (Figures 5.24 and 5.25) every 2 seconds per segment (close to the period of the first mode) are calculated with respect to the deformation of the isolation layer. The equivalent stiffness starts at a very high level because the rubber bearings restore toward the initial loading stiffness during the interval

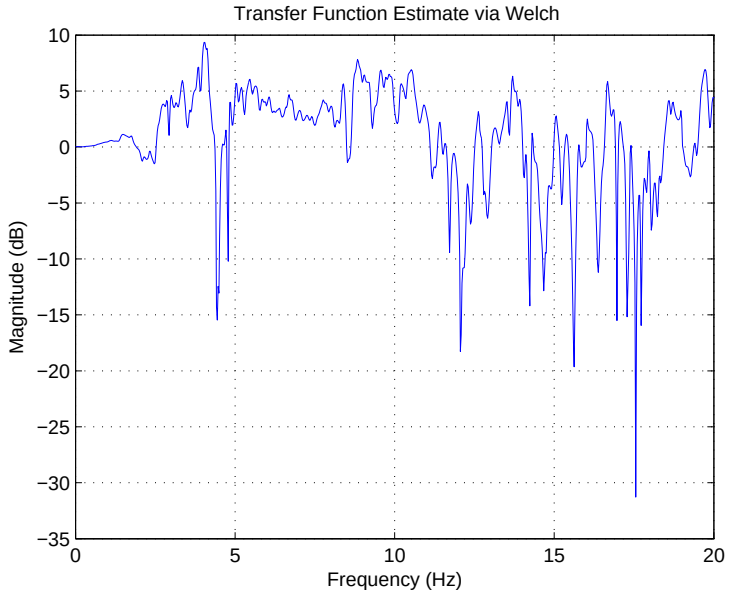

Figure 5.17: Estimated transfer function of superstructure in x direction (input: acceleration on the 1st floor, output: acceleration on the roof)

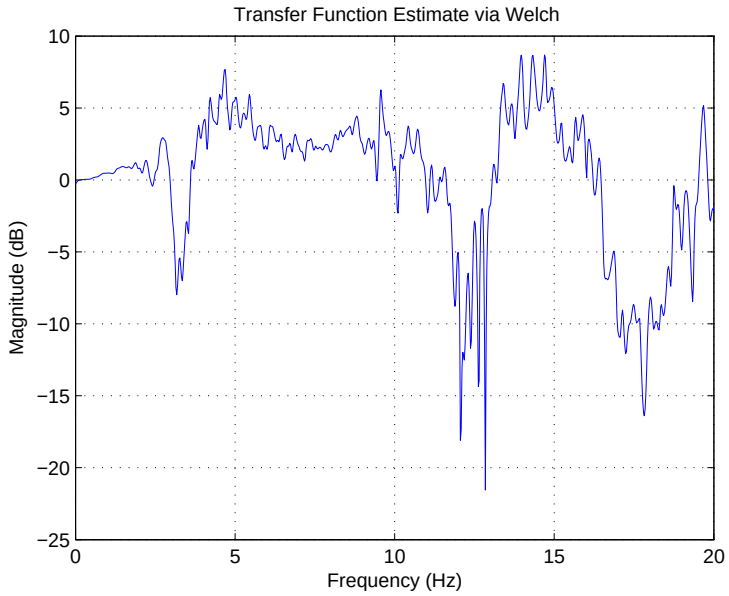

Figure 5.18: Estimated transfer function of superstructure in y direction (input: acceleration on the 1st floor, output: acceleration on the roof)

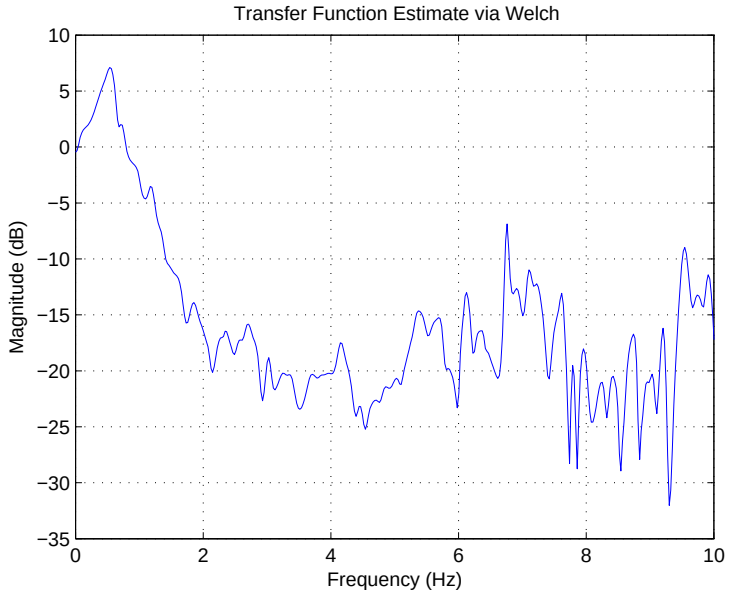

Figure 5.19: Estimated transfer function of whole structure in x direction (input: acceleration on the ground, output: acceleration on the roof)

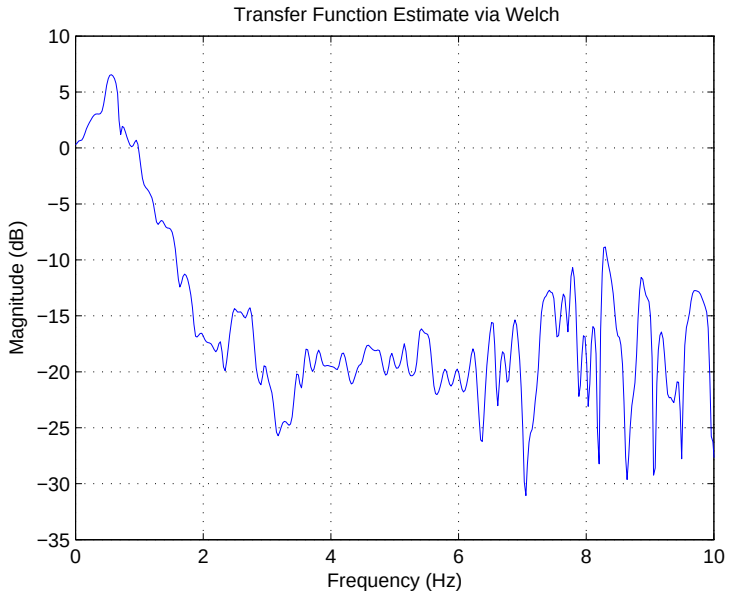

Figure 5.20: Estimated transfer function of whole structure in y direction (input: acceleration on the ground, output: acceleration on the roof)

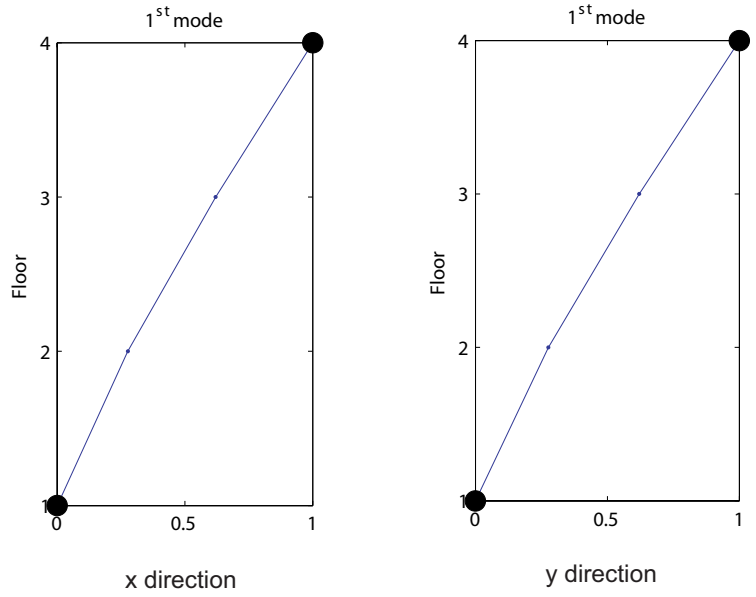

Figure 5.21: Expanded 1st mode shape

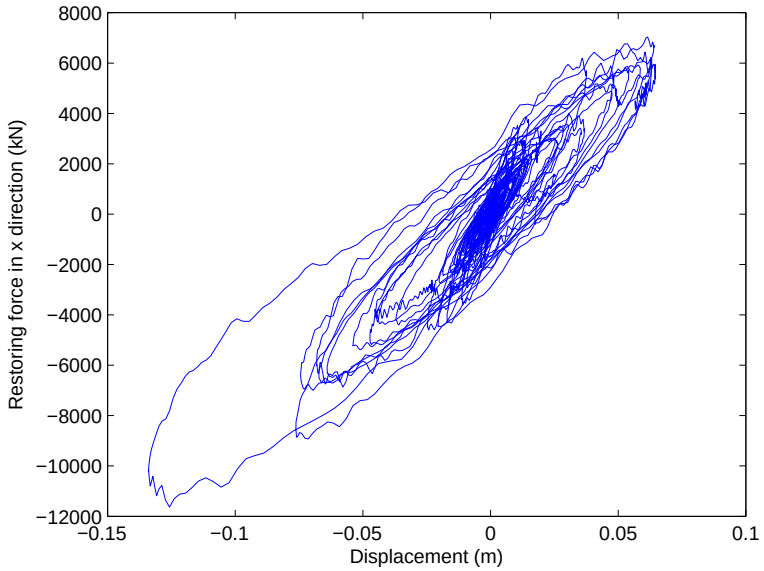

Figure 5.22: Hysteresis loop of isolation layer in x direction

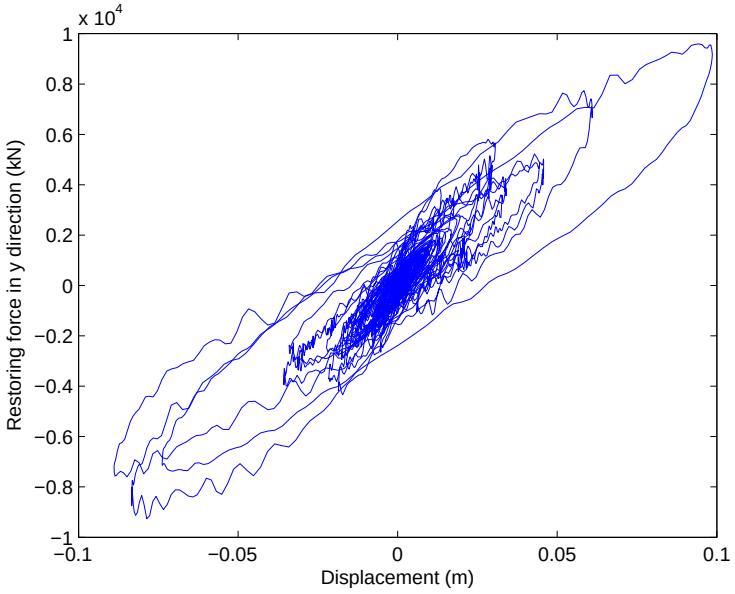

Figure 5.23: Hysteresis loop of isolation layer in y direction

between severe earthquakes yielding extreme deformation. To remove this effect, the equivalent values are recomputed based on the data set between 50 s to 180 s, as plotted in Figure 5.26 and Figure 5.27. The time span for each segment is set at 1 second for more samples. The range of deformation is set between 0 to 0.02 m for aftermentioned comparison. The equivalent stiffness in both directions shows that its dependence on deformation. The same pattern as Raiosha's results is confirmed.

5.2.2.2 Kushiro-oki Earthquake in 2004

In oder to track the state and characteristics of the isolation layer, the proposed method is applied to another acceleration response (Figures 5.28 and 5.29) observed during Kushiro-oki earthquake occurred on November 29$^{\text{th}}$, 2004. The deformation of the isolation layer is calculated in the same way, as plotted in Figure 5.30. The maximum deformation is 4.3 cm in y direction.

The superstructure are identified by the subspace identification method to obtain the first mode shapes in both directions. The estimated restoring force are plotted against the deformation in Figures 5.31 and 5.32 from 20 s to 180

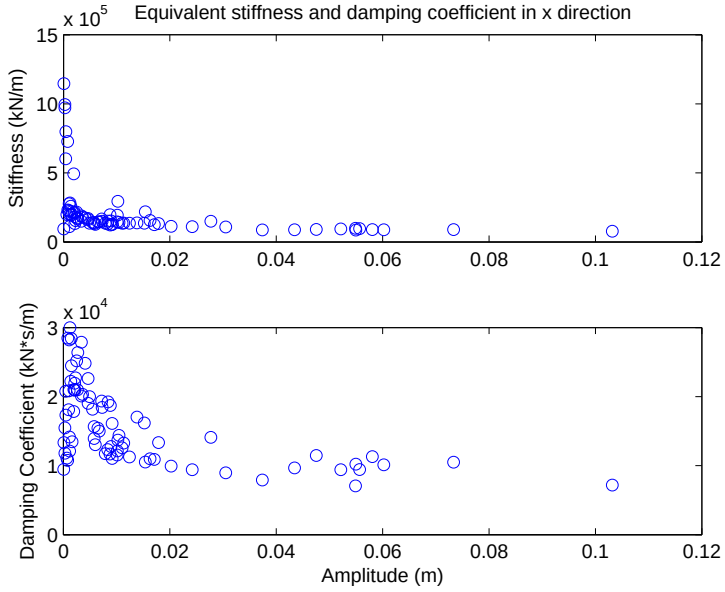

Figure 5.24: Equivalent stiffness and damping coefficient in x direction (from 20 s to 180 s, 2 s per segment)

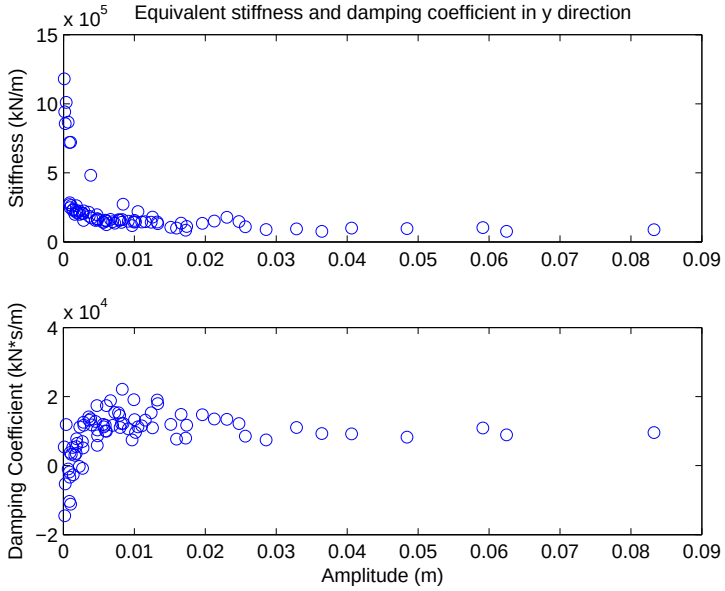

Figure 5.25: Equivalent stiffness and damping coefficient in y direction (from 20 s to 180 s, 2 s per segment)

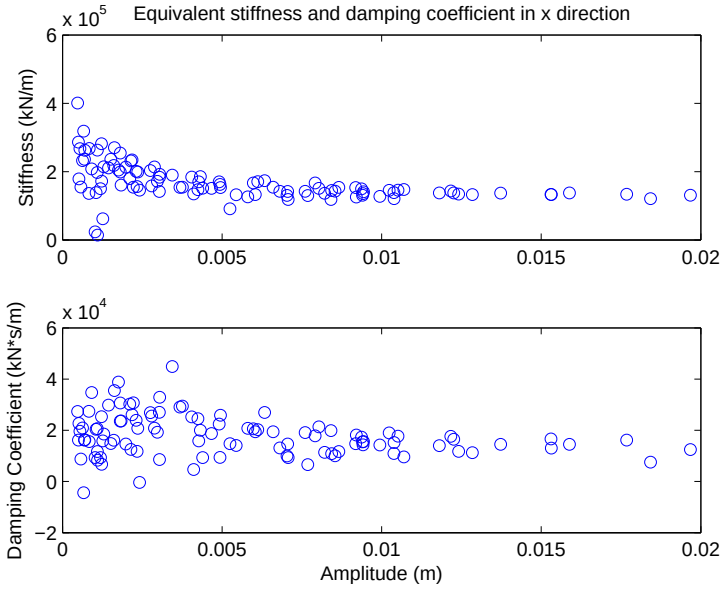

Figure 5.26: Equivalent stiffness and damping coefficient in x direction (from 50 s to 180 s, 1 s per segment)

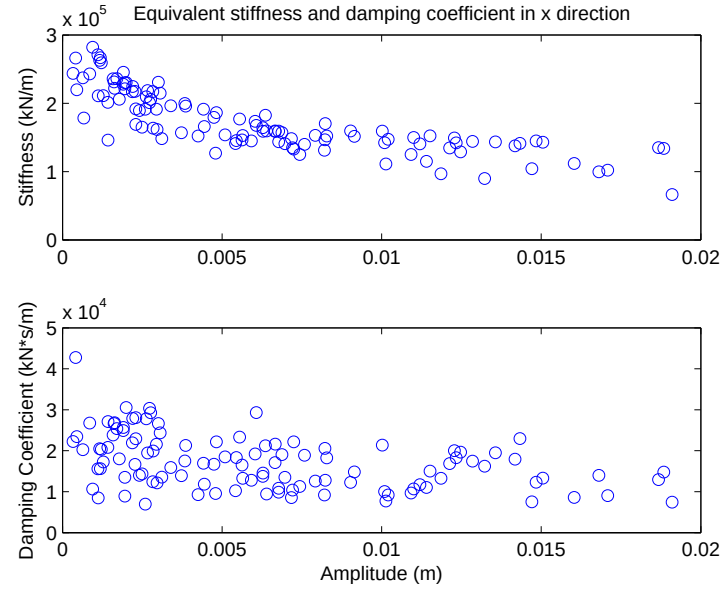

Figure 5.27: Equivalent stiffness and damping coefficient in y direction (from 50 s to 180 s, 1 s per segment)

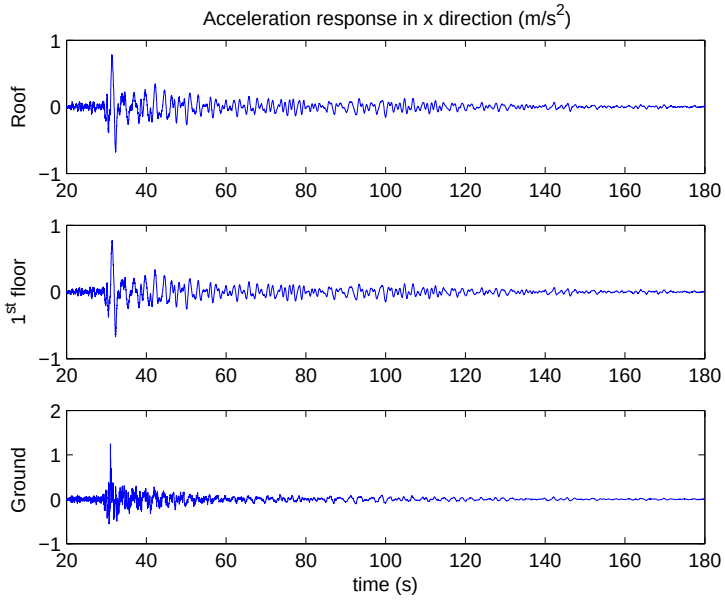

Figure 5.28: Acceleration responses in x direction

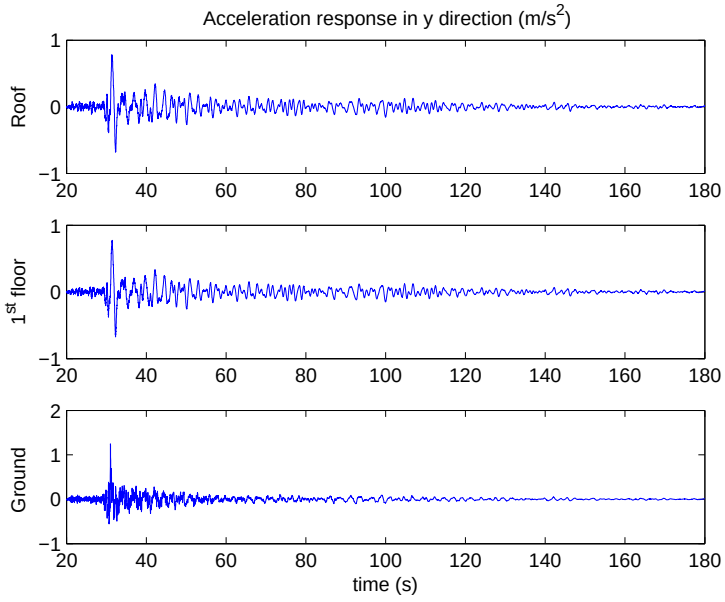

Figure 5.29: Acceleration responses in y direction

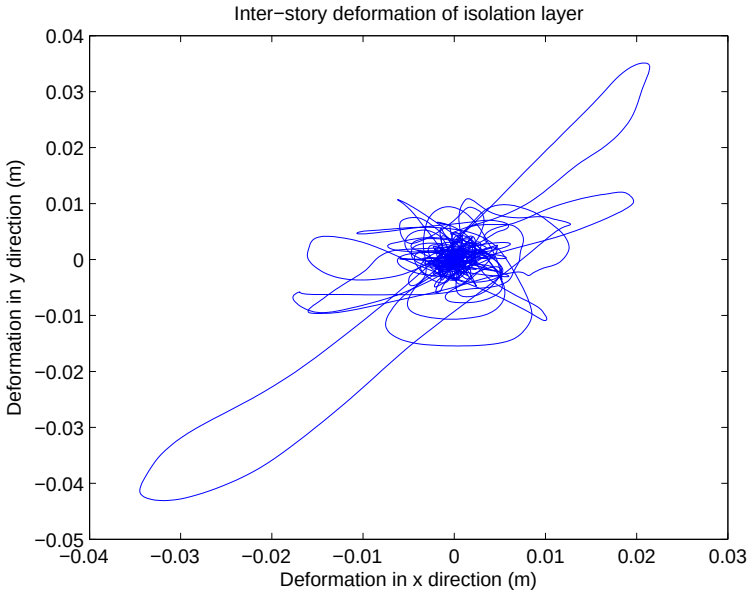

Figure 5.30: Deformation of isolation layer

s. The equivalent stiffness and damping coefficient are shown in Figures 5.33 and 5.34. Comparing with Figures 5.26 and 5.27, the equivalent stiffness in both directions has smaller variance and is slightly higher in small deformation range.

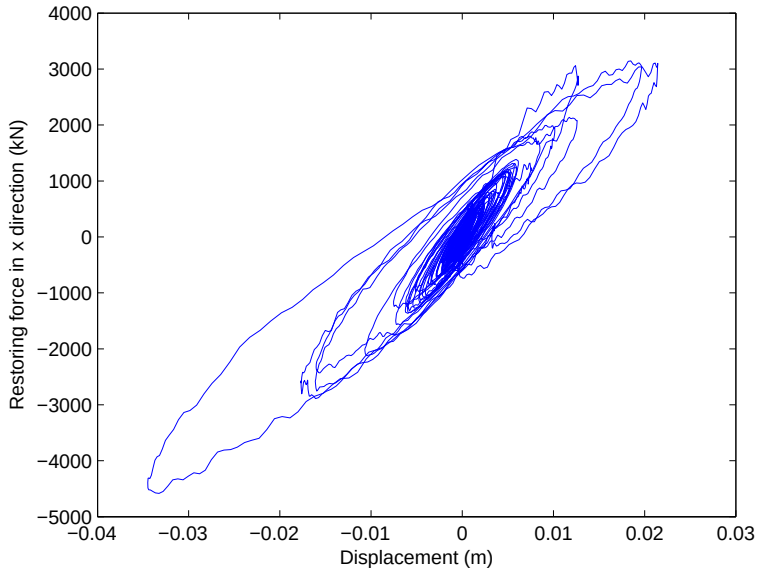

Figure 5.31: Hysteresis loop of isolation layer in x direction

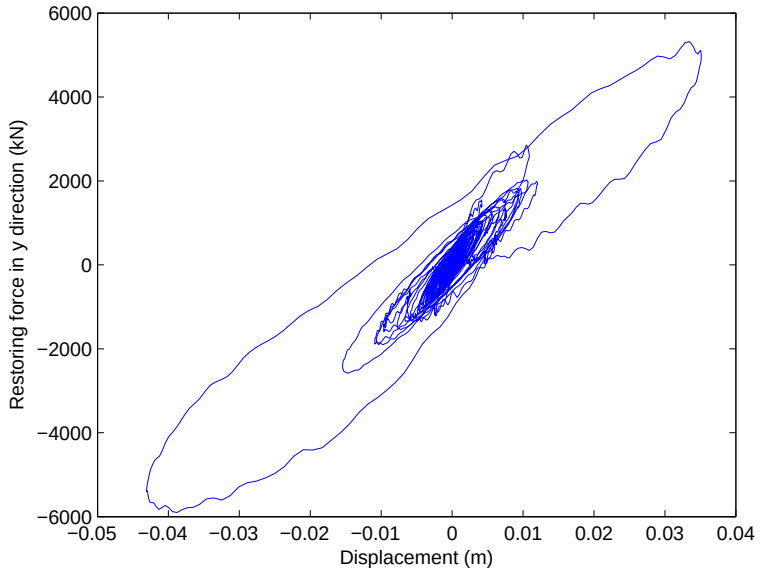

Figure 5.32: Hysteresis loop of isolation layer in y direction

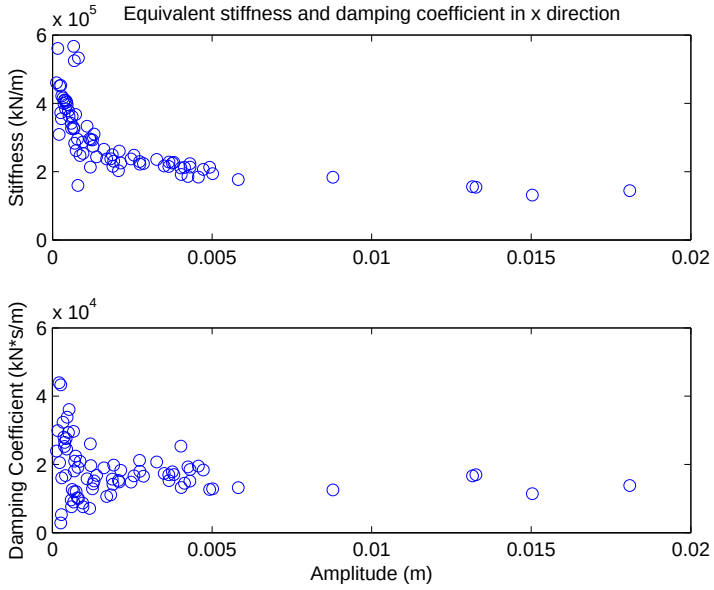

Figure 5.33: Equivalent stiffness and damping coefficient in x direction (from 20 s to 180 s, 2 s per segment)

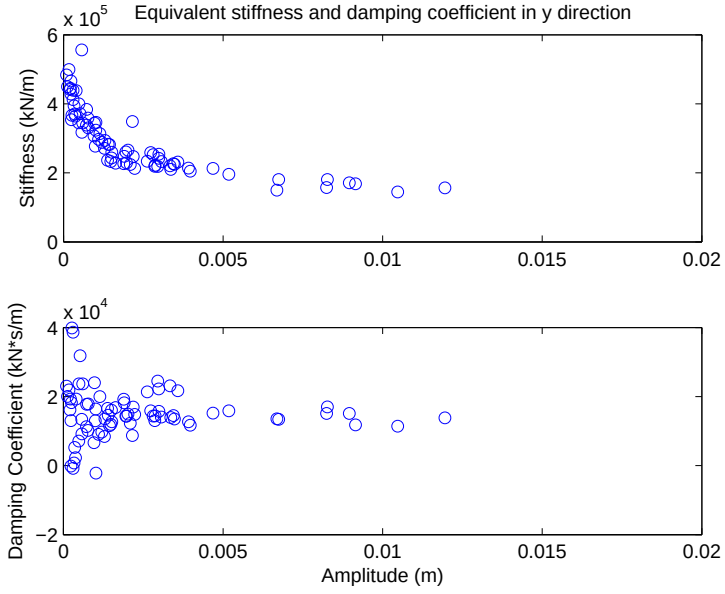

Figure 5.34: Equivalent stiffness and damping coefficient in y direction (from 20 s to 180 s, 2 s per segment)

5.3 Conclusions

The restoring force estimation method was applied to two real base-isolated structures, Raiosha at Keio University and a hospital in Kushiro City. The estimated restoring force has strong hysteresis property in both cases. The amplitude-dependent equivalent stiffness and damping coefficient were adopted to describe the nonlinearity of the isolation layer. The equivalent stiffness of the base isolation layer depends on the deformation and decreases with increasing deformation. The identified results by the proposed method reconfirmed the experimental observation of nonlinearity in the isolation layer made up of rubber bearings.

Chapter 6

Conclusions

This thesis made contribution to identifying the base-isolated structures subjected to severe earthquakes, which possess strong hysteretic nonlinearity. The identification methods were investigated in two schemes.

One scheme separates the whole structure into a linear superstructure and a nonlinear base isolation layer. A new method based on component mode synthesis was presented for estimating the restoring force of an isolation layer. The hybrid motion equation involving the modal coordinates and the physical coordinates is derived by using a substructuring technique. This method is applicable when the number of sensors is limited because only the mode shape information of the superstructure and the estimated mass are needed for estimating the restoring force. It was shown that the proposed method is not sensitive to the mass distribution and the expanded mode shapes but will be scaled by the total mass. The effectiveness of this method was validated in simulations and in application to real base-isolated structures. The amplitude-dependent equivalent stiffness and damping coefficient are adopted to describe the nonlinearity of the isolation layer. The identified results by the proposed method reconfirmed the experimental observation of nonlinearity in the isolation layer.

The other scheme separates the whole structure into an underlying linear structure and a nonlinear component. A nonlinear identification technique named NIFO has been presented to identify hysteretic systems in this scheme. The hysteretic restoring force is modeled by polynomial approximation of displacement and velocity. The idea of reverse path is attractive for its simplicity. It is able

to extract the underlying linear model out of nonlinear systems, makes the traditional dynamic characteristics meaningful for indicating the state of nonlinear systems. However, polynomial approximation can not yield the exact hysteretic force due to the inherent multivalued-property of hysteretic systems, so that NIFO can not identify the exact underlying linear model. To overcome the difficulties, SSV model is suggested to model the nonlinear hysteretic force. Further study should be made to explore possible algorithms of nonlinear identification methods.

In the first scheme, the identification of the superstructure is necessary for mode shape extraction. The identifiability condition for substructural identification was investigated by spectral analysis and parametric methods in order that we can make sure that the identified results are accurate and reliable in what condition. An eternal excitation will always assure the identifiability of the superstructure. In case of free vibration, spectral analysis in the frequency domain cannot obtain the identifiability of a superstructure. If the base layer is governed by a linear feedback law, the identifiability of the superstructure is lost unless there are at least two regulators. By making the regulators nonlinear, identifiability can be regained with parametric methods. In a free-vibration field test, the identification of a linear substructure under linear feedback laws can be guaranteed if a nonlinear device is attached to the rest of the structure. The feedback, determined by the characteristics of the regulator, has a greater influence on the identifiability than does the model structure or the identification method.

Appendix A

Subspace Identification

The subspace identification formulates and solves a major part of the identification problem on a signal level. The main characteristic of these schemes is the approximation of a subspace defined by the span of the column or row space of matrices determined by the input-output data. The parametric time-invariant model is calculated from these spans by exploiting their special structure, such as the shift-invariance property. Subspace identification methods take advantage of robust numerical techniques such as QR factorization and singular value decomposition (SVD). For brevity, only an archetypical procedure is illustrated in this paper.

Given a deterministic-stochastic state-space model with a p-dimensional output y_t and a m-dimensional input u_t

$$\begin{aligned} x_{t+1} &= Ax_t + Bu_t + w_t \\ y_t &= Cx_t + Du_t + v_t \end{aligned} \tag{A.1}$$

where w_t and v_t are unmeasurable disturbances respectively called process error and measurement error and x is a n-dimensional state space vector.

From Eq. (A.1) we can formulate the k-step ahead predictor y_{t+k} by expanding x_{t+k}. Then we form the equation

$$Y_r(t) = O_r x_t + S_r U_r(t) + V(t) \tag{A.2}$$

where

$$Y_r(t) = \begin{bmatrix} y_t \\ y_{t+1} \\ \vdots \\ y_{t+r-1} \end{bmatrix}, U_r(t) = \begin{bmatrix} u_t \\ u_{t+1} \\ \vdots \\ u_{t+r-1} \end{bmatrix}$$

$$O_r = \begin{bmatrix} C \\ CA \\ \vdots \\ CA^{r-1} \end{bmatrix}, S_r = \begin{bmatrix} D & 0 & \cdots & 0 \\ CB & D & \cdots & 0 \\ \vdots & \vdots & \ddots & \vdots \\ CA^{r-2}B & CA^{r-3}B & \cdots & D \end{bmatrix}$$

And the kth block component of $V(t)$ is

$$V_k(t) = CA^{k-2}w_t + CA^{k-3}w_{t+1} + \cdots + Cw_{t+k-2} + v_{t+k-1} \tag{A.3}$$

$O_r$is the extended observability matrix for the system. To eliminate the term with $U_r(t)$ and make the noise influence from $V(t)$ disappear asymptotically, we introduce

$$\mathbf{Y} = [\, Y_r(1) \quad Y_r(2) \quad \cdots \quad Y_r(N) \,]$$

$$\mathbf{X} = [\, x_1 \quad x_2 \quad \cdots \quad x_n \,]$$

$$\mathbf{U} = [\, U_r(1) \quad U_r(2) \quad \cdots \quad U_r(N) \,]$$

$$\mathbf{V} = [\, V(1) \quad V(2) \quad \cdots \quad V(N) \,]$$

We can rewrite Eq. (A.2) as

$$\mathbf{Y} = O_r\mathbf{X} + S_r\mathbf{U} + \mathbf{V} \tag{A.4}$$

and form an $N \times N$ matrix orthogonal to the matrix $\mathbf{U}$

$$\Pi^{\perp}_{\mathbf{U}^T} = \mathbf{I} - \mathbf{U}^T(\mathbf{U}\mathbf{U}^T)^{-1}\mathbf{U} \tag{A.5}$$

Multiplying Eq. (A.4) by $\Pi^{\perp}_{\mathbf{U}^T}$ will eliminate the term with $\mathbf{U}$, yielding

$$\mathbf{Y}\Pi^{\perp}_{\mathbf{U}^T} = O_r\mathbf{X}\Pi^{\perp}_{\mathbf{U}^T} + \mathbf{V}\Pi^{\perp}_{\mathbf{U}^T} \tag{A.6}$$

By correlating with a suitable matrix Φ (Van Overschee & de Moor, 1996), the noise term can be removed as well. Thus we have

$$G = \frac{1}{N}\mathbf{Y}\Pi^{\perp}_{\mathbf{U}^T}\Phi^T \tag{A.7}$$

The column space can reduced by using singular value decomposition (SVD). If has rank n, only the first n singular values will be non-zero. So we have

$$G = USV^T = \begin{bmatrix} U_1 & U_2 \end{bmatrix} \begin{bmatrix} S_1 & 0 \\ 0 & S_2 \end{bmatrix} \begin{bmatrix} V_1^T \\ V_2^T \end{bmatrix} = U_1 S_1 V_1^T \tag{A.8}$$

where S_1 is the $N \times N$ upper left part of S.

An estimate of the extended observability matrix may be obtained as $\hat{O}_r = U_1 S_1$. We finally can estimate the system matrices C by using the first block row of O_r and estimate the system matrix A by using the shift property. Once we have C and A, we can estimate the matrices B and D by solving a linear least-squares problem. It is worth noting that the left and right weighting matrices for the oblique projection G determine a wide class of subspace algorithms, such as N4SID (Van Overschee & De Moor, 1993), MOESP (Verhaegen, 1994) and CVA (Larimore, 1990).

References

Abe, M., Yoshida, J. & Fujino, Y. (2004). Multiaxial behaviors of laminated rubber bearings and their modeling. i: experimental study. *Journal of Structural Engineering*, **130**, 1119–1132. 2, 77

Adams, D. & Allemang, R. (1998). Survey of nonlinear detection and identification techniques for experimental vibrations. *Proceedings of the International Conference on Noise and Vibration Engineering*, 269–281. 5, 6

Adams, D. & Allemang, R. (2000). A frequency domain method for estimating the parameters of a non-linear structural dynamic model through feedback. *Mechanical Systems and Signal Processing*, **14**, 637–656. 11, 55, 58

Adams, D. & Allemang, R. (2001). Residual frequency autocorrelation as an indicator of non-linearity. *International Journal of Non-Linear Mechanics*, **36**, 1197–1211. 8

Adams, D.E. (2002). Frequency domain arx model and multi-harmonic FRF estimators for non-linear dynamic systems. *Journal of Sound and Vibration*, **250**, 935–950. 9

Akaike, H. (1967). Advanced seminar on spectral analysis of time series. 40, 44, 53

Al-Hadid, M. & Wright, J. (1989). Developments in the force-state mapping technique for non-linear systems and the extension to the location of non-linear elements in a lumped-parameter system. *Mechanical Systems and Signal Processing*, **3**, 269–290. 9

Andronikou, A.M., Bekey, G.A. & Hadaegh, F.Y. (1983). Identifiability of nonlinear systems with hysteretic elements. *Journal of Dynamic Systems, Measurement and Control, Transactions ASME*, **105**, 209–214. 12

Baber, T. & Noori, M. (1986). Modeling general hysteresis behavior and random vibration application. *Journal Of Vibration, Acoustics, Stress, and Reliability in Design*, **108**, 411–420. 25

Bendat, J. (1990). *Nonlinear system analysis and identification from random data*. Wiley New York. 11, 55

Benedettini, F., Capecchi, D. & Vestroni, F. (1995). Identification of hysteretic oscillators under earthquake loading by nonparametric models. *Journal of Engineering Mechanics*, **121**, 606. 10, 62

Bouc, R. (1967). Forced vibration of mechanical systems with hysteresis. *Proceedings of the 4th Conference on Nonlinear Oscillations, Prague, Czechoslovakia*, 315. 3, 25

Box, G. & MacGregor, J. (1974). The analysis of closed-loop dynamic-stochastic systems. *Technometrics*, **16**, 391–398. 41, 45

Carli, F. (1999). Nonlinear response of hysteretic oscillator under evolutionary excitation. *Advances in Engineering Software*, **30**, 621–630. 25

Charalampakis, A.E. & Koumousis, V.K. (2008). Identification of Bouc-Wen hysteretic systems by a hybrid evolutionary algorithm. *Journal of Sound and Vibration*, **314**, 571–585. 13

Chatterjee, A. & Vyas, N.S. (2001). Stiffness non-linearity classification through structured response component analysis using Volterra series. *Mechanical Systems and Signal Processing*, **15**, 323–336. 9

Choi, D., Chang, J. & Powers, E. (1982). Bispectral identification of non-linear mode interactions. *Proceedings of the International Modal Analysis Conference*. 8

Collis, W., White, P. & Hammond, J. (1998). Higher-order spectra: the bispectrum and trispectrum. *Mechanical Systems and Signal Processing*, **12**, 375–394. 8

Craig, R. (1985). A review of time-domain and frequency-domain component mode synthesis method. *Combined Experimental/Analytical Modeling of Dynamic Structural Systems*, 1–30. 16

Craig, R. & Bampton, M. (1968). Coupling of substructures for dynamic analysis. *AIAA Journal*, **6**, 1313–1319. 20

Crawley, D.F. & O'Donnell, K.J. (1987). Force-state mapping identification of nonlinear joints. *AIAA journal*, **25**, 1003–1010. 10

Demetriades, G., Constantinou, M. & Reinhorn, A. (1993). Study of wire rope systems for seismic protection of equipment in buildings. *Engineering Structures*, **15**, 321–334. 3

Doebling, S., Farrar, C., Prime, M. & Shevitz, D. (1996). Damage identification and health monitoring of structural and mechanical systems from changes in their vibration characteristics: A literature review. Tech. rep., LA–13070-MS, Los Alamos National Lab., NM (United States). 5

Forssell, U. & Ljung, L. (1999). Closed-loop identification revisited. *Automatica*, **35**, 1215–1241. 41

Fritzen, C., Jennewein, D. & Kiefer, T. (1998). Damage detection based on model updating methods. *Mechanical Systems and Signal Processing*, **12**, 163–186. 9

Fujita, T., Suzuki, S. & Fujita, S. (1989). Hysteretic restoring force characteristics of high damping rubber bearings for seismic isolation. In *ASME Pressure Vessels and Piping Conference*, 23–28. 2

Gloth, G. & Göge, D. (2004). Handling of non-linear structural characteristics in ground vibration testing. *Proceedings of the International Seminar on Modal Analysis (ISMA), Leuven*. 6

Gustavsson, I., Ljung, L. & Söderström, T. (1977). Identification of processes in closed loopidentification and accuracy aspects. *Automatica*, **13**, 59–75. 41, 42

Guyan, R. (1965). Reduction of stiffness and mass matrices(Simultaneous stiffness and nondiagonal mass matrix reduction in structural analysis). *AIAA Journal*, **3**, 380. 23

Hammond, J.K., Lo, H.R. & Seager-Smith, J. (1987). Identification of nonlinearities in vibrating systems using optimal control techniques. *Proceedings of the International Modal Analysis Conference, London*, 1467–1473. 10, 62

Heaton, T., Hall, J., Wald, D. & Halling, M. (1995). Response of high-rise and base-isolated buildings to a hypothetical mw 7.0 blind thrust earthquake. *Science*, **267**, 206–211. 1

Hemez, F. & Doebling, S. (2001). Review and assessment of model updating for non-linear, transient dynamics. *Mechanical Systems and Signal Processing*, **15**, 45–74. 5

Hurty, W. (1960). Vibrations of structural systems by component-mode synthesis. *Journal of the Engineering Mechanics Division, ASCE*, **86**, 51–69. 16

Hwang, H. (1998). Identification techniques of structure connection parameters using frequency response functions. *Journal of Sound and Vibration*, **212**, 469–479. 16

Hwang, J., Wu, J., Pan, T. & Yang, G. (2002). A mathematical hysteretic model for elastomeric isolation bearings. *Earthquake Engineering and Structural Dynamics*, **31**, 771–789. 2

Jeary, A. (1996). The description and measurement of nonlinear damping in structures. *Journal of Wind Engineering and Industrial Aerodynamics*, **59**, 103–114. 3

Kelly, J.M. (1997). *Earthquake resistant design with rubber*. Springer-Verlag. 2

Kerschen, G., Lenaerts, V., Marchesiello, S. & Fasana, A. (2001). A frequency domain versus a time domain identification technique for nonlinear parameters applied to wire rope isolators. *Journal of Dynamic Systems, Measurement, and Control*, **123**, 645. 11

Kerschen, G., Golinval, J. & Hemez, F. (2003). Bayesian model screening for the identification of nonlinear mechanical structures. *Journal of Vibration and Acoustics*, **125**, 389. 8

Kerschen, G., Worden, K., Vakakis, A. & Golinval, J. (2006). Past, present and future of nonlinear system identification in structural dynamics. *Mechanical Systems and Signal Processing*, **20**, 505–592. 5, 54

Kikuchi, M. & Aiken, I.D. (1997). An analytical hysteresis model for elastomeric seismic isolation bearings. *Earthquake Engineering and Structural Dynamics*, **26**, 215–231. 2

Kwok, N.M., Ha, Q.P., Nguyen, M.T., Li, J. & Samali, B. (2007). Bouc-Wen model parameter identification for a MR fluid damper using computationally efficient GA. *ISA Transactions*, **46**, 167–179. 13

Kyprianou, A., Worden, K. & Panet, M. (2001). Identification of hysteretic systems using the differential evolution algorithm. *Journal of Sound and Vibration*, **248**, 289–314. 13

Larimore, W. (1990). Canonical variate analysis in identification, filtering, andadaptive control. *Decision and Control, 1990., Proceedings of the 29th IEEE Conference on*, 596–604. 97

Ljung, L. (1999). *System identification theory for the user*. Prentice-Hall PTR. 5, 43, 51

Ljung, L., Gustavsson, I. & Soderstrom, T. (1974). Identification of linear, multivariable systems operating under linear feedback control. *Automatic Control, IEEE Transactions on*, **19**, 836–840. 41, 44

Llorca, F., Gerard, A., Brenot, D. & Hennequin, D. (1994). Identification of joint stiffness parameters using a free interface component mode synthesis method. *International Congress on Air- and Structure-borne Sound and Vibration, 3rd, Montreal, Canada*, 789–796. 16

Loh, C. & Chung, S. (1993). A three-stage identification approach for hysteretic systems. *Earthquake Engineering and Structural Dynamics*, **22**, 129–150. 13

Ma, F., Zhang, H., Bockstedte, A., Foliente, G.C. & Paevere, P. (2004). Parameter analysis of the differential model of hysteresis. *Journal of Applied Mechanics*, **71**, 342–349. 13

Ma, F., Ng, C. & Ajavakom, N. (2006). On system identification and response prediction of degrading structures. *Structural Control and Health Monitoring*, **13**, 347. 13

Marchesiello, S. & Garibaldi, L. (2008a). A time domain approach for identifying nonlinear vibrating structures by subspace methods. *Mechanical Systems and Signal Processing*, **22**, 81–101. 11, 55

Marchesiello, S. & Garibaldi, L. (2008b). Identification of clearance-type nonlinearities. *Mechanical Systems and Signal Processing*, **22**, 1133–1145. 11, 55

Masri, S., Sassi, H. & Caughey, T. (1982). Nonparametric identification of nearly arbitrary nonlinear systems. *Journal of Applied Mechanics*, **49**, 619–628. 61

Masri, S.F. & Caughey, T.K. (1979). A nonparametric identification technique for nonlinear dynamic problems. *Journal of Applied Mechanics*, **46**, 443–447. 9, 10, 61

Mori, A., Moss, P., Cooke, N. & Carr, A. (2003). The behavior of bearings used for seismic isolation under shear and axial load. *Earthquake Spectra*, **15**, 199. 2

Naeim, F. & Kelly, J. (1999). *Design of seismic isolated structures*. John Wiley New York. 2

Nelles, O. (2001). *Nonlinear system identification: from classical approaches to neural networks and fuzzy models*. Springer Verlag. 5

Ng, T., Goodwin, G. & Anderson, B. (1977). Identifiability of MIMO linear dynamic systems operating in closed loop. *Automatica*, **13**, 477–485. 41

Ni, Y., Ko, J.M. & Wong, C.W. (1998). Identification of non-linear hysteretic isolators from periodic vibration tests. *Journal of Sound and Vibration*, **217**, 737–756. 12

Ni, Y., Ko, J. & Wong, C. (1999). Nonparametric identification of nonlinear hysteretic systems. *Journal of Engineering Mechanics*, **125**, 206–215. 10

Nichols, J., Seaver, M. & Trickey, S. (2006). A method for detecting damage-induced nonlinearities in structures using information theory. *Journal of Sound and Vibration*, **297**, 1–16. 8

Ozdemir, H. (1976). *Nonlinear transient dynamic analysis of yielding structures*. Ph.D. thesis, University of California, Berkeley. 3

Rice, H. & Fitzpatrick, J. (1988). A generalised technique for spectral analysis of non-linear systems. *Mechanical Systems and Signal Processing*, **2**, 195–207. 10, 54

Rice, H. & Fitzpatrick, J. (1991). A procedure for the identification of linear and non-linear multi-degree-of-freedom systems. *Journal of Sound and Vibration*, **149**, 397–411. 11, 55

Richards, C. & Singh, R. (1998). Identification of multi-degree-of-freedom non-linear systems under random excitations by the "reverse path" spectral method. *Journal of Sound and Vibration*, **213**, 673–708. 11, 55

Roberts, J.B. & Sadeghi, A.H. (1990). Sequential parametric identification and response of hysteretic oscillators with random excitation. *Structrual Safety*, **8**, 45–68. 13

Robinson, W. (1982). Lead-rubber hysteretic bearings suitable for protecting structures during earthquakes. *Earthquake Engineering and Structural Dynamics*, **10**, 593–604. 2

Schoukens, J., Rolain, Y., Swevers, J. & De Cuyper, J. (2000). Simple methods and insights to deal with nonlinear distortions in FRF-measurements. *Mechanical Systems and Signal Processing*, **14**, 657–666. 9

Skinner, R., Robinson, W. & McVerry, G. (1993). *An introduction to seismic isolation*. John Wiley and Son Ltd. 2

Söderström, T., Gustavsson, I. & Ljung, L. (1975). Identifiability conditions for linear systems operating in closed loop. *International Journal of Control*, **21**, 243–255. 41, 48

Söderström, T., Ljung, L. & Gustavsson, I. (1976). Identifiability conditions for linear multivariable systems operating under feedback. *Automatic Control, IEEE Transactions on*, **21**, 837–840. 41, 45

Sohn, H. (2003). A review of structural health monitoring literature 1996-2001. Tech. rep., LA–13976-MS, Los Alamos National Lab., NM (United States). 41, 47

Stewart, J., Conte, J. & Aiken, I. (1999). Observed behavior of seismically isolated buildings. *Journal of Structural Engineering*, **125**, 955–964. 2, 76

Tang, H., Xue, S., Chen, R. & Sato, T. (2006). Online weighted LS-SVM for hysteretic structural system identification. *Engineering Structures*, **28**, 1728–1735. 13

Tobita, J. (1996). Evaluation of nonstationary damping characteristics of structures under earthquake excitations. *Journal of Wind Engineering and Industrial Aerodynamics*, **59**, 283–298. 2, 76

Trendafilova, I., Lenaerts, V., Kerschen, G., Golinval, J., Van Brussel, H. & Heylen, W. (2000). Detection, localisation and identification of nonlinearities in structural dynamics. *Proceedings of the International Seminar on Modal Analysis (ISMA), Leuven*. 8

Vakakis, A. & Ewins, D.J. (1994). Effects of weak non-linearities on modal analysis mechanical systems. *Mechanical Systems and Signal Processing*, **8**, 175–198. 9

Van Overschee, P. & De Moor, B. (1993). N4SID: numerical algorithms for state space subspace system identification. *Proceedings of the IFAC World Congress*, 361–364. 97

Van Overschee, P. & de Moor, B. (1996). *Subspace identification for linear system*. Kluwer Academic Publishers. 5, 43, 96

Vanhoenacker, K., Schoukens, J., Swevers, J. & Vaes, D. (2002). Summary and comparing overview of techniques for the detection of nonlinear distortions. *Proceedings of the International Seminar on Modal Analysis, Leuven (Belgium)*, 1241–1256. 6

Verhaegen, M. (1994). Identification of the deterministic part of MIMO state space models given in innovations form from input-output data. *Automatica*, **30**, 61–74. 97

Wang, J., Chen, T. & Huang, B. (2004). Closed-loop identification via output fast sampling. *Journal of Process Control*, **14**, 555–570. 41

Wen, Y.K. (1976). Method for random vibration of hysteretic systems. *Journal of the Engineering Mechanics Division*, **102**, 249–263. 3, 25

Worden, K. (2000). Nonlinearity in structural dynamics: the last ten years. In *Proceedings of the European COST F3 Conference on System Identification and Structural Health Monitoring*, vol. 3, 29–52. 5

Worden, K. & Tomlinson, G. (2001). *Nonlinearity in structural dynamics: detection, identification, and modelling*. Institute of Physics Publishing. 5, 7

Yar, M. & Hammond, J. (1987). Parameter estimation for hysteretic systems. *Journal of Sound and Vibration*, **117**, 161–172. 12

Yoshida, J., Abe, M. & Fujino, Y. (2004). Constitutive model of high-damping rubber materials. *Journal of Engineering Mechanics*, **130**, 129–141. 3, 25

Yoshimoto, R., Mita, A., Okada, K., Iwaki, H. & Shiraishi, M. (2003). Damage detection of a structural health monitoring system for a seven-story seismic isolated building. *Proceedings of SPIE*, **5057**, 594. 26

Yoshimoto, R., Mita, A. & Okada, K. (2005). Damage detection of base-isolated buildings using multi-input multi-output subspace identification. *Earthquake Engineering and Structural Dynamics*, **34**, 307–324. 69

Yun, C. & Bahng, E. (2000). Substructural identification using neural networks. *Computers and Structures*, **77**, 41–52. 16

Zhang, H., Foliente, G., Yang, Y. & Ma, F. (2002). Parameter identification of inelastic structures under dynamic loads. *Earthquake Engineering and Structural Dynamics*, **31**, 1113–1130. 12

Zhang, J., Sato, T. & Iai, S. (2007). Support vector regression for structural identification via component-mode synthesis. *Structural Engineering and Mechanics*, **25**, 631. 16